統計的手法を用いた超伝導コイルのトレーニングクエンチ特性の評価と安定性設計

平成13年3月

古瀬 充穂

学位論文

統計的手法を用いた超伝導コイルのトレーニングクエンチ特性の評価と安定性設計

平成１３年３月

横浜国立大学大学院

工学研究科

電子情報工学専攻

古瀬 充穂

要約

超伝導電磁石の設計において、電流密度の向上と安定性の向上は相反する関係にあり、要求される性能を満たしつつ適度な安定化を施すことが最も重要なポイントとなる。しかしながら現在用いられている安定性評価基準は、擾乱エネルギーの大きさが与えられたときに電磁石が安定か否かを判断するものであり、実際に生じる擾乱の形態、発生頻度を考慮したものではない。そのため設計者は発生する擾乱を経験から予測し、それに対して既存の安定化基準に即した設計を行うという方法が一般的である。超伝導電磁石の更なる性能向上と経済性の両立には、発生し得る擾乱の大きさを正しく評価し、それに対して適切な安定化を施すことが必要不可欠であり、そのための安定性評価手法と設計手法の確立が望まれる。

低温超伝導電磁石の予期せぬクエンチの主要原因は導体の動きによる機械的擾乱であり、この機械的擾乱の定量化と発生頻度の予測から、設計の段階で電磁石のクエンチ特性を知ることができれば、トレーニングを起こさないような設計が可能となる。このような観点から新しい超伝導電磁石安定性評価に関する手法を提案し、その有効性を示してきた。

この手法は、導体の微少な動きによる擾乱のエネルギーを導体の機械的特性や通電電流から定量化し、擾乱が導体寸法不整による局所的な導体押さえ力劣化部分で起こると考え、寸法不整をガウス分布に従う不規則過程として計算機上で模擬した巻線中でのクエンチ発生回数の期待値を求めるものである。いくつかの異なる構造の超伝導コイルに対してこの手法を適用した結果、実際の界磁巻線の励磁試験結果をよく説明できることが示された。またその過程から、安定性を向上させる方法、もしくは電流密度を向上させるための最適設計に関する指針が得られることが示された。

擾乱の発生によってクエンチが生じるか否かは、擾乱エネルギーに対する冷媒の冷却能力に左右される。機械的擾乱のようなパルス的局所的発熱に対しては、機器の運用環境下における冷媒の過渡熱伝達特性を正しく評価することが重要である。超伝導発電機の回転子では、遠心加速度によりヘリウムは超臨界状態になり、界磁巻線の安定性評価においては遠心加速度下での超臨界圧へ

リウムの過渡熱伝達特性の把握が必要となる。しかし遠心加速度下での短時間のパルス的発熱に対する精度の良い温度測定が困難であるため、測定例が無かった。そこで、電子技術総合研究所と共同で、回転クライオスタットを用いて遠心加速度下での超臨界圧ヘリウムの過渡熱伝達特性を初めて測定し、冷却の機構に関する知見を得ることができた。

これらの成果は今後開発される大型超伝導電磁石について安定性設計のための指針を与えるものであり、これにより適度な安定化による経済性と性能向上を満たす電磁石の製造が可能になると考えられる。

また本安定性評価手法は発熱・冷却特性の他にコイル内の電磁・機械的応力分布の把握が重要な要素であり、これら要素理論の裏付けのための各種実験を行い、理論確立を目指した。

目次

序論

今日、実用的な超伝導線材の開発をうけて、本格的に超伝導機器の製造が行われるようになってきた。超伝導を用いれば高い密度の電流を損失無く流すことができるので、機器の大幅な高効率化、小型軽量化を図ることができる。逆に、従来の機器と同じ体格で製造すれば、常伝導金属では実現できないような大容量化を果たすことが可能である。従来の電気機器は、機器構造や冷却方式の改善、新たな支持材料や絶縁材料の開発等によって少しずつ性能を延ばしてきたが、導電材料を超伝導化することによって飛躍的な性能向上が期待でき、そういう意味で、電力機器・エネルギー機器の革命的進歩となる。すでに国内では 70MW 級超伝導発電機の開発に成功しており、電力機器の超伝導化の先駆けとして注目された。

高エネルギー物理分野では、要求される仕様から、電磁石の超伝導化はすでに必須のものとなっている。しかし電力機器については、超伝導化による性能・効率の向上と開発・製造コストのバランスや信頼性が重視される。超伝導電力機器の普及の妨げはまさに経済性と安定性にあり、これらの追求が大きな課題の一つである。

一般に電流密度の増加と安定性は相反する関係にあり、両者の妥協点をできるだけ高くすることが電磁石の設計において重要なポイントであるが、設計パラメータと安定性の関係が理論的に明らかになっていないため、どの程度の安定化を施すかについては、設計製造者の勘と経験に頼るところが大きいのが実状である。

一方、経験則も設計においては重要な情報である。電気学会超電導応用電力機器調査専門委員会において、昭和年代と平成年代に国内で設計製作された超伝導マグネットについて、設計思想と性能についてのアンケートが二度実施されている[1,2]。このアンケートにおいて数十のマグネットの設計パラメータや構造、運転状況についての情報が集まっており、これらから設計の指針について知見を得ることができる。アンケートの具体的な内容は文献を参照していただきたいが、たとえば、マグネットの安定度を測る簡易なパラメータとして知られている安定化係数と蓄積エネルギーの関係を表したデータでは、昭和年

代では完全安定化を含めた安定よりの設計が好まれていたが、平成年代ではより安定化係数を大きくした設計が行われるようになっている、といった傾向が見て取れる。さらにそういったマグネットのトレーニングの有無も知ることができ、安定で、かつ電流密度を高くとれるマグネットの設計について、先例を参考にすることができる。

しかし、安定化係数だけでマグネットの安定性を論じることはできず（事実、安定化係数2前後でもトレーニングをみせ、3以上でも安定なマグネットも報告されている）、マグネットの構造まで深く考慮した多角的な評価をする必要があるし、トレーニングを見せるような不安定なマグネットに関する情報は圧倒的に少ない。アンケートの結果だけを信じて設計製造するのは危険である。結局、設計パラメータから安定性を論じることができる理論や手法の確立が最も望まれるところである。

一般にトレーニングを伴う電流劣化現象の主要原因は、強大な電磁力による導体の動きという機械的擾乱であることが、様々な実験的検証から広く知られている[3]。総延長数百 m から数 km に及ぶ導体の中の、わずか数 mm ほどの長さにわたって、数μm 動いただけで、そのときの発熱により常伝導の芽が生じ、コイル全体が常伝導転移する。このような導体の動きが生じないように様々な手段を用いて導体の固定がなされるが、局所的で微少な機械的擾乱を完全に防ぐことは困難であり、今日でも大型高電流密度超伝導コイルの不安定性要因の筆頭に機械的擾乱が挙げられる。連続的に生じるような擾乱についてはあらかじめ予測と対策がたてやすく、パルス的な擾乱でも磁束跳躍については、ピンニングを施した均一な性能の長尺線材の開発によって問題にならなくなりつつある。

よって不安定性の主要原因である機械的擾乱を定量的に把握し、その発生頻度の予測を設計の段階で行うことができれば、設計の段階でマグネットのトレーニング現象を予測することが可能であるし、さらにクエンチ電流が確実に要求性能を越えるような設計が可能になると考えられる。

第 1 章　統計的手法を用いた超伝導コイルのクエンチ特性評価手法の概要

1.1　機械的擾乱の定量化と最小クエンチエネルギー(MQE)

超伝導巻線を構成する超伝導導線や巻枠、スペーサ等の構造材には、表面の粗さや寸法の不均一といった寸法不整が、どんなに寸法管理をしても不可避的に伴う。これにより巻線に対して外部から導体固定のための応力を加えても、巻線中に均一にいきわたらず、固定力にも不整が生じる。局所的に押さえが弱くなっている箇所で、導体に加わる電磁力（一般にフープ力）が押さえ力を上回ると、その部分で導体の動きが生じ、機械的擾乱が発生すると考えられる。この局所的な擾乱は、様々な実験結果から、継続時間が数百μ秒~数 m 秒のパルス的なもので、わずか数ミクロンの距離の導体の動きでも、常伝導の芽を生じさせるに十分な発熱があることが知られている[4]。

具体的に巻線内での導体の動きは図 1.1 に示すようなたわみであると考えられる。このとき導体が受ける仕事のうち、導体に蓄えられる位置エネルギーを差し引いた、発熱に寄与するエネルギーE_dは、通電電流 I で突然素線が動いたとすると、(1.1)式で与えられる[5]。

$$E_d = \frac{(B_n I)^2 (l/2)^5}{45 E I_d} \tag{1.1}$$

ここに l は導体が動く部分の長さ、B_n は導体が動く方向に対して垂直な方向の磁界、E は導体のヤング率、I_d は断面二次モーメントである。このエネルギーが、一度にパルス的に放出されるものと仮定する。

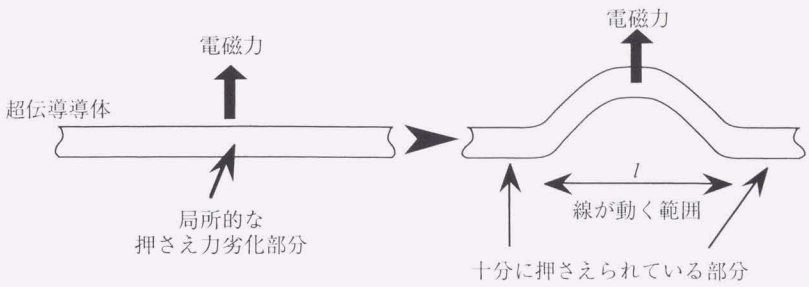

図 1.1　超伝導導体の動き

超伝導巻線がクエンチするか否かは、擾乱エネルギーE_dが導体の最小クエンチエネルギー(MQE)を越えるかどうかで判断できる。

導体の MQE は、発熱が線方向に一次元的に拡がると仮定すると、(1.2)式のような一次元熱伝導方程式を解き、発熱が巻線全体に拡がっていってしまう最小の発熱を求めることにより得られる[6]。

$$S\frac{\partial}{\partial x}\left(\kappa\frac{\partial T}{\partial x}\right)-Sc\frac{\partial T}{\partial t}+Q(T)-W(T)=0 \tag{1.2}$$

ここに S は導体断面積、κは熱伝導率、c は比熱、T は温度、$Q(T)$は温度 T における発熱量、$W(T)$は冷却量である。冷却量については、線の動きというパルス的機械的擾乱に対する過渡熱伝達特性を考慮することが MQE を正しく評価するための鍵となる。

(1.1)式で与えられるエネルギーが、導体のどれくらいの長さに渡って生じるかについては、導体やコイルの構造に依存する。層間スペーサがあるコイルの場合はスペーサと導体の接触部分の長さ、ラザフォードケーブルのような撚り線が用いられている場合は素線同士の接触部分の長さと考えられる。擾乱の継続時間は、クエンチ時に音響センサで観測される音響信号の幅から、およそ 500μsec から 1msec であることが知られている[4]。

1.2 統計的クエンチ特性評価

求めた MQE を(1.1)式の E_d に代入し、素線が動く部分の長さ l について式を解くと、(1.3)式のようになる。

$$\mathrm{MML}=\left\{\frac{1440(\mathrm{MQE})EI_{\mathrm{d}}}{\left(B_{\mathrm{n}}l\right)^{2}}\right\}^{1/5} \tag{1.3}$$

ここで与えられる長さ MML とは、導体が動いてもクエンチを起こさないような最大長さであり、最大可動域長さ(Maximum Movable Length)の略である。つまり、クエンチをエネルギーの大小での評価でなく、導体の長さの次元で考えることにする。MML は通電電流と、巻線内の導体が経験する磁界の関数である。

導体の動きは局所的押さえ力劣化部分で起き、押さえ力の変動を起こすのは導体や構造材の寸法不整であると仮定したが、一般に導体の長さ方向のうねりや厚さの寸法誤差といった不整量の特性は、ガウス分布をする不規則過程と考えることができる。そのパワースペクトル密度$\Phi_0(\omega)$は高速道路の路面や鉄道線路と同様に考えて、(1.4)式のようになる[7]。

$$\Phi_0(\omega)=\frac{A}{\omega^4} \tag{1.4}$$

ωは空間振動数、A は変動の標準偏差を決める定数である。こういったガウス分布に従う不整量は、モンテカルロ法を用いて計算機上で模擬することができる。つまり導体の長さ方向の寸法不整を計算機上で再現することができる。導体長手方向（x 方向）の寸法不整を計算機上で模擬したものを $y(x)$とする。

$$\begin{aligned} y(x)&=\sum_{k=1}^{N}a_k\cos\left(\omega_k x+\phi_k\right)\\ a_k&=\sqrt{4\Phi_0(\omega_k)\Delta\omega}\\ \Delta\omega&=\left(\omega_{\mathrm{u}}-\omega_{\mathrm{l}}\right)/N\\ \omega_k&=\omega_{\mathrm{l}}+(k-1/2)\Delta\omega \qquad ;k=1,2,\cdots,N \end{aligned} \tag{1.5}$$

ここにω_uは高域遮断周波数、ω_lは低域遮断周波数、Nは十分に大きな整数である。またϕ_kは0から2πで一様なかつ互いに独立な確率変数である。

巻線を考えたときは、このような寸法不整を持つ導体がn層重ねられている。このとき各導体の仮想平面に対する不整の標準偏差σ_nは導体一本のときの$\sqrt{n}$倍になる。

巻線に挟み込む形で力を加えたとき，各導体は圧縮による抗力と加えられる応力がつりあうまで変形する。抗力は，圧縮による変形量にコイルのばね定数κを乗じたもので，弾性領域であればκは一定値である（コンプライアンスはばね定数の逆数である）。このとき寸法不整により各導体が相互に及ぼしあう接触面力に不整が生じる。導体間の接触面力は，図 1.2 のような導体のばねモデルを用いて計算することができる。導体を，電磁力や遠心力といった体積力の働く質点と，変形により生じる抗力の平面力を表す２つのばねで表している。コイルで導体がn層積層されている場合は，このばねモデルをn層積層し，力の釣り合いから導体間の接触面力を求めることができる。

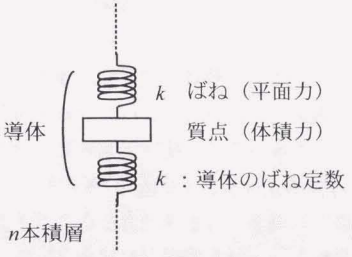

図 1.2　コイルのばねモデル

モデルのばねのばね定数kは，コイルのばね定数κに対し，$k = \kappa / 2n$である。

計算機上で模擬した寸法不整$y(x)$に対し，導体間接触面力の不整は(1.6)式で近似される。

$$\Delta F(x) = \kappa y(x) \tag{1.6}$$

つまり接触面力は平均値周りに$\Delta F(x)$だけ変動する。この近似は、圧縮力により巻線が著しく塑性変形しなければ成り立つ。実際のコイルにおいて、そのような応力を加えることはまず無く、近似が妥当であることは明らかである。

このような導体間の接触面力に対し、それとは垂直な方向に導体が動こうとしたとき、それを留める押さえ力は、接触面力に静止摩擦係数を乗じた摩擦押さえ力である。

この導体押さえ力の不整の中で、通電による電磁力が摩擦押さえ力を上回る部分で導体の動きが生じ、その部分の長さがMML以上であればクエンチが起きる。よってある通電電流、応力状態において、模擬した押さえ力分布の中でそのような箇所を数え上げることにより、巻線が潜在的に持つクエンチ発生回数の期待値を求めることができることになる。実際の巻線の総延長より十分長い不整分布を模擬すれば、期待値はより確からしくなり、実際の巻線総延長あたりに換算すれば、クエンチ発生回数の確率となる。

励磁を模擬して通電電流を 0 から増し、各通電電流におけるクエンチ発生回数の確率を積分すれば、これがその通電電流に到達するまでに経験せねばならないトレーニングクエンチの回数になる。ここで、一度動いた部分が、再び動く可能性があるかについて検討しなければならない。一般に導体に動きが生じると、その部分はより安定した場所に移動して落ち着き、押さえ力が回復して二度とクエンチの芽にはならないと考えられる。実際にクエンチ後の励磁ではクエンチ時に観測される音響信号が減ることが多く、カイザー効果として知られている[8]。しかし、線が動くフリースペースが大きい場合等では、再び同じ場所が動く可能性を考える必要がある。一度動いた部分は今まで貯め込まれた応力が緩和され、再びその部分に電磁力による応力が蓄積していくようなモデルにすればよい。このようなモデルでも、トレーニングの途中でクエンチ電流が下がるマグネットのような記憶の悪いコイルを模擬することはできない。これについては今後検討の必要がある。

クエンチ発生確率の積分値が 1 を越えるところで最初のトレーニングが（ファーストトレーニング）、以降 1 増える毎にトレーニングが起きると仮定すると、トレーニングのクエンチ電流を予測することができる。

以上のトレーニングクエンチ特性評価手法を、形状・導体・冷却方式が異なる２つの超伝導巻線について適用し、実際の励磁試験結果と比較を行った。コイル毎のモデルの相違と具体的な計算について、次章以降に示す。

第２章　大口径超伝導マグネットのクエンチ特性予測

国際熱核融合実験炉（ITER）用の導体の安定性試験をするための超伝導電磁石が、日本原子力研究所那珂研究所で製作された。このマグネットは、長尺の導体を均一磁界下に置くため、口径が大きい。製造後、三度の励磁試験が行われたが（３回目は増力用の補助コイルがインサートされた。これについては今回は検討は行わない）、設計より低い電流値でトレーニングが見られた。この安定性評価用超電導磁石(以降 MAST)にクエンチ特性予測手法を適用する。

2.1　大口径超伝導マグネットの諸元と構造、励磁試験結果

図 2.1 は MAST の縦断面図、表 2.1 は諸元である。

マグネットは 34 のダブルパンケーキコイルから成り、上下をフランジで挟み込み、これを結ぶ 96 本の締め付けボルトで固定されている。導体は銅比 3.2 の NbTi 角形モノリス導体で、パンケーキ間とダブルパンケーキ内の層間に GFRP のスペーサが挟まれている。スペーサは図 2.2 に示すように冷却チャネルが設けられており、冷媒がコイル内に行き渡るようになっている。マグネット軸方向に対するチャネルの位置は、パンケーキを積層して組み立てる時に特に合わせることはしていない。冷却は液体ヘリウム浸漬冷却である。

導体の寸法や臨界電流、ダブルパンケーキコイルの形状は、製造の段階で測定し、仕様を満足することを確認してから、マグネットの組み立てを行っている。

表 2.1　MAST 諸元

コイル	34 ダブルパンケーキコイル
冷却	液体ヘリウム浸漬冷却
内／外径	1.5m／1.8m
総ターン数	2236
蓄積エネルギー	21MJ (at 6T)
テンション	$10kg/mm^2$
導体	角形モノリシック
導体サイズ	4.0mm×7.9mm ±0.05mm
銅比 NbTi : Cu	1 : 3.2

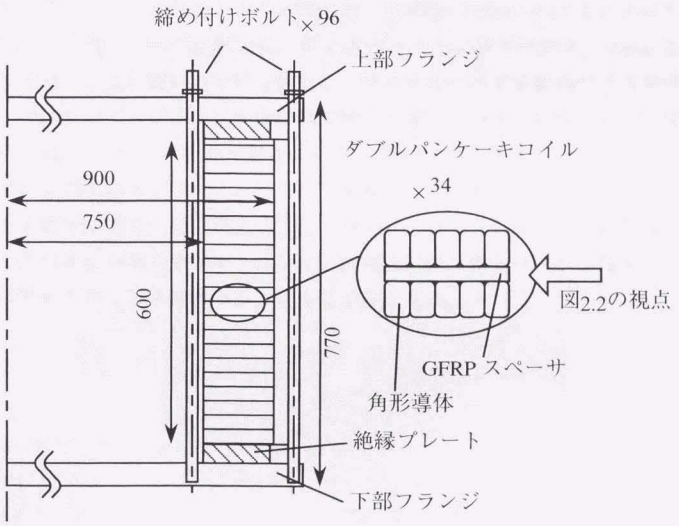

図 2.1　MAST 縦断面図

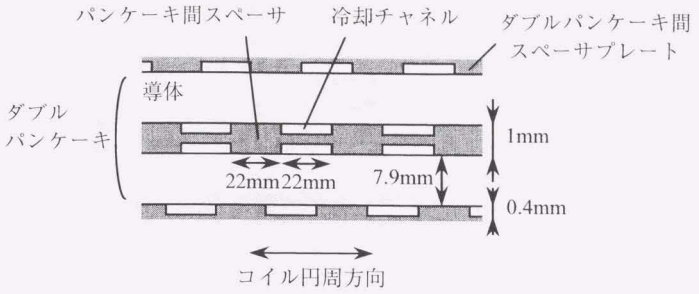

図 2.2　パンケーキとスペーサプレート

MAST の初回と２回目の励磁試験結果を図 2.3 に示す。各励磁試験ではそれぞれ５回ずつクエンチさせている。図中の一点鎖線は実測された導体の臨界電流である。２回目の励磁試験では、締め付けボルトの径を初回の 16mm から 13mm に削り、より強い力で引っ張ることでコイルに対する締め付け力を増した。この改良によってクエンチ電流は大幅に増加している。以降、初回の励磁試験を Case1、２回目の励磁試験を Case2 と表記する。表 2.2 に Case1 と 2 の締め付け力の相違とファーストクエンチ電流を示す。締め付け力の増加によりクエンチ電流が 250A ほど向上することがわかったが、Case2 でも臨界電流に比してかなり低い電流でトレーニングが観測された。電流マージンは大きく、発生磁界を大きくできるポテンシャルは十分にある。

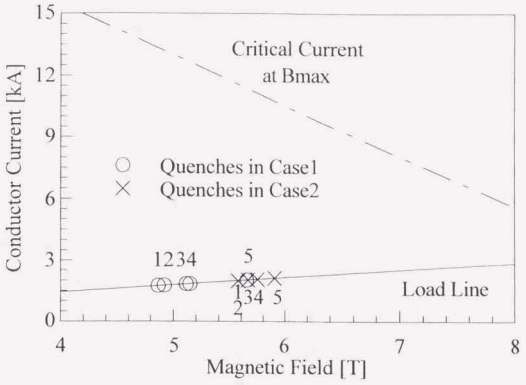

図 2.3　MAST 励磁試験結果

表 2.2　励磁試験条件とファーストクエンチ電流

	Case1	Case2
締め付けボルト径	16mm	13mm
コイルに対する圧縮応力	10.5MPa	12.0MPa
ファーストクエンチ電流	1740A	1992A

パンケーキは張力を持って巻かれており、エポキシ含浸されている。それでも、励磁試験の前後でマグネットに取り付けられた歪みゲージからパンケーキが動いた形跡が見られ、また音響センサの反応から機械的擾乱によってクエンチが起きたことが伺える。また軸方向の押さえ力の増加によるコイルのクエンチ電流の増加は、半径方向への導体の動きによりクエンチが引き起こされたことを示していると考えられる。エポキシ含浸は、冷却による熱収縮から、ターン間や層間が剥離することがあり、マグネットに部分的に、あるいは全部に渡って導体が動けてしまう空間が生じてしまったことが考えられる。

2.2 大口径超伝導コイルのクエンチ特性評価

第1章で述べた理論を用いて MAST のクエンチ特性評価を行った。具体的な評価手順を以下に示す。

導体の動きは前節で述べたように、コイルの半径方向におきると仮定した。このとき導体が動かないように押さえる力は、締め付けボルトによって与えられるマグネット軸方向の応力による、摩擦押さえ力である。さらにパンケーキはテンションを加えながら巻線されているため、半径方向内側に向かうテンションによる締め付け力も、導体が動かないように固定する力になる。

(1.1)式の擾乱定量化において、導体の機械的定数であるヤング率と断面二次モーメントは、導体の仕様から E=130GPa（ほぼ銅のヤング率と仮定）、I_d=42×10^{-12}m^4（角形導体のフラットワイズ方向への曲げより）とした。マグネット内の各導体に加わる磁界は、有限要素解析により求めた。

MQE は液体ヘリウムの過渡熱伝達特性を考慮した文献[6]のコードを用い、擾乱の継続時間は 500μsec、長さはスペーサと導体の接触部分の長さである 22mm とした。この擾乱部分の長さは MQE の結果にあまり影響しないことがわかっている[6]。また MQE は経験磁界の関数であるが、クエンチをするような磁界の強い場所を考えるので、マグネット内での最大磁界で計算し、これで近似した。MML は(1.3)式より求まるが、このときの B_n も B_{max} と近似した。MML の計算結果を図 2.4 に示す。図より MML は数 cm から 10cm 程度のオーダーであることがわかる。

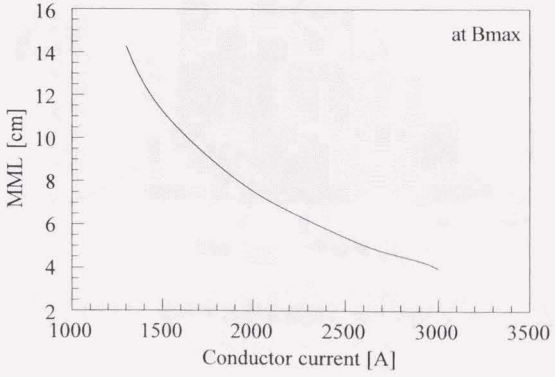

図 2.4 MAST の MML 計算結果 (at B_{max})

MAST のダブルパンケーキコイルに使用された導体は、巻線前に寸法を測定し、仕様を満足していることが確認されている。このときの測定データ（74点）は、導体の幅の平均 7.90mm、標準偏差 22.7μm であった。ヒストグラムを図 2.5 に示す。導体仕様が 7.9mm±50μm であることから、ガウス分布では約 2σが 50μm 以下であったことがわかる。そこで導体の標準偏差σ_cは 25μm とした。またスペーサもこれと同じ標準偏差σ_s=25μm とした。このときパンケーキ 1 層とスペーサ 1 層を合わせた寸法不整の標準偏差は、2 層より 25μm の$\sqrt{2}$倍でσ_0=35μm である。マグネットはこれが n=68 層重なっているので、全体の不整の標準偏差はさらに$\sqrt{68}$倍である。そこで標準偏差$\sigma = \sqrt{n}\sigma_0$の寸法不整データを式(1.5)より計算した。押さえ力の不整は、スペーサで導体がしっかり押さえられているとすれば、スペーサ間隔の 2 倍周期より短い不整は無いと考えられ、またコイルの 1 周より長い周期の不整も無いと考えられる。ゆえにそれぞれ高域遮断周波数ω_h=142.8rad/m と低域遮断周波数ω_l=1.19rad/m とした。（不整データはパワースペクトル密度が空間周波数の 4 乗に反比例するため、低域側が重要で、高域は問題にならない。）不整データの長さ方向の刻みは十分小さくする必要があるが、これはサンプリング定理よりスペーサ間隔とした。

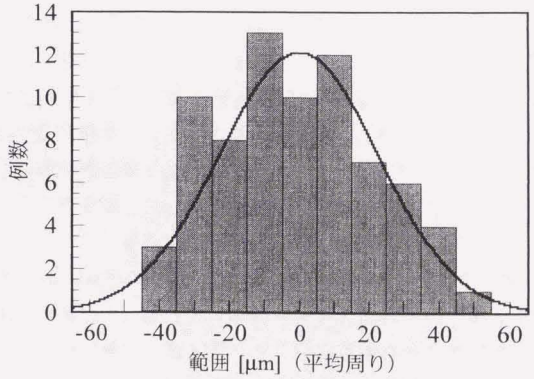

図 2.5　導体高さ測定結果のヒストグラム

マグネット内の応力分布は図 2.6 のようなバネモデルから求めた。ここで、パンケーキ 1 層と絶縁プレート 1 枚を合わせたものを一まとめに考え、これを体積力である電磁力が加わる質点と、面積力である相互間接触面力と変形を表す 2 つのバネで表してある。これが n=68 層積み上げられ、フランジで挟み込まれ、これを結ぶ締め付けボルトで挟み込み力が加えられているモデルである。パンケーキのバネ定数 k は、コイル全体のバネ定数κより $k = \kappa / 2n$ で与えられる。κは、MAST に取り付けられた歪みゲージにより励磁中の歪みを測定し、その値から求めた。κは 5GPa に相当する。これは、低温でのエポキシのヤング率に近い値である。96 本分の締め付けボルトのバネ定数 k_0 は SUS の低温でのヤング率 200GPa より求めた。

ボルトはあらかじめ引っ張って伸ばし、これによりコイルに対して締め付け力（初期押さえ力）を加えるが、励磁によりコイルが軸方向に縮むと、それにつれてボルトも縮み、もとの長さに戻ると初期押さえ力は無くなる。このとき層間の接触面力は体積力である電磁力のみによって生じ、フランジに接している部分の接触面力は無くなる。（構成材やコイルの自重の影響は無視する）このときは図 2.6 の右側のモデルを使って接触面力を求めなければならない。モデルの切り替えは、フランジに接している部分のバネの力が f_{y1} または f_{y68} が 0 になったときに行えばよい。

バネモデルで求めた層間の接触面力を平均値として、式(1.6)に従い接触面力は長さ方向に不整分布を持つ。(1.6)式のコイルのバネ定数κは上記の通りである。接触面力に対して最大静止摩擦係数μを乗じたものが最大摩擦押さえ力であり、摩擦による導体押さえ力の最大値である。摩擦係数は、低温でのエポキシ対エポキシの摩擦係数の実測値である 0.7 とした[9]。しかし摩擦係数はこのクエンチ特性予測手法において支配的なパラメータでなく、0.3 から 1.0 の範囲で変化させても予測結果にほとんど影響しないことを述べておく。

通電時に導体には電磁力が働くため，図５の通り，導体の上面の面力 f_{yi} と下面の面力 f_{yi+1} は異なる。従って，摩擦押さえ力は導体の上面と下面で異なるが，導体にフープ力が加わったとき，どちらか摩擦押さえ力が小さい方から滑りが起きる。しかしもう片面の摩擦力が電磁力を上回っていれば、導体は動かない（ここで動摩擦力は小さいとして無視する）。よって導体の動きを考えるときは、導体の両側の摩擦押さえ力の内、大きい方を考えればよい。以降の摩擦押さえ力は、この大きい方の摩擦押さえ力を言うことにする。

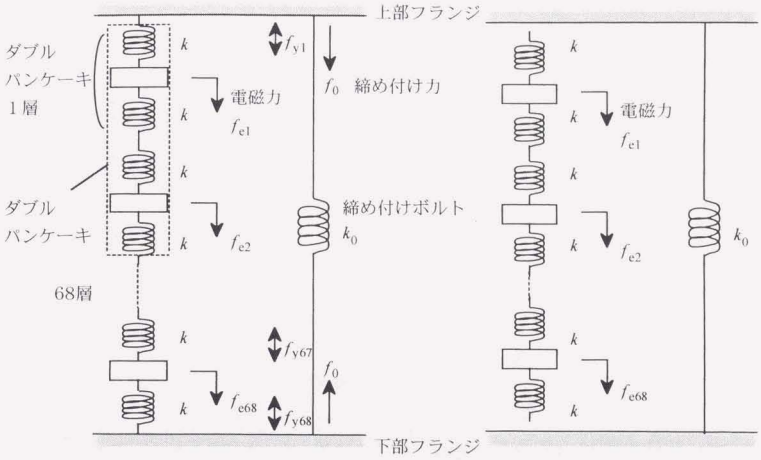

図 2.6　コイル内応力分布を求めるためのバネモデル（右は締め付けボルトの締め付け力が無くなった後のモデル）

ある通電電流においてこの最大摩擦押さえ力を計算機上で模擬した一例を図 2.7 に示す。寸法不整の模擬においてサンプリングを 22mm 間隔としたが、これを計算上の 1 セグメントとし、図 2.7 の横軸はそのセグメントの位置、縦軸はそのセグメントあたりの摩擦押さえ力を 1m あたりに換算した力である。また図中の破線はフープ力からテンションを引き算したものである（1m あたり）。

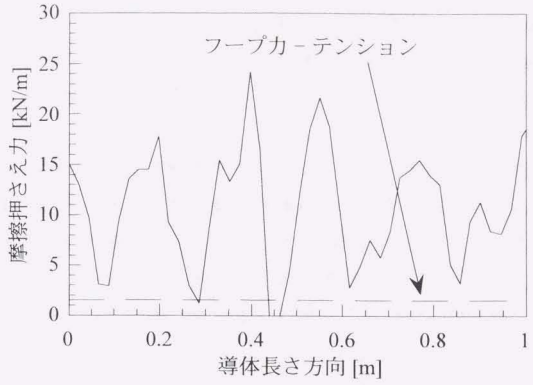

図 2.7　摩擦押さえ力の模擬例（1 セグメント 22mm あたり。図中の破線は電磁力 － テンション）

図 2.7 の通り、摩擦押さえ力は平均値周りに大きく変動し、場所によっては完全に 0 になる部分もありうる。

巻線張力のコイル半径方向内側向き成分は、図 2.8 より以下のように計算できる。

$$\int_0^{\pi/2} r\,\mathrm{d}\theta\rho\sin\theta = F_\mathrm{T}$$
$$\therefore F_\mathrm{T} = r\rho \tag{2.1}$$

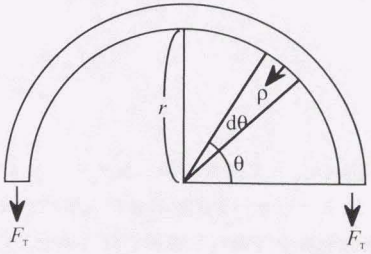

図 2.8　コイル内のテンションの半径方向成分

例えば、半径 80cm の位置でのテンションは、F_T = 10kg/mm^2×4mm×7.9mm = 316kg より、ρ = 3.9kN/m である。これは約 1200A 通電時の半径方向電磁力に相当する。テンションは半径方向内向きに作用するため、導体が外向きに動こうとするときは、フープ力が摩擦押さえ力とテンションの合計を越えなければならない。

フープ力 − テンションが摩擦押さえ力を上回った場合、その部分がフリーになると仮定すると、その区間に加わる電磁力はその両側で支えなければならない。計算機上の応力模擬モデルの上では、両側のセグメントに電磁力を二分して受け持つものと仮定する。もしこの力が両側で受けきれない場合は、さらにその外側のセグメントで受け持たなければならない。（図 2.9）

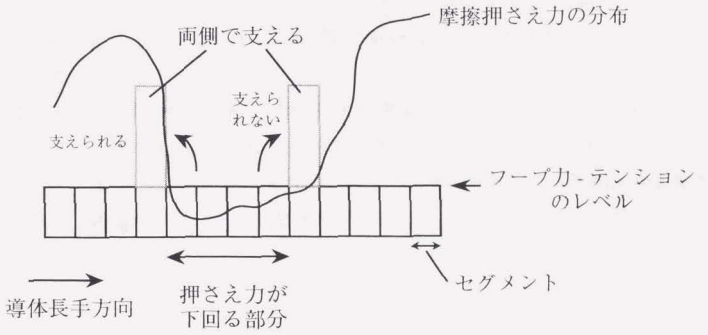

図 2.9　導体支持のモデル

導体が長い部分に渡って撓んだ場合、その移動距離Δ$y(x)$（図 1.1 の弓なりのたわみの頂部分を x=0 とする）は式(2.2)で与えられる[5]。

$$\Delta y(x) = \frac{B_n I (l-x)^2 (l+x)^2}{24 E I_d} \tag{2.2}$$

しかし導体が動けるスペースは、密巻きのコイルゆえに、導体が持つ寸法不整分しかないと考えられる。つまりパンケーキコイルが 33 ターンのため、標準偏差 $\sqrt{33}\sigma_c$ のガウス分布に従う距離だけ動ける部分が導体長さ方向に分布することになる（可動距離が負になった場合は 0 とする）。各セグメントでの

移動距離を(2.2)式より求め、その点での模擬された可動距離に到達した場合は、そこで導体が外側のターンに触れるために固定され、それ以上長い範囲に渡って導体のたわみは生じないと仮定した。本来ならテンションによって導体がつぶれて隙間は小さくなっていると考えられるが、ここではその効果は小さいと見なして無視した。（先のテンションの例では 0.5MPa 程度で、応力としては小さい。）

導体が動いた部分は（両側で支えられた場合も次のターンに接触して固定された場合も）応力が緩和されたとみなし、それら全てのセグメントの電磁力を 0 とした。（励磁試験の通電範囲内では一度動いた部分が再び動くようなことはないと判断したため）

このような仮定により、コイルのかなり長い部分（たとえば半周以上）にわたって導体の動きがモデル上で制限される。一例として、1500A、4T のとき、$\Delta y(0)$=100μm となるようなたわみ部分長さは l=7.6cm である。（このときの MML は 9.7cm）

導体が動いた部分の長さが、そのときの通電電流における MML よりも長い場合はクエンチが起き、MML より短い場合は、動きが生じでもクエンチは起きない。クエンチ発生回数の期待値を通電電流毎に計算し、実際の導体長さでわり算して確率を求め、ある通電電流 I までの確率の積算をしたものが図2.10である。

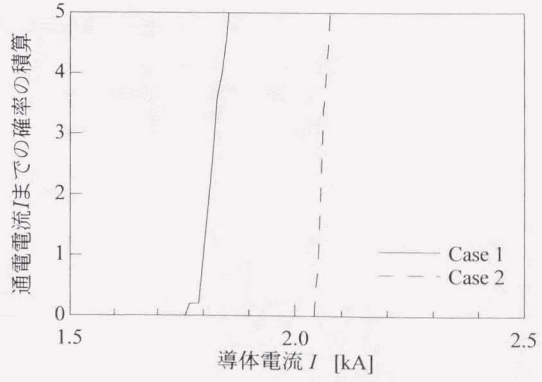

図 2.10　通電電流 I までのクエンチ発生確率の積算

第1章より、この確率の積算が1になるときファーストクエンチが、以降1増える毎にクエンチが起きると仮定すると、トレーニングクエンチ電流が予測でき、その予測結果と図 2.3 の励磁試験結果を合わせてプロットしたものが図 2.11 である。

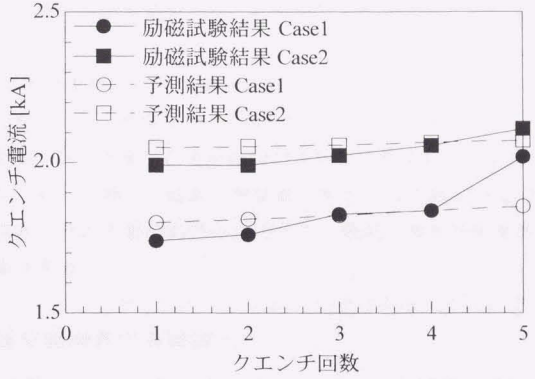

図 2.11　トレーニングクエンチ予測結果と励磁試験結果の比較

図 2.11 の通り、トレーニングクエンチ予測は、若干の誤差はあるものの、励磁試験結果をよく説明できることがわかる。

第3章　超伝導発電機界磁巻線のクエンチ特性予測

次に超伝導発電機界磁巻線のクエンチ特性予測を行い、励磁試験結果との比較を行った結果について述べる。発電機界磁巻線は前章の大口径マグネットとは全く異なるタイプの巻線であり、モデルや近似方法等、相違点について詳述する。

国内の超伝導発電機開発は、通商産業省工業技術院のニューサンシャイン計画「超伝導電力応用技術開発」の一環として行われ、本稿執筆時点で7万kW級超伝導発電機（モデル機）の実証試験が成功裏に終了し、当初計画の20万kW級機（パイロット機）の試設計が始まったところである[10]。本章ではモデル機用に製作された3種類のロータのうち、低速応高電流密度型B機の界磁巻線を対象とする。

3.1　超伝導発電機界磁巻線諸元

界磁巻線を超伝導化した超伝導発電機は、空心でも発電に必要な高磁界が得られるため、同期リアクタンス低減による限界送電電力の向上および電圧安定性の改善、発電機効率の1%程度の向上、発電機重量と寸法の半減といった様々なメリットを持つ。これら優れた特性を持つ超伝導発電機は、21世紀の早い時点で実用化されるものとして期待されている[11]。

表3.1は低速応高電流密度型7万kW級超伝導発電機の諸元、表3.1はロータ断面図である[M]。界磁巻線に用いられる超伝導導体の諸元は表3.2に示す通り、素線9本を撚り合わせた成形撚線で、外周部に絶縁のためのポリイミドテープと、冷媒流路形成のためのプリプレグテープを巻いてある。導体断面図を図3.2に示す。

表 3.1　7 万 kW 級超伝導発電機諸元

ロータ	
極数	2
回転速度	3600rpm (60Hz)
直径	890mm
軸受け間距離	4900mm
界磁巻線	
形状	鞍型
コイル数	10（5 コイル/極）
磁束密度	最大 4.5T（at 3000A）
導体	9 本撚成形撚線

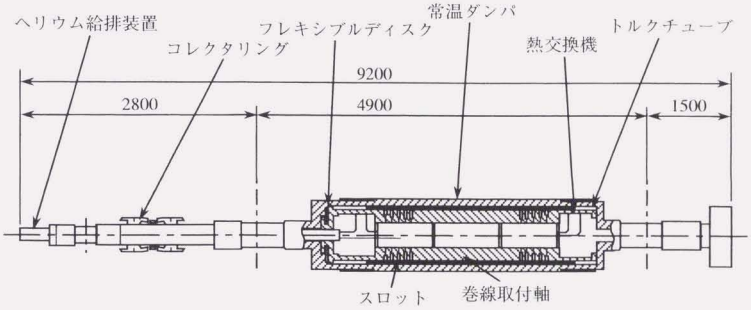

(a)　縦断面図

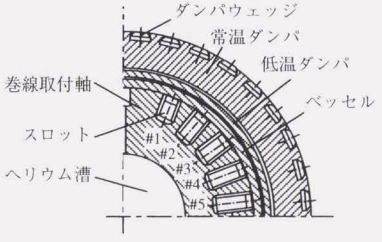

(b)　横断面図

図 3.1　7 万 kW 級超伝導発電機回転子断面図

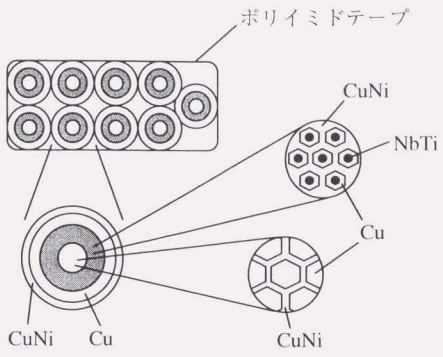

図 3.2　導体及び素線の断面図

表 3.2　界磁巻線導体諸元

導体（成形撚線）	
断面寸法	2.9mm×(7.4mm+0μm,-200μm)
素線本数	9 本
フィラメント径	9μm
臨界電流	5100A (7.6T) at 4.2K 4900A (7.3T) at 4.6K
導体絶縁	カプトンテープ半重ね巻 プリプレグテープすかせ巻
素線	
素線径	φ1.6mm
Cu : CuNi : NbTi	2 : 0.7 : 1

界磁巻線は 1 極あたり 5 個、計 10 個のコイルを直列接続したもので、それぞれのコイルは巻線取付軸に刻まれている鞍型のスロットに納められている。各コイルは超伝導導体の積層段数が異なるため、スロットの深さが異なる異深スロット構造を採用している。界磁巻線の固定は、巻線後の絶縁テープの樹脂の加熱硬化と、図 3.3 のスロット断面図のように上下左右に配置した絶縁スペーサによって行われ、ロータ外側から金属円筒のベッセルを焼きばめし、巻線

の上下方向に一定の押さえ力が加えられている。左右方向には積極的な押さえ力の付加は行っていない。

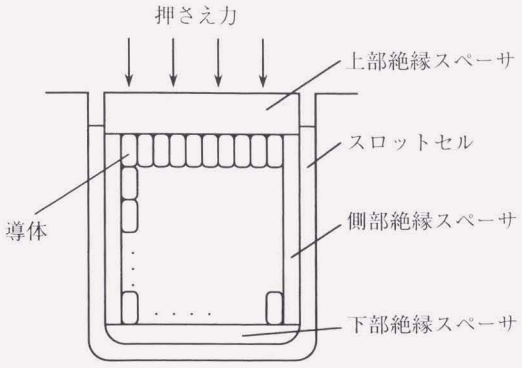

図 3.3　スロット断面図

3.2　超伝導発電機界磁巻線のクエンチ特性評価

界磁巻線はテンションをかけて巻かれているが、鞍型コイルの直線部分ではテンションによる導体の固定が難しい。導体に加わる力は、ロータの半径方向にベッセルによる巻線固定力、回転時に遠心力が、半径方向と円周方向にはそれぞれ電磁力があり、ロータ円周方向への電磁力は巻線直線部にとっては拡がろうとするフープ力に相当する。そこで機械的擾乱は巻線直線部で起きるものと仮定し、直線部のみに着目した。またテンションは引き張り方向の力であるため、導体の動きに関する本手法上では無視する。

導体は素線が束ねられているため、ロータ円周方向には素線の動きが生じると仮定した。この仮定にはいくつかの理由がある。まず、導体全体が動くと仮定すると断面二次モーメントが大きく、かなり大きい電磁力が必要になる。また導体の MQE は概算で素線の本数倍と考えられ、MML が大きくなる。導体は樹脂の加熱硬化により固定され、長い部分に渡って導体が動くとは考えにくい。逆に素線に着目した場合、図 3.2 に示すように比較的フリースペースは大きいと考えられ、素線の動きによる擾乱がクエンチを引き起こすと仮定する

のが妥当である。導体内の素線が1本動いたとき、導体内の応力バランスが崩れ、他の素線も同時に動くと考えれば、結局導体全体が動いたのと同じことになる。そこで、導体を1本の素線で代表させ、導体の中心部での力がこの素線に加わるというモデルとした。素線が動こうとするとき、これを留めようとする力は、巻線の半径方向の接触面力による摩擦押さえ力であるが、接触面力は導体の平面力が導体内部に行き渡ると仮定し、導体間接触面力が代表される素線に加わるものとした。摩擦係数は丸形素線間の値であるが、MAST のときと同様に評価上重要な値ではない。ここでは$\mu = 0.7$ とした[13]。

(1.1)式の擾乱定量化においては素線の機械的定数であるヤング率と断面二次モーメントはそれぞれ E=130GPa（ほぼ銅のヤング率と仮定）、I_d=3.2×10^{-13}m^4（丸形素線の曲げより）とした。コイル内の磁界分布は有限要素解析によるデータがあるので、これを参考にし、導体中央での磁界が導体を代表する素線に加わると仮定した。

界磁巻線の励磁試験は、ロータを静止させた状態と回転させた状態で行われた。静止状態での励磁では巻線は 4.2K の液体ヘリウムの浸漬冷却となるが、回転状態では毎分 3600 回転の遠心加速度約 4kG が巻線だけでなく冷媒のヘリウムに加わり、ヘリウムは 4 気圧 4.6K の超臨界圧状態になる。よって MQE の計算では遠心加速度下における超臨界圧ヘリウムの過渡熱伝達特性を考慮しなければならない。しかし過渡熱伝達特性については過去に測定例が無かったため、遠心加速度下での超臨界圧ヘリウムの定常熱伝達特性のデータ[14]を用いて MQE の計算を行った。この熱伝達特性については次節で詳述する。使用したコードは MAST と同じ文献[6]のものであるが、表 3.2 の通りこの導体は CuNi をバリアとして持っており、三層構造になっている。そこでコードの中の安定化材の物性値を、Cu と CuNi の値から断面積比で按分して求め、計算を行った。MML は式(1.3)より求まる。このときの B_n も B_{max} とした。擾乱が加わる範囲は図 3.4 より、素線同士の接触部分の長さとして 2mm、継続時間は MAST と同様に 500μsec とした。

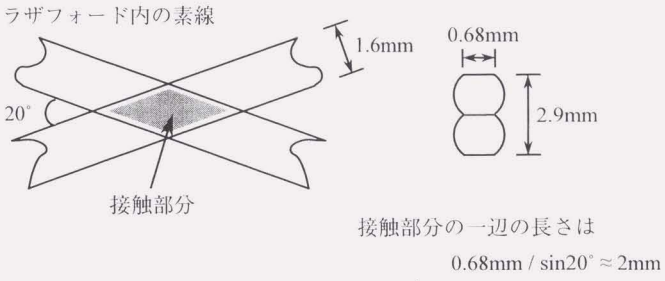

図 3.4　擾乱が加わる部分の長さ（素線の接触部分の長さ）

素線 1 本に巻線最大磁界が加わったときの MML の計算結果を図 3.4 に示す。ただし図 3.5 の横軸は導体の通電電流に換算してある。

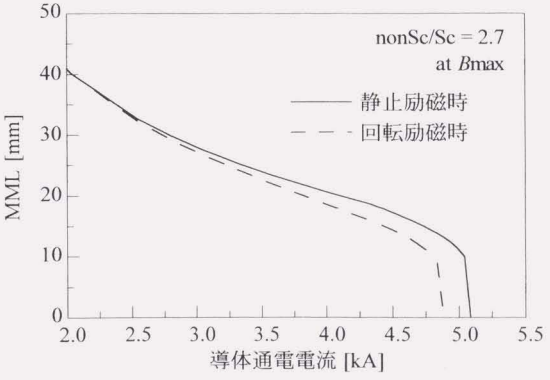

図 3.5　発電機界磁巻線の MML 計算結果 (at B_{max})

図より、MML は数 mm から数 cm のオーダーであり、静止励磁の方が大きく、臨界電流付近で急激に小さくなることがわかる。

寸法不整データは、前述の仮定の通り、接触面力は導体の表面力を考える

ため、導体寸法の不整データを模擬した。表 3.2 の仕様より、導体の高さは平均+0μm、-200μm で管理されている。そこで標準偏差は 3σ=100μm とした。1000 個のデータのうち 3 つが範囲を超えるという標準偏差である。本来は+0μm はローラにより導体をつぶしていることを意味するが、出っ張っている部分は接触面力が大きくなり、導体の動きを生じにくくさせる。着目すべきはへこんでいる部分であり、妥当な仮定である。寸法不整データの計算は式(1.5)に従い、低域遮断周波数はω_l=0.02rad/m、高域遮断周波数はω_h=15.7krad/m とした。低域遮断周波数は、静止励磁試験時の巻線押さえ板の寸法が半周期となるように、高域遮断周波数は MAST のときと同様にほとんど意味を持たないので大きな値としておいた。サンプリング間隔は 0.2mm と十分小さくした。静止励磁試験ではベッセルははめず、巻線押さえ板をスプリングで押しつける形で巻線の固定を行っている。励磁前に巻線に加えられている初期固定力は、静止励磁試験時 18MPa、回転励磁試験時 21MPa であった。

巻線内の応力分布の計算は、MAST と同様のバネモデルを用いて行った。界磁巻線の場合はボルトによる締め付けは無く、上部フランジから与えられる初期固定力のみが積極的固定力である。また回転励磁時は接触面力が作用するロータ半径方向に遠心力が加わるため、質点に電磁力と遠心力が加わるようなモデルになっている。バネモデルを図 3.6 に示す。遠心力は初期固定力に抗う向きであり、固定を弱くする要因である。

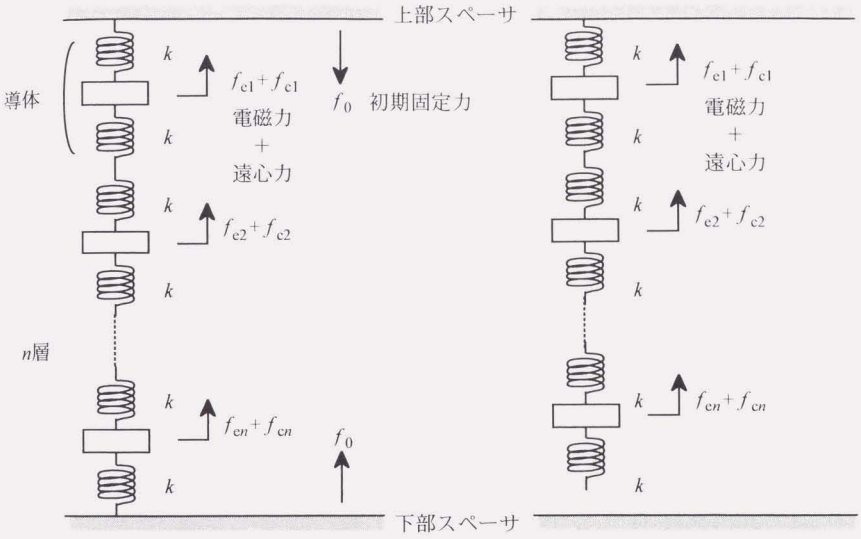

図 3.6　巻線内応力分布を求めるためのバネモデル（右は遠心力により巻線が下部スペーサより離れた後のモデル）

異深スロット構造により、巻線毎に導体数 n は異なる。

励磁による巻線のロータ半径方向の収縮と、遠心力の影響で、巻線が下部スペーサから離れるような場合は、図 3.6 の右側のモデルを用いた。このときは初期固定力が全く作用しない。

導体のバネ定数 k は、巻線のバネ定数κより $k=\kappa/2n$ で与えられる。κは、有限要素解析により算出した。詳細は第 4 章で述べる。

ある通電電流における摩擦押さえ力の分布の計算例を図 3.7 に示す。横軸はセグメント（幅 0.2mm）の位置、縦軸はそのセグメントあたりの摩擦押さえ力を 1m あたりに換算した力、破線はフープ力である。

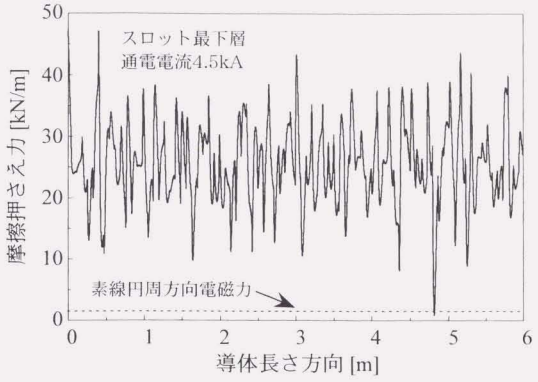

図 3.7　摩擦押さえ力の模擬例（1 セグメント 0.2mm あたり）

フープ力が摩擦押さえ力を上回った場合、MAST のケースとは異なり、MML を越えるような動きが生じたときのみ応力緩和が起き、それ以外の場合は電磁力がその場に蓄積していくモデルとした。つまり、励磁によりフープ力が大きくなっていき、押さえ力が上回っても両側で支持することはせず、また MML より短くてもその部分の電磁力はそのままとした。MML を越える長さに成長したときにクエンチとカウントし、その区間のすべての電磁力を 0 にリセットした。これは、ラザフォードケーブルの素線の場合は連続的な支持構造であり、動く場合はクエンチの時に導体内の素線が一度に動くという仮定からである。また同様の理由から素線の動く範囲についても考慮しなかった。

模擬した押さえ力分布の中で電磁力が摩擦押さえ力を上回る部分で、かつその部分の長さが MML を越える部分を勘定し、巻線のストレート部分の長さからクエンチ確率を求めた。ここで、素線が動くと導体中の他の素線も同時に動き、1 つのクエンチが起きるという仮定であった。ある通電電流 I までのクエンチ確率の積算が 1 になったときがファーストクエンチである。安定性評価においてはファーストクエンチの電流値が最も重要であるので、ここではファーストクエンチ電流の予測のみを記す。予測結果と励磁試験結果の比較を表 3.3 に示す。

実際のロータ界磁巻線の励磁試験は、ロータを静止させた状態で臨界電流

付近まで通電し、トレーニングがあることを、また回転させた状態で定格通電（3kA）と過渡時最大 3780A でクエンチしないことを確認している[12]。表 3.3 より、静止励磁時のファーストクエンチ電流を予測できていることがわかる。これを根拠に、回転励磁では予測される電流値からトレーニングが起きると考えられる。

表 3.3　ファーストクエンチ電流予測結果と励磁試験結果の比較

	静止励磁	回転励磁
試験結果	4.3kA	――
予測結果	4.1kA	4.4kA

図 3.5 の MML では静止状態の方が回転状態より大きくなっているのに、予測結果では静止励磁時より回転励磁時の方がファーストクエンチ電流が大きくなっている。これは、巻線に対する押さえ力が回転励磁試験の方が大きいためであり、巻線押さえ力が安定性向上に大きく寄与することを示している。静止励磁試験と回転励磁試験の関係、およびクエンチ電流の巻線押さえ力依存性は次章で詳述する。

この章では発電機のトルクの影響は考慮しなかった。定常トルクの導体 1 本 1m あたりの分担分は 0.46kN/m で、定格運転時に加わる電磁力 13.5kN/m の 3%にすぎず、これを上乗せしても実際にクエンチする時の電磁力 27.7kN/m に遠く及ばない。発電機の三相突発短絡でも過渡時最大 3.5pu しかかからず、定常トルクや突発三相時の瞬時トルクは巻線の安定性にほとんど影響しないことがわかる。実際に発電機の励磁試験と突発短絡試験で、クエンチせずに運転できることが確かめられている[12]。

3.3　遠心加速度下における超臨界圧ヘリウムの過渡熱伝達特性

前節のクエンチ特性評価においては、回転励磁時の MQE の計算において、遠心加速度下における超臨界圧ヘリウムの定常熱伝達特性を用いた。この根拠となった、超臨界圧ヘリウムの過渡熱伝達特性の測定結果について述べる。

回転場の生成には、電子技術総合研究所の高速回転クライオスタットを用いた。クライオスタットの断面図を図 3.8(a)に示す。ヘリウムが入るサンプル

スペースは高さ 20cm、直径 20cm のアルミ合金製円筒容器で、FRP のシャフトでエアタービンにつながり、容器自体が回転する。容器内部には４枚のディスクがあり、このディスクの１つに図 3.8(b)のように加熱用導体兼温度計として白金コバルト細線（以下 Pt-Co 線）を、地面に対して垂直になるように設置した。このときの Pt-Co 線の回転半径は 9cm であった。回転により Pt-Co 線には線に対して垂直な方向に遠心加速度が加わる。

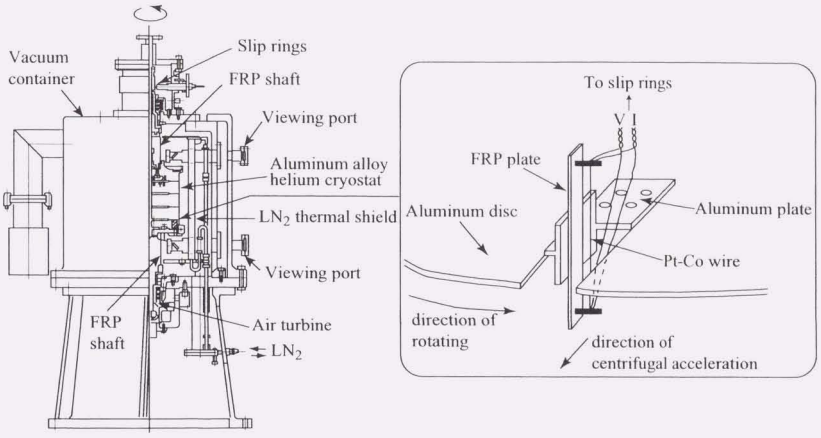

(a)　高速回転クライオスタット断面図　　(b)　測定サンプル

図 3.8　熱伝達特性測定装置図

Pt-Co 線は極低温用の工業用温度計に用いられる材料で、白金に微量のコバルトを混ぜることによって極低温域における抵抗値や感度が大きくなっている。サンプルに用いた Pt-Co 線の直径は 20μm、長さは 40mm である。液体ヘリウム温度での抵抗測定では 1.1Ωだった。この Pt-Co 線の熱時定数は 4.2K で 10μsec 程度[15]であり、数 100μsec から数 msec の発熱に対する温度測定においては十分にはやく、線のバルク温度と表面温度は等しいと考えて良い。

Pt-Co 線に接続されている電流・電圧リードはスリップリングを介して外部と接続することができる。電流リードは定電流パルス電源に接続し、電流値 $I(t)$ は Pt-Co 線と直列に接続した（常温部の）シャント抵抗（1Ω標準抵抗器）の

電圧を測定して求めた。電圧リードは時分割能 5μsec のトランジェントレコーダに接続し、パルス電流を流したときの電圧変化 $V(t)$を記録した。抵抗 $R(t)= V(t) / I(t)$ とあらかじめ測定しておいた抵抗温度依存性より時刻 t における温度 $T(t)$ が得られる。また Pt-Co 線の表面熱流束は次式(3.1)で与えられる。

$$q(t) = \frac{I(t)V(t)}{S} \tag{3.1}$$

ここに S は加熱面表面積で、S=2.5×10^{-2}cm^2 である。

定電流パルスで加熱した場合、温度変化により抵抗値が変わるため、$V(t)$も時間的に変化する。ゆえに(3.1)式の熱流束も時間の関数であるが、加熱開始直後のわずかな時間では熱流束は変化せず、このときの熱流束を初期熱流束と呼ぶことにする。液体ヘリウムの過渡熱伝達特性においては過渡核沸騰状態における熱流束に相当する。以降、Pt-Co 線に入力した熱量の大きさは、この初期熱流束で表すことにする。

測定はクライオスタットの回転数を 0rpm から 6000rpm まで変化させて行った。このとき Pt-Co 線周囲に加わる遠心加速度は 1G から 3600G になる。液体ヘリウムの圧力は容器内の液残量に依存するが、1G,400G,900G,1600G では液体状態、3600G では 2.4 気圧に達し、超臨界状態であった。

図 3.9(a)~(d),(d')は、初期熱流束にして 23kW/m^2~47kW/m^2 を入力したときの、各遠心加速度下での Pt-Co 線の温度の時間変化の測定結果である。横軸は加熱開始からの時間である。

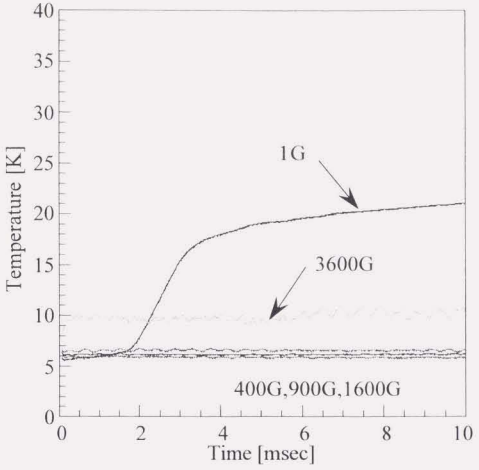

(a) 23kW/m^2

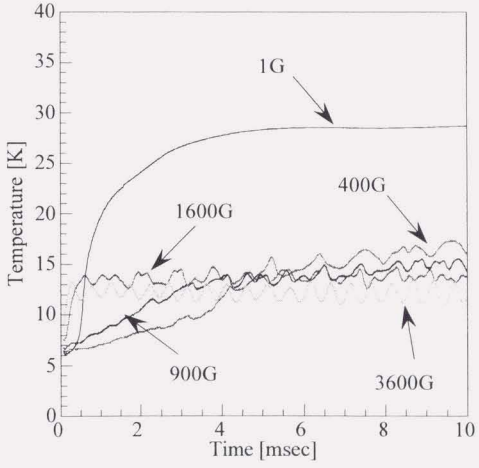

(b) 32kW/m^2

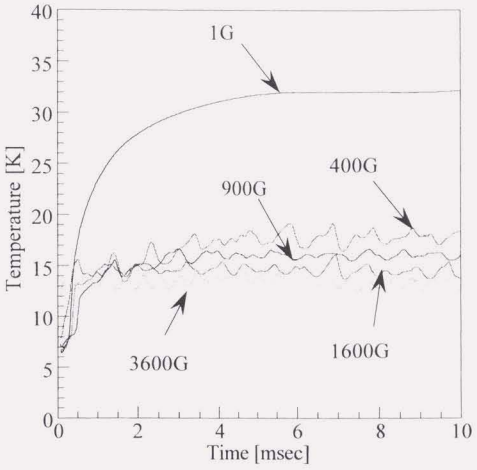

(c) 37kW/m^2

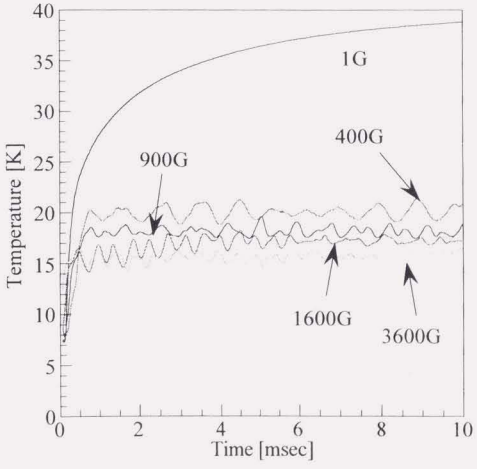

(d) 47kW/m^2

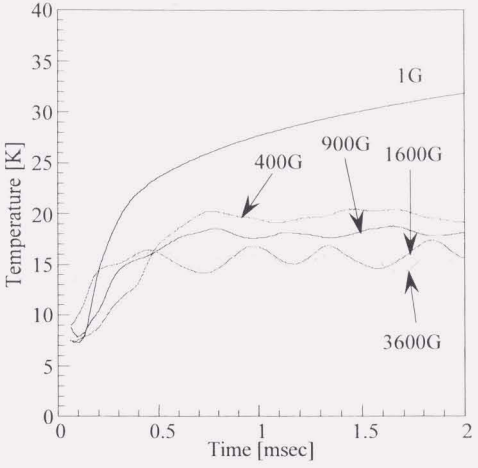

(d') 47kW/m^2 拡大図

図 3.9 遠心加速度下でのパルス加熱に対する Pt-Co 線の温度の時間変化

どの条件においても、膜沸騰状態では温度の周期的振動が見られた。これは気泡の加熱面からの離脱周期（気泡離脱周期）と一致することがわかっている[15]。3600G の超臨界状態でも温度の周期振動が見られるが、相変化の無い超臨界状態では気泡の生成は起こらない。しかし 2.4 気圧程度の超臨界圧ヘリウムの密度はわずかな温度変化でも大きく変化する。そのため加熱面付近に密度の異なる泡状の粗密が生じ、その移動が気泡の振る舞いと似ているため、擬似的な沸騰現象が起きていると考えられる。図 3.10 に気泡の離脱周期と遠心加速度の関係のグラフを示す。気泡離脱周期は遠心加速度の-1/3 乗に比例することがわかっているが[15]、超臨界でのデータもこの線上に乗っている。

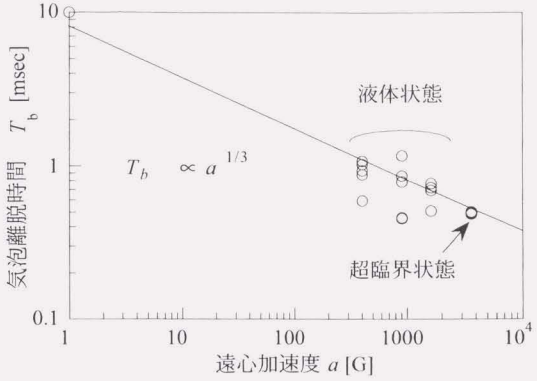

図 3.10　気泡離脱時間と遠心加速度の関係

図 3.9 より明らかに、3600G では過渡核沸騰状態が見られない。これは超臨界状態のヘリウムは相変化を起こさないためである。沸騰冷却では液相から気相に相変化する際に大きなエンタルピーの変化があり、これにより大きな冷却効果がもたらされる。核沸騰状態と過渡核沸騰状態ではこの効果により温度上昇は極めて低く抑えられる。これに比べて超臨界状態では相変化による熱の奪取が起きず、伝熱により暖まった超臨界ヘリウムの泡状の塊が自然対流により加熱面より離れていくだけである。よって沸騰冷却のような良好な冷却は期待できない。擬似的な沸騰現象は起きるが、蒸気膜で覆われて伝熱が制限される膜沸騰状態と同様に、加熱面の温度上昇は大きく、泡の離脱による冷却効果は小さい。自然対流による冷却が支配的となる。

図 3.9(d')は同(d)の加熱開始直後のグラフを拡大したものである。3600G の超臨界状態では加熱開始後 200μsec 程度で温度は定常状態になっている。

図 3.11 は温度が定常になったときのバス温度からの温度上昇ΔT とその時の熱流束をプロットしたものである。1600G 以下ではヘリウムは液体状態であり、核沸騰、膜沸騰の区別があり、バーンアウトがある。しかしながら 3600G ではグラフの傾きは一直線であり、超臨界圧ヘリウムの自然対流による冷却特性を示している。

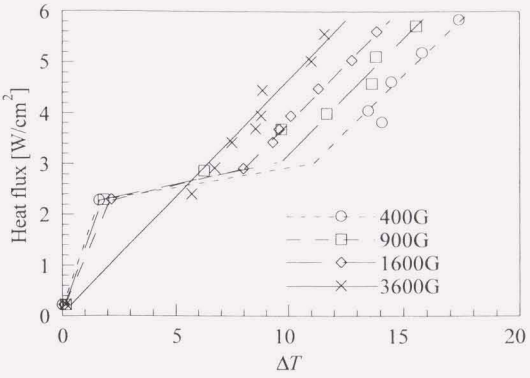

図 3.11　遠心加速度下での定常熱伝達特性

熱流束が小さい領域では液体状態の核沸騰冷却は超臨界圧状態の自然体流冷却より優れた冷却能力を持ち、温度は低く押さえられる。しかし限界熱流束を越えると液体状態では膜沸騰冷却に移行し、自然対流冷却が支配的となる。この場合は対流速度を速める高遠心加速度下の方が優れた冷却能力を持つことになる。

3600G での定常熱伝達特性をレイレイ数(Ra)とヌセルト数(Nu)の無次元量で評価したものが図 3.12 である。レイレイ数とヌセルト数はそれぞれ以下の式で算出した。

$$Ra = ad^3\beta\Delta T\rho^2 C_p / \lambda\mu \tag{3.2}$$

$$Nu = \alpha d / \lambda \tag{3.3}$$

ここに、

a	:	遠心加速度	m/s^2
C_p	:	比熱	J/kg·K
d	:	伝熱面等価直径	m
α	:	熱伝達係数	W/m^{2}K
β	:	体積膨張率	1/K

λ	:	熱伝導率	W/m·K
μ	:	粘性係数	Pa·s
ρ	:	密度	kg/m^3

である。図中の破線は平板加熱面に対する遠心加速度下の超臨界圧ヘリウムの定常熱伝達特性のデータより得られたもので、$Nu=0.13\times Ra^{1/3}$ は自然対流熱伝達の実験式としてよく知られている式である[14]。

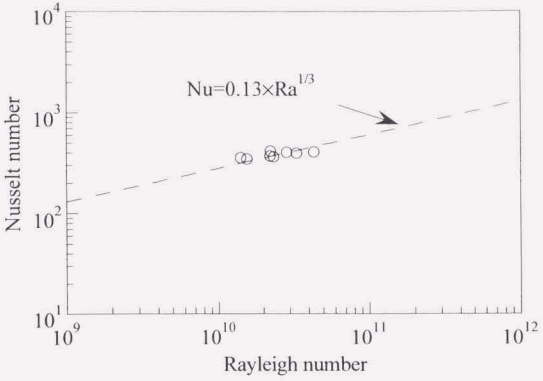

図 3.12　3600G での定常熱伝達特性 (Ra-Nu)

以上の議論より、遠心加速度下の超臨界圧ヘリウムは、加熱開始後 200μsec 程度で定常熱伝達が確立することがわかった。導体の突発的動きという機械的擾乱の継続時間は 500μsec から 1msec 程度であることから、このような発熱に対しては過渡熱伝達特性の影響は小さいと考えられる。よって前節のクエンチ特性評価手法において回転時の MQE の計算では遠心加速度下の超臨界圧ヘリウムの定常熱伝達特性を用いた。

第4章　超伝導コイルの安定性設計

前章までで統計的トレーニングクエンチ特性手法の概略と、全く異なるタイプの二つの超伝導コイルに手法を適用した結果を示してきた。注意深くモデルを作成すれば、クエンチ特性の予測が可能であることが示された。そこで、さらに踏み込んで、安定性と電流密度を両立させる超伝導コイルの設計に関する指針について検討を行った。

4.1　大口径超伝導マグネットの安定性向上のための指針

MAST は図 2.3 の励磁試験結果が示すとおり、臨界電流よりかなり低い電流値でトレーニングが起きている。よって MAST では、クエンチ電流を増す、つまり安定性を向上させる方策について検討を行った。

MAST のクエンチ特性評価の過程において、ファーストクエンチが起きるのは、コイルが電磁力により軸方向に縮み、ボルトによる初期締め付け力が抜けきってしまう電流値であることがわかった。つまり、コイルに対する締め付け力が足りていないため、電磁力が摩擦押さえ力を上回り、導体の動きが生じてクエンチが起きていた。実際、締め付け力を増した Case2 では Case1 に比べてクエンチ電流が増加しており、締め付け力の増加が安定性の向上につながることが示されている。

しかし、コイルに対する締め付け力は Case2 で 12MPa 加えており、ボルトに加わる応力は塑性領域に近い値である。よってこれ以上締め付けボルトを引っ張る、もしくは径を削るのは難しいし、過度な締め付けはコイルにダメージを与える可能性もある。

そこで、初期締め付け力を増す代わりに、締め付けボルトのバネ定数を変えたときの安定性向上効果について検討した。つまり、ボルトを軟らかくして、コイルの収縮に合わせてボルトも縮み、コイル内に押さえ力を残す構造を考えた。

図 4.1 は締め付けボルトのバネ定数を小さくしたとき（Case2 のバネ定数を 1 とした）のファーストクエンチ電流の予測結果である。ボルトのバネ定数以外の条件は第 2 章と全く同じである。予測結果では、ボルトのバネ定数を現在

の 30%まで減らせば、トレーニング無く臨界電流まで励磁できる可能性が示されている。

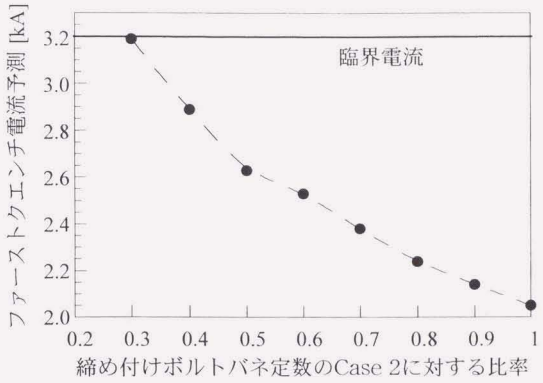

図 4.1　ファーストクエンチ電流の締め付けボルトバネ定数に対する依存性

具体的にバネ定数を減らす方法については、以下の通りである。

1) 締め付けボルトの断面積を減らす
2) 締め付けボルトの長さを長くする
3) ヤング率の低い材料の使用
4) さらばねの使用

1)は耐荷重の問題から Case2 以上に削ることは難しい。2)は、単純に 2 倍の長さのボルトを使えばバネ定数を半分にでき、有効な方法であるが、スペースが必要になる。3)は現在の SUS から、Ti 合金のような軟らかく降伏応力の高い材料に変えれば、ヤング率の分だけバネ定数を減らせる。SUS304 と Ti-5Al-2.5Sn の特性について表 4.1 にまとめた。4)は低温で十分な反力の出るさらばねを用いればよく、複数枚を直列に接続すればバネ定数をかなり減らせる。また自然とボルト長も長くなり、バネ定数低減効果が大きい。

表 4.1　SUS304 と Ti-5Al-2.5Sn の物性値比較

	SUS304	Ti-5Al-2.5Sn
降伏応力	400MPa	1.4GPa
ヤング率	205GPa	130GPa
収縮率 (300K to 4.2K)	2.65/1000	1.70/1000

注：コイルの収縮率は 3.30/1000 で、Ti 合金を使う場合は収縮率の相違に注意する必要がある。

よって 2),3),4)の複合により、バネ定数は容易に大幅に低減できる。例えば、Case2 と同径同長の Ti-5Al-2.5Sn ボルトを用いると、初期締め付け力は 12.0MPa から 10.8MPa に落ちるが（熱収縮率の違いより）、バネ定数は 63%になる。この時のファーストクエンチ予測は 2.35kA であった。さらにさらばねを入れてボルト長が 2 割ほどのびれば、長さの効果で合わせて 50%、さらばねの効果を入れれば 30%は不可能ではないと考えられる。

以上のように MAST の安定性は、コイルの大幅な改造をしなくても、締め付けボルトの交換によって安定性を大幅に向上させられる可能性があることが、クエンチ特性評価手法に基づいて示された。

4.2　発電機界磁巻線の最適設計に関する指針

発電機界磁巻線は、安定性についてはほぼ問題ない。ただし、今後の超伝導機の普及のためには、さらなる経済性の追求と、安定性を保ちつつ大容量化、高電流密度化することが必要不可欠である。本節では安定性と電流密度の関係について、クエンチ特性評価手法を用いて検討した結果について述べる。巻線の設計においては、導体銅比の選定がキーポイントとなる。一般に銅比は既存の安定性評価基準や設計製造者の経験、生じる交流損失等から決定されるが、機械的擾乱の発生抑制の観点から銅比選定の指針を探った。

導体の銅比を大きくすることは、導体の軟らかさが増して巻線押さえ力が加わったときに寸法不整を吸収し、接触押さえ力の不整を低減させる効果がある。しかしながら安定化材の増加は電流密度を低下させ、同じ磁界を発生させる場合に負荷率が大きくなる。これは逆にクエンチの可能性を増すことにもな

る。よってどこかにクエンチ確率を小さくし、電流密度を最大にとれる銅比が存在するはずである。

発電機界磁巻線の導体の素線の断面構造は図 3.2 に示すとおり、再外層にバリア用の CuNi 層があり、その内側に銅のみの層、さらにその内側に NbTi、CuNi、Cu の複合フィラメント領域がある。簡単のため、銅比の変更は銅層とフィラメント層の境界の半径を変えることにより実現させるものとした。このとき CuNi の量は変わらないと仮定した。ここで、Cu と CuNi を合わせた断面積(nonSc)の NbTi 断面積(Sc)との比(nonSc/Sc)を、便宜上銅比と呼ぶことにする。

図 4.2 は巻線の剛性を評価するための有限要素解析プログラム用の導体モデルである。モデルは 1/4 断面の素線と、導体を包むカプトンテープからなる。このモデルに図の上部から均一の押さえ力が加わったときの変形の様子を有限要素法により数値解析を行った。計算にはそれぞれの構成材の低温での圧縮変位特性を考慮した。コア部分とフィラメント領域は硬化により弾性変形するものとし、銅領域が塑性変形するとした。図 3.3 に示すように導体はスロット中に縦に配置されており、導体の縦方向に力が加わる。よって図 4.2 のモデルは 1 つの導体の 1/4.5 スケールとなる。ある力が加わったときのモデルの変形量を 4.5 倍すれば 1 導体の変形量であり、これを加わる力を変えて応力対変位の特性を計算した。さらに前述のように銅の量を変えて応力ひずみ特性を求めた。その結果を図 4.3 に示す。

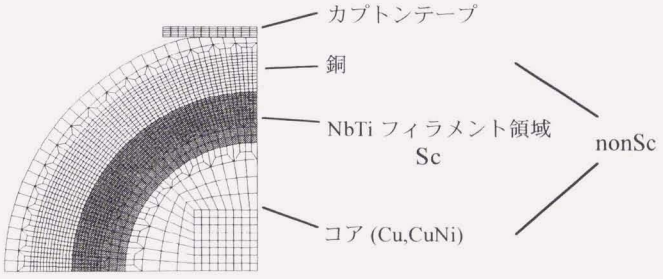

図 4.2　剛性評価用モデル（1/4 素線）

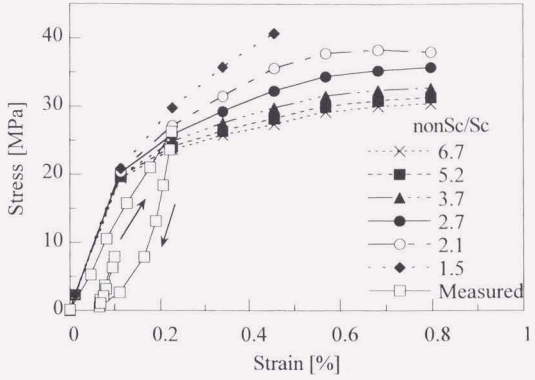

図 4.3　様々な銅比に対する巻線の圧縮変位特性

図 4.3 中の初期押さえ力近傍のグラフの傾きが、巻線のバネ定数κである。

図 4.3 に示すとおり、銅比が大きくなると塑性領域での傾きは小さくなり、押さえ力に対して変形が大きくなる。つまり寸法不整のある導体に対して押さえ力を加えたときに変形が進み、十分に接触押さえ力が各導体に加わることになる。逆に銅比が小さくなると傾きが大きく堅くなり、寸法不整が吸収されず、摩擦押さえ力に大きなばらつきが生じる。

図 4.3 には数値解析結果とともに、発電機界磁巻線と同じ導体を使って製作したモデルコイルの低温での圧縮歪み特性も示してある。モデルコイルの形状と測定装置を図 4.4 に示す。

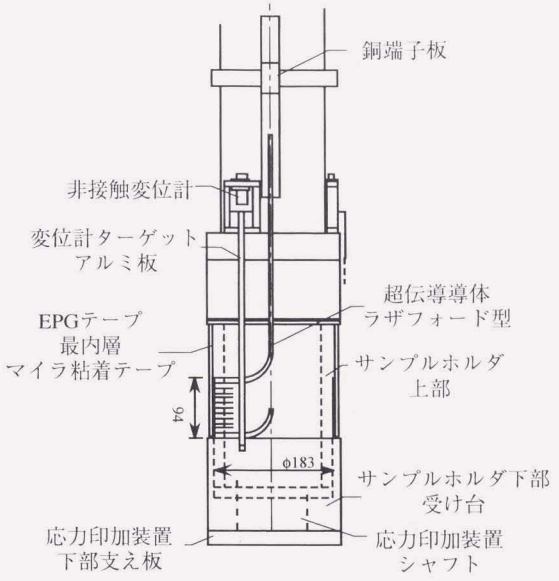

図 4.4　低温下での巻線応力歪み特性測定用モデルコイルと測定装置図

モデルコイルは FRP 製円筒ボビンにラザフォード型超伝導導体（発電機界磁巻線のものと同じ。銅比 2.7）を 1 層 11 ターン巻き付け、外周からバインドテープで保護してある。下部受け台はこのボビンとは独立に上下できる円筒形状で、中心を通る応力印加装置のシャフトにより受け台を持ち上げることでコイルに対して圧縮応力を与えることができる。応力はすべてコイルに集中する構造であり、受け台は変形しないものとすると、下部受け台に据え付けたアルミターゲットの変位から応力印加時のコイルの圧縮変形量を非接触変位計で測定することができる。

図 4.3 の通り、矢印のように応力を増加、減少させる過程でヒステリシスを描いた。これはボビンと下部受け台の円筒どうしの摩擦によるものと考えられる。低温、常温ともほぼ同じ特性で、傾きのヤング率は応力増加時で 6GPa であった。これはエポキシの低温でのヤング率に近い値である。また有限要素解析結果よりは軟らかい結果となった。これは素線の隙間の存在等が影響してい

るものと考えられる。また応力印加装置の性能と、コイルの過去の履歴から、塑性領域までは測定できなかった。

測定結果は、正確なコイル部分の変位とコイルにかかる応力を測定することが困難であることから、多分に誤差が含まれていると見るべきだが、有限要素解析の結果は測定結果に近い値であり、数値解析が実際のコイルの特性を再現できていると言える。3.2 節の発電機界磁巻線のクエンチ特性評価においては、この数値解析結果のデータを用いた。

界磁巻線の銅比を変えたときのファーストクエンチ電流予測の結果を図 4.5 に示す。横軸は銅比(nonSC/SC)で、縦軸は予測されたクエンチ電流である。同時に臨界電流も示してある。銅の量が大きくなると巻線の剛性が低下し、導体の動きによるクエンチ確率が減少し、クエンチ電流は増加する（図中破線)。ある銅比から、ファーストクエンチ電流が臨界電流に到達し、臨界電流までトレーニングクエンチを起こさなくなる。しかし銅比が大きすぎると、電流密度の低下により臨界電流が減少し（図中太線)、クエンチ電流は減少する。予測結果では銅比 nonSc/Sc=3.2 でクエンチ電流が最大になっている。このように、ファーストクエンチ電流を最大にする銅比を示すことができた。

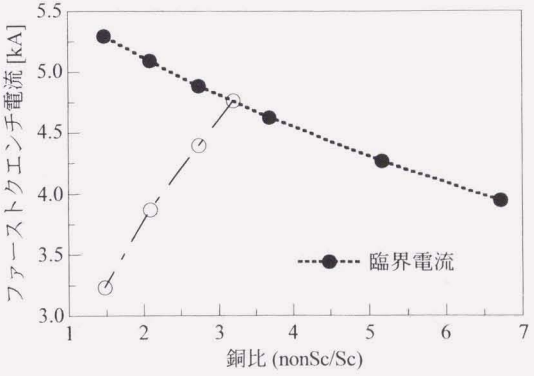

図 4.5　導体銅比に対するファーストクエンチ電流予測値

先にも述べたとおり、銅比の決定は様々な要因から決定されるが、機械的

擾乱の抑制の観点から最適銅比を選定できる設計のための指針が得られることは、設計上の大きなメリットである。

また銅比 3 前後でクエンチ電流を最大にできるという予測結果は、従来の設計製造者の経験則によく合致する。経験則を理論的に裏付けることができたことも、提案するクエンチ特性評価手法大きな成果の一つである。

4.3 超伝導発電機界磁巻線の高電流密度化と、回転・静止励磁における安定性の関係

7 万 kW 級機は 20 万 kW 級パイロット機の同径縮長で開発されたため、基本構造を変えずとも軸長を伸ばせば20万kW級機の製作は可能と考えられる。界磁巻線の直線部はその分伸びるため、前節や前章で論じた機械的擾乱によるクエンチ確率は高くなるが、それでも大幅なクエンチ電流の低下の心配はない。しかし、今後の現用機との競争のため、さらなる高電流密度化が課題であり、巻線電流密度の上昇に対する安定性評価が重要になってくると考えられる。今後開発が必要とされる技術課題として、具体的に界磁巻線の電流密度の 3 割向上が挙げられており[10]、この点について検討を行った。

巻線の構造を変えず、電流密度の向上を運転電流の上昇だけで行うことを考えると、定格電流が現行の 3kA から 3.9kA になる。さらに発電機は最大界磁電流として 1.2pu のマージンを持たせているため、少なくともファーストクエンチ電流は 4.7kA 以上でなければならない。図 4.5 の通り、現行の導体では臨界電流を上回り、課題はクリアできない。線材の設計のしなおしが必須である。

そこで、仮に臨界電流が現行の導体の 3 割増と 5 割増の導体が製造されたとして（それ以外の導体断面構造や剛性等は変わらないものとする）、それらの導体で 20 万 kW 級機の界磁巻線を製作したときのクエンチ電流の予測を行った。結果を図 4.6 に示す。現行の導体を Standard Case、臨界電流 3 割増を High Case I、5 割増を High Case II と表記してある。また現行の定格電流の 1.2pu を I_{max0}、3 割増を I_{max1} とする。

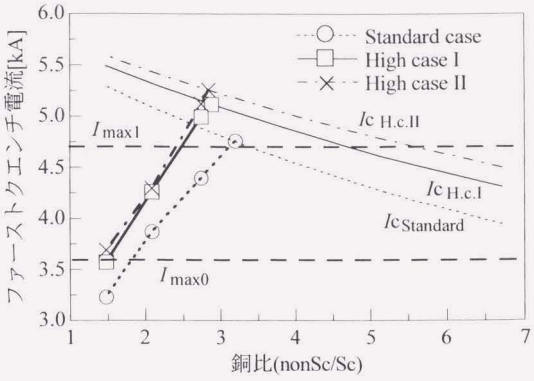

図 4.6　予想されるパイロット機のクエンチ特性予測

図 4.6 の通り、High Case I と II では大幅にクエンチ電流が向上し、銅比 2.9 付近で 5kA を越える通電が可能という数値解析結果が得られた。よってこのような導体の使用により、さらなる界磁巻線の高電流密度化が実現できるものと期待される。

次に、静止励磁試験と回転励磁試験における界磁巻線安定性の関係について述べる。ロータの製作の過程で静止励磁試験を行い界磁巻線の安定性評価を行うが、この段階で回転励磁時の安定性について理論的予測が可能であれば、回転励磁時に必要な巻線押さえ力を求めることができ、励磁試験において重要な情報となる。そこで、静止励磁時と回転励磁時のファーストクエンチ電流の巻線初期押さえ力に対する依存性をクエンチ特性評価手法により求めた。導体は先の臨界電流 3 割増の High Case I を想定した。予測結果を図 4.7 に示す。

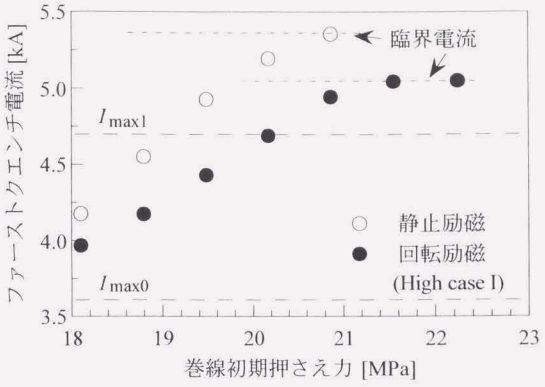

図 4.7　静止・回転励磁におけるファーストクエンチ電流の巻線初期押さえ力依存性

図 4.7 より、回転励磁において要求される界磁電流を満足するために必要な巻線初期押さえ力がわかるとともに、そのような初期押さえ力下で静止励磁試験を行った時のファーストクエンチ電流がわかる。これらの予測結果は巻線の励磁試験において大いに役立つ情報である。

4.4　クエンチ特性評価手法による安定性設計とコイル設計の手順

前章までのクエンチ特性評価手法により、超伝導コイルのクエンチ電流値を定量的に評価することが可能になった。また、安定性を向上させる方法、電流密度を向上させる方法といった、コイル設計方法についても情報が得られることを示してきた。

また以上より、クエンチ電流を支配する主要要因は、MML、導体の押さえ力の大きさと、その不整のばらつきの大きさであることがわかる。MML は導体の構造・構成・冷却条件に関わる量であり、導体の押さえ力とそのばらつきの大きさはコイルの構造・構成に関わる量であって、安定性の設計にあたってはこれらの量を、クエンチ電流が要求値を上回るように設計する必要がある。表 4.2 にはこれらの量を決める導体及びコイルの構造・構成の設計パラメータ

およびそれに関わる諸量を示してある。コイルの安定性設計にあたってはこれらの諸量に基づき設計パラメータを決めることになる。安定性設計の手順が図4.8 に示してある。コイルの形状・規模・磁界性能の要求条件に従って、コイル・導体の設計を行う。これに基づきクエンチ電流支配要因量を算出し、前章までで述べた手法に従いクエンチ電流を算出する。その結果が要求値を満たさなければ、導体／コイルの設計パラメータを変更する。一般に MML は導体の大幅な変更がなければあまり大きく変えられない。導体の押さえ力の増強、押さえ力の不整の抑制が安定性向上の効果が大きい。銅比を大きくすると導体の変形裕度が大きくなり、導体の押さえ力の不整を抑えるのに有効である。このような手順を踏むことにより、コイルのクエンチ電流が確実に要求性能（定格）を越えるような設計が可能になる。

表 4.2　安定性設計に関わる導体／コイル構造・構成に関わる諸量

支配要因量	導体／コイル設計パラメータ	導体／コイルの構造・構成諸量
MML	MQE	・冷媒熱伝達特性・冷媒温度，導体の熱伝導率 ・銅比／常電導転移時の抵抗 ・超電導体の J_c（運転時の磁界における） ・通電電流値
	導体の曲げ剛性	・導体形状（断面２次モーメント） ・導体のヤング率
導体の押さえ力	導体の摩擦力	・コイル押さえ力 ・導体にかかる電磁力，外力（遠心力等） ・導体間，導体／スペーサ間の摩擦係数
	導体固定構造	・巻線構造 ・プリストレス
導体の押さえ力の不整	導体（およびスペーサ）の寸法不整	・導体寸法公差管理
	コイル構造	・コイル形状，寸法，ターン数，層数等
	コイルのコンプライアンス	・コイル構造 ・導体のコンプライアンス（銅比，形状等） ・スペーサのコンプライアンス

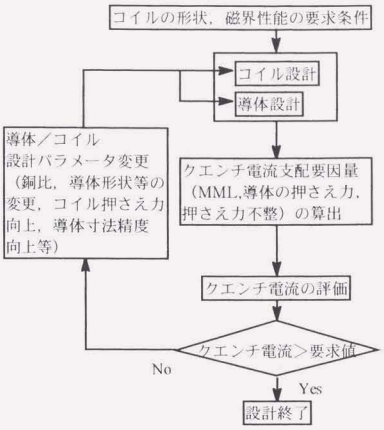

図 4.8　安定性設計の手順

結論

本論文では、低温大型高電流密度超伝導マグネットのトレーニングクエンチの主要原因である機械的擾乱に着目し、従来困難とされてきた擾乱の定量化と発生頻度の予測から、超伝導巻線の確率統計的トレーニング特性を予測する手法を提案した。また、手法を２つの異なるタイプの超伝導巻線に適用し、その特性予測が実際の励磁試験結果をよく説明できること、さらにその過程で安定性を向上させる方法や電流密度を向上させるための設計の指針、クエンチ電流が要求性能を越えるための設計法について情報が得られることを示した。

また、手法を構成する理論の実験的検証を行い、仮定や近似の妥当性の裏付けを行った。特に熱伝達特性は、実験を通して冷却の機構について多くの重要な知見を得ることができ、手法の枠を越えて活用できる。

今日多くの超伝導マグネットが製作されるようになり、製造経験の蓄積が極端に不安定なマグネットを少なくしているが、機械的擾乱以外にも、導体構造やコイル構造の複雑化から新たな電磁気的不安定性の問題が表面化してきており、本手法だけで安定性を論ずることはできなくなっている。しかし、未だに機械的擾乱は不安定性要因の筆頭であることに変わりはなく、安定性と高電流密度化を両立させる超伝導コイルの設計のための理論の確立が強く望まれる中、設計の段階でクエンチ特性の予測ができ、安定性設計に関する知見が得られる本手法は強力な武器になると考える。

謝辞

本研究の遂行にあたり、日頃からご指導、ご助言下さった、塚本修巳教授、大山力教授、雨宮尚之助教授、山岸一人助手、上智大学の高尾智明助教授、新潟大学の福井聡助教授に御礼申し上げます。

また、本研究に関連する論文の執筆に当たり、資料、データ、機材、実験環境の提供やご助言を下さった皆様方に、この場を借りて御礼申し上げます。

電子技術総合研究所　淵野修一郎様、玉田紀治様、石井格様、樋口登様、
岡野眞様、名取尚武様
電力中央研究所　鳥居慎治様、秋田調様
三菱電機株式会社　守田正夫様、下畑賢司様、前田進様、吉村秀人様
超電導発電関連機器材料技術研究組合　平尾俊樹様、渋谷正豊様
日本原子力研究所　吉田清様

本研究に関連する実験の補助や、ご助言を下さった塚本研究室の皆様に御礼申し上げます。

参考文献

[1] 「超電導マグネットの技術動向」、電気学会技術報告 No.309(199-10)

[2] 「わが国におけるマグネットの技術開発」、電気学会技術報告 No.664

[3] M.N.Wilson, "Superconducting magnets", Oxford University Press, 1983

[4] 山村昌、菅原昌敬、塚本修巳、山口貢、山本充義、「超電導工学」、電気学会、1991

[5] 高尾智明、「機械的擾乱に対する超伝導マグネットの安定性」、平成 3 年度博士論文、横浜国立大学

[6] N.Amemiya, T.Takao and O.Tsukamoto, "Disturbance characteristics and stability of high current density superconducting wires", *Fusion Engineering and Design 20*, pp.339-344, 1993

[7] 星谷勝, "確率論手法による振動解析", 鹿島出版, 1979

[8] Y.Iwasa, "Case Studies in Superconducting Magnets", Plenum, 1994

[9] A.Iwabuchi, H.Arai, Y.Yoshino, T.Shimizu, M.Sugimoto, K.Yoshida, T.Kashima and H.Inui, " Frictional Properties of Ceramics, MoS_2 Coated Films and Polyethylene Fibre Reinforced Plastics at 4.2K in Liquid Helium," Cryogenics, Vol. 35, No. 1, pp.35-40, 1995

[10] 渋谷正豊、平尾俊樹、長村英博、塩原亮一、前田進、宮池潔、「20 万 kW 級超伝導発電機の試設計と今後の課題」、平成 12 年電気学会全国大会講演論文集[5]、5-239

[11] 仁田旦三、「超電導発電機」、平成 10 年電気学会全国大会講演論文集[5]、S27-5

[12] 鈴木一市、前田進、中村嘉延、増永顕、中村史朗、小寺溢男、下畑賢司、米谷晴之、谷周一、田宮洋一、平尾俊樹、「7 万 kW 級高電流密度低速応型超電導発電機の研究開発」、平成 12 年電気学会全国大会講演論文集[5]、5-237

[13] T. Takao, D. Yoshino, T. Kubosaka, N. Momma, I. Nitta, A. Iwabuchi and F. Odajima, "Influence of Surface Roughness and Precooling by Liquid Nitrogen on Frictional Coefficients at Liquid Helium Temperature", Proceedings of the Seventeenth International Cryogenic Engineering Conference, Institute of Physics

Publishing, pp.299-302,1998

[14] R. Nakajima, K. Sato, K. Miyake, M. Kumagai and Y. Kobayashi, "Liquid and Supercritical Helium Heat Transfer of Horizontal Upward Facing Surfaces under High Centrifugal Acceleration Fields", ASME HTD-Vol.229, Heat Transfer in Superconducting Equipment, Book No. G00721 (1992), pp.39-44.

[15] O.Tsukamoto, M.Furuse, T.Takao, N.Tamada ,S.Fuchino, I.Ishii and N.Higuchi, "Transient Heat Transfer Characteristics of Liquid Helium in Centrifugal Acceleration Field", Advances in Cryogenic Engineering, Vol.43B, Plenum Press, pp.1489-1496, 1998

本論文に関連する発表論文

論文発表

[1] T.Takao, O.Tsukamoto, M.Furuse and K.Tsuchiya, "Statistical Estimation of Quench Characteristics of Quadrupole Magnets", IEEE Trans. on Appl. Super., Vol 7, No.2, pp.183-186, 1997

[2] O.Tsukamoto, M.Furuse, T.Takao, N.Tamada, S.Fuchino, I.Ishii and N.Higuchi, "Transient Heat Transfer Characteristics of Liquid Helium in Centrifugal Acceleration Field", Advances in Cryogenic Engineering, Vol.43B, Plenum Press, pp.1489-1496, 1998

(CEC/ICMC'99 Russell B.Scott Award, Honorable Mention, Research Paper 受賞)

[3] O.Tsukamoto, M.Furuse, T.Takao, M.Morita, S.Maeda and T.Hirao, "Designing Stable and High-Current Density Rotor Windings of Superconducting Generator", IEEE Trans. on Appl. Super., Vol 9, No.2, pp.244-247, 1999

[4] M.Furuse, O.Tsukamoto, T.Takao, S.Fuchino, I.Ishii, M.Okano and N.Tamada, "Transient Heat Transfer Characteristics of Supercritical Helium in High Centrifugal Acceleration Field", Advances in Cryogenic Engineering Vol.45, pp.1151-1158, 2000

[5] M.Furuse, O.Tsukamoto, T.Takao and K.Yoshida, "Analytical Estimation of Quench Current of Large Bore Superconducting Magnet", IEEE Trans. on Appl. Super. Vol. 10, No.1, pp.653-656, 2000

[-] M.Furuse, O.Tsukamoto, S.Torii, S.Akita and M.Shibuya, "Study on Designing High Current Density Rotor Windings of Superconducting Generator and Relation of the Stabilities in Static and Rotating Conditions", presented at ASC2000, IEEE Trans. on Appl. Super.掲載予定

国際会議プロシーディング

[6] S.Fuchino, I.Ishii, N.Tamada, O.Tsukamoto, M.Furuse and T.Takao, "Transient Heat Transfer of Liquid Helium in Rotating Machines", Proceedings of Fifteen International Conference on Magnet Technology, Part 1, Science Press, pp.526-529, 1998

[7] O.Tsukamoto, M.Furuse, T.Takao, M.Morita and T.Hirao, "A Method to Estimate Stability of Rotor Windings of Superconducting Generator in Rotating Condition", Proceedings of Fifteen International Conference on Magnet Technology, Part 1, Science Press, pp.522-525, 1998

口頭発表

[8] 古瀬充穂、塚本修巳、高尾智明、玉田紀治、淵野修一郎 ; "回転場における液体ヘリウムの過渡熱伝達特性", 電気学会超電導応用電力機器・回転機合同研究会, 1996

[9] 古瀬充穂、塚本修巳、高尾智明、玉田紀治、淵野修一郎 ; "回転場における液体ヘリウムの過渡熱伝達特性", 1996 年度秋季低温工学超電導学会, 1996

[10] 塚本修巳、古瀬充穂、高尾智明、守田正夫、平尾俊樹 ; "超電導発電機界磁巻線の安定性評価に関する手法", 電気学会超電導応用電力機器・リニアドライブ合同研究会, 1998

[11] 古瀬充穂、塚本修巳、高尾智明、淵野修一郎、玉田紀治、岡野眞、名取尚武、石井格 ; "遠心力場における超臨界圧ヘリウムの過渡熱伝達特性", 1999 年度春季低温工学超電導学会, 1999

[12] 古瀬充穂、塚本修巳、高尾智明、吉田清 ; "大口径マグネットのクエンチ特性評価と安定性向上法", 1999 年度秋季低温工学超電導学会, 1999

[13] 古瀬充穂、塚本修巳 ; "超伝導発電機界磁巻線の高電流密度化と安定性設計", 電気学会超電導応用電力機器・リニアドライブ合同研究会, 2000

Statistical Estimation of Quench Characteristics of Quadrupole Magnets

Tomoaki Takao
Faculty of Science and Technology, Sophia University, Tokyo, Japan

Osami Tsukamoto and Mitsuho Furuse
Faculty of Engineering, Yokohama National University, Yokohama, Japan

Kiyosumi Tsuchiya
National Laboratory for High Energy Physics, Tsukuba, Japan

Abstract—Quench tests of 9 quadrupole magnets for TRISTAN accelerator were performed at National Laboratory for High Energy Physics (KEK). Those magnets, with same specifications, had different training characteristics. Each magnet has 4 coils of the same winding configuration connected in series, and, in total, quench behaviors of 36 coils of the same configuration were obtained. Quenches were considered to be caused by conductor motions. In the paper, we explain the training behavior of the coils based on our previously derived theory which statistically estimates expected number of quenches for the magnet current to reach a certain value. The theoretically estimated results are compared with the experimental results and the validity of our theory is discussed. It is also shown that the theory is useful to design stable and high-current density magnets.

I. Introduction

To estimate the stability of a superconducting magnet, it is common to experimentally or theoretically evaluate minimum quench energies (MQEs) of the magnet conductor. However, there is not enough knowledge about how much the MQE values should be to obtain a stable magnet, because it is hard to estimate the size of disturbances occurring to the magnet conductor. It is widely known that main disturbances causing quenches are abrupt conductor motions. A minute conductor motion of $1 \sim 2\ \mu$m has enough energy to cause a quench of a high-current density conductor. Therefore, it is considered that quantitative estimation of the disturbance energy is difficult.

We derive a theory which statistically estimates sizes of disturbances due to conductor motions and training characteristics[1]–[3]. In the theory, it is assumed that supporting force of the magnet conductor fluctuates because of irregularity in conductor dimensions and electric insulator thicknesses and that a conductor motion occurs where the supporting force is exceeded by the electromagnetic force to the conductor. The number of places along the conductors where conductor motions causing quenches occur can be statistically estimated by assuming that the irregularities in the conductor dimensions and the insulator thicknesses follow gaussian distributions. Therefore, the expected number of quenches of the quadrupole magnets can be estimated by the calculation. The theory takes not only mechanical properties of the conductors but also electromagnetic and mechanical forces applied to the conductors into consideration. We already applied the theory to explain the experimental results to study on the relation between copper-to-superconductor ratio in SSC prototype conductors and the training characteristics[1]. The theory was also applied to the field windings of the model rotor of the superconducting generator[2], [3]. The results, estimated based on the theory, reasonably agreed with the experimental results.

In this paper, we try to apply our theory to the results of the quench tests of 9 quadrupole magnets for the TRISTAN electron-positron collider at KEK[4], [5]. Each of the quadrupole magnets has 4 coils of the same configuration, and, therefore, 36 coils of the same configuration in total were tested. Experimental results are therefore statistically significant.

II. Training Characteristics of 9 Quadrupole Magnets

A cross-sectional view and specifications of the quadrupole magnet are shown in Fig. 1 and Table I. Each of the 4 coils of the quadrupole magnet has pancakes of 24, 27, 37, and 41 turns in the order from innermost layer, and copper wedges are inserted between the turns in the inner doublepancakes. The 4 coils are connected in series. The conductor of the coils is the Rutherford type

TABLE I
SPECIFICATIONS OF QUADRUPOLE MAGNET

Length	1,450 mm
No. of coils	4 coils
No. of layers	4 layer/coil
Inner diameter	140 mm
Outer diameter	218 mm
Nominal current	3,405 A
Maximum field	6 T at 3,405 A
Collar	SUS316LN

Manuscript received August 27, 1996.

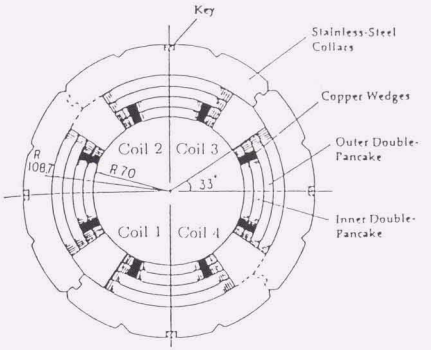

Fig. 1. Cross-section perpendicular to center axis of quadrupole magnet.

TABLE II
SPECIFICATIONS OF CONDUCTOR AND STRAND

Conductor	Rutherford type conductor
Height	3.09 mm
Small width	1.19 mm
Large width	1.35 mm
No. of stands	27 strands
Critical current	more than 9,500 A at 5T
Insulation	Kapton tape
Strand	
Material	NbTi and Cu
Cu ratio	1.8
Diameter	0.683 mm

conductor (made of 27 strands) having about 1 degree of keystone angle. The specifications of the conductor and the strand are listed in Table II.

In the test, each the magnet was excited up to 4000 A at the rate of 10 A/sec. The quench-training characteristics were observed. Quenches were caused by frictional heating caused by conductor motions. Because burst signals from the AE sensors on the magnet were detected with simultaneous spike signals in the terminal voltage of the magnet just before a quench[4]. About 80 % of the total quench events in the 9 magnets occurred in the inner pancake of the coil, therefore, we focused our attention on the inner pancakes in the analysis. The training curves in the inner pancakes of the coils of the 9 quadrupole magnets are shown in Fig. 2. The magnet conductor current is limited to 4000 A because of the capacity of the power supply. The current marked by "o" in Fig. 2 is the supply limit, 4000 A. As shown in the figure, training-quench behaviors of the nine magnets were different, through the magnets were based on the same design.

III. Theoretical Analysis

Fig. 3 (a) and (b) show the cross-sections of the winding of a coil (half of the coil) and the corresponding analytical model of the winding. The coils were wound of the Rutherford type conductors wrapped with Kapton tapes coated with semi-cured epoxy resin and cured after the winding. The conductors were fixed by the adhesive force between the epoxy and conductor. However, the adhesive force was easily exceeded by the electromagnetic force and the conductors were supported mainly by frictional force. The frictional supporting forces of the conductors are given by the compressive force applied to the conductor surface by collars. Even if the fixing force by the collars and the electromagnetic force applied to the conductors are uniform, the supporting force along the conductor fluctuates due to the irregularities in the conductor dimensions and the thickness of the Kapton tape. The irregularities in the dimensions can be numerically calculated, assuming that the irregularities in dimensions follow the random gaussian process and knowing the standard deviation of the irregularity. In the analysis, we assume that copper surface layers of the conductor strands and the Kapton tapes are deformed by the compressive force applied by the collars, because the stiffnesses of Cu and Kapton are much lower than the stainless steel collar. The procedure to calculate the fluctuations in the conduc-

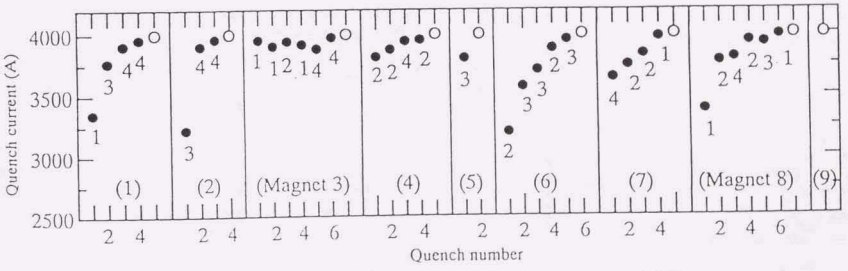

Fig. 2. Training characteristics of the nine quadrupole magnets at KEK. (The numerals in the figure show which coil initiated the quenches.)

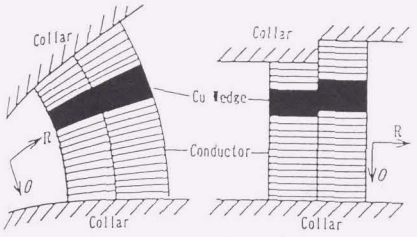

(a) Part of magnet. (b) Analytical model.

Fig. 3. Schematic illustrations of analytical model.

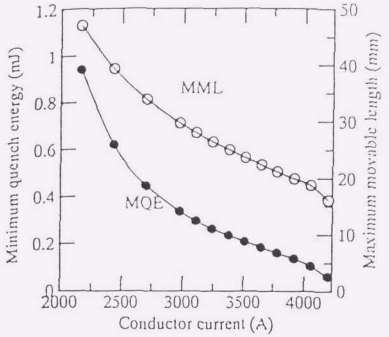

Fig. 4. Estimated MQE and MML.

tor supporting force are described in detail in [2]. Based on the calculated fluctuations, we can statistically determine the length of the poorly supported part along the conductor where the magnetic force exceeds the frictional supporting force. If disturbance energy, released by the conductor motion at the poorly supported part, is larger than MQE of the conductor, the conductor quenches. The relation between the length of the moving part of the conductor and the size of disturbance energy can be calculated by our theory taking account of magnetic field, conductor's Young's modulus and the geometrical moment of inertia of the conductor[7]–[9]. The length of the moving part releasing disturbance energy equal to the strand's MQE is the maximum movable length (MML)[7], [8]. If the length of the poorly supporting part of the conductor is longer than MML, the moving part is a potential source of a quench. A quench of a stranded conductor such as the Rutherford type conductor is most probably initiated by a quench caused by a strand motion. Therefore, it is necessary to calculate the MQE of the single strand. In the calculation of the strand's MQE the spatial length and duration time of the frictional heating due to the disturbance are assumed to be 1 mm and 500 μsec, and transient heat transfer characteristics of liquid helium are taken into account. The details of the calculation of MQE and MML are described in [6] and [7], [8], respectively. The calculated MQE and MML of the strand of the conductor whose specifications are listed in Table II are shown in Fig. 4.

IV. Comparison of Theoretical Analysis and Experimental Results

In the theoretical analysis, we assume that the diameters of the strands have irregularities following the Gaussian distribution with the standard deviation of $3\sigma = 18 \sim 20$ μm and that the frictional coefficient at the interfaces between the strands and Kapton tapes is $\mu = 0.3 \sim 0.9$. We assume that value of 3σ, because the allowance of the strand diameter is $\pm 20\mu$m (design value).

Fig. 5 shows the average training characteristics of the 9 magnets and the theoretically estimated quench characteristics. In Fig. 5, the tested quench currents of the 9 magnets at nth quench are averaged and the value is plotted at the nth quench event and the theoretical results are for $3\sigma = 18$ μm and $\mu = 0.9$.

In the quench test, the quenched coil was identified at each quench event of the magnet as is shown in Fig. 2. We can assume that each of the 4 coils of the quadrupole magnet, therefore, 36 coils in total had independent training characteristics. From Fig. 2, we can count the total number (m_{1st}) of the coils, whose first quench currents were less than a certain given value I_{q0}. m_{1st} vs. I_{q0} are plotted in Fig. 6 (a). In the figure, the left side vertical axis is the accumulated probability of quenches ($m_{1st}/36$) and the right side vertical axis is the total number of quenched coils (m_{1st}). For example, in Fig. 6 (a) the total number of quenched coils is 5 and the accumulated probability is 14 % at $I_{q0} = 3600$ A (see the experimental curve), which means that 5 coils out of 36 coils (14 % of the all coils) had the initial quench currents less than 3600 A. Theoretically calculated values of the accumulated probability of

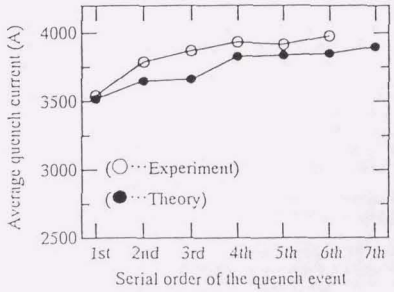

Fig. 5. Theoretical and experimental training characteristics of magnets.

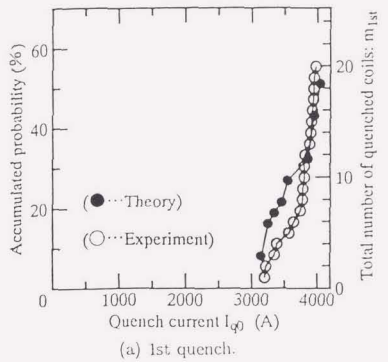

(a) 1st quench.

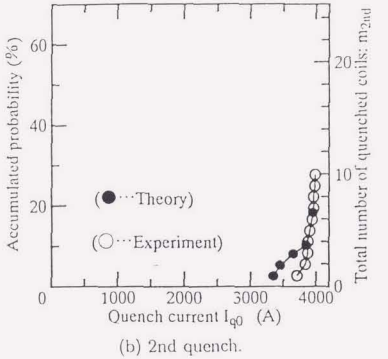

(b) 2nd quench.

Fig. 6. Total number of quenched coils and accumulated probability of quench vs. I_{q0} for the first and second quenches.

quenches based on the above theory are also plotted (for $3\sigma = 18\mu$m and $\mu = 0.9$) in Fig. 6 (a). Experimental and theoretical results for the case of the second quench are also plotted in Fig. 6 (b). m_{2nd} is the total number of the coils whose 2nd quench currents were less than I_{q0}. From both Figs. 5 and 6, agreement of the theoretical and the experimental results is reasonably good.

To increase stability of the magnet and to decrease the number of training quenches to reach to a design current, it is effective to decrease the standard deviation σ of the irregularities in the dimensions of magnet conductors. Expected numbers of the training quenches for one of the coils to reach to the nominal value of 3405 A are also calculated for various values of 3σ based on the theory described above assuming that clamping force to the conductor is constant and they are plotted in Fig. 7. From the figure, the number of training quenches is effectively decreased with decreasing of σ.

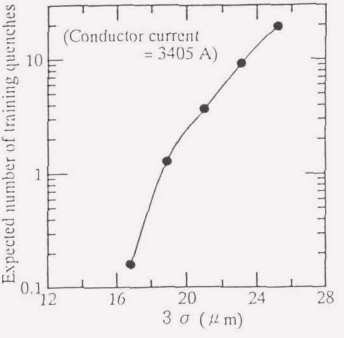

Fig. 7. Influence of number of training quenches on 3σ.

V. Concluding Remarks

We statistically analyzed the quench characteristics of the quadrupole magnets for TRISTAN collider based on our previously derived theory. The theoretical data agreed reasonably well with the experimental results and the validity of our theory was confirmed.

Magnet designer can use the theory to optimize the conductor and winding configurations for the given expected number of quenches.

References

[1] T. Takao, P. C. Michael, O. Tsukamoto, "Influence of copper-to-superconductor ratio on the stability of high current density superconductor," *IEEE Trans. on Magn.*, vol. 30, No. 4, Part II, pp. 2439-2442, 1994.

[2] T. Takao, K. Iwasaki, O. Tsukamoto, "Statistical estimation of disturbance energy due to conductor motion in rotor windings of superconducting generator," *IEEE Trans. on Appl. Super.*, vol. 5, No. 2, pp. 361-364, 1995.

[3] T. Takao, et al., "Quench characteristics of rotor winding of superconducting generator in static and rotating conditions" *IEEE Trans. on Magn.*, vol. 32, No. 4, pp. 2365-2368, 1996.

[4] T. Ogitsu, K. Tsuchiya, A. Devred, "Investigation of wire motion in superconducting magnets," *IEEE Trans. on Magn.*, vol. 27, No. 2, pp. 2132-2135, 1991.

[5] K. Tsuchiya, K. Egawa, K. Endo, N. Ohuchi, A. Terashima, Y. Morita, "Superconducting quadrupole magnets for TRISTAN mini-beta insertions," *Cryogenic Engineering*, vol. 28, No. 4, pp. 199-208, 1993. (in Japanese)

[6] N. Amemiya, T. Takao, O. Tsukamoto, "Disturbance characteristics and stability of high current density superconducting wires," *Fusion Engineering Design*, vol. 20, pp. 339-344, 1993.

[7] T. Takao, O. Tsukamoto and S. Honjo, "Probability of premature quenches due to conductor motion in superconducting windings," *Cryogenics*, vol. 31, pp. 504-509, 1991.

[8] O. Tsukamoto, "Disturbance due to conductor motion and stability of large-scale superconductors," *Fusion Engineering Design*, vol. 20, pp. 327-332, 1993.

[9] T. Takao et al., "Study on fluctuations in supporting force of conductors caused by fluctuations in conductor dimensions." *IEEE Trans. on Appl. Super.*, vol. 3, No. 1, Part II, pp. 484-487, 1993.

TRANSIENT HEAT TRANSFER CHARACTERISTICS OF LIQUID HELIUM IN CENTRIFUGAL ACCELERATION FIELD

O.Tsukamoto,[1] M.Furuse,[1] T.Takao,[2]
N.Tamada,[3] S.Fuchino,[3] I.Ishii,[3] N.Higuchi[3]

[1]Yokohama National University
Yokohmana, Kanagawa, 240, Japan
[2]Sophia University
Chiyodaku, Tokyo, 102, Japan
[3]Electrotechnical Laboratory
Tsukuba, Ibaraki, 305, Japan

ABSTRACT

Transient heat transfer of liquid state helium in centrifugal acceleration fields up to 1300G have been investigated for studying the stability characteristics of the rotor field windings of a superconducting generator. In the experiment, temperature resistive platinum-0.5% cobalt (Pt-Co) thin wire was used as the temperature sensor and heater to measure the heat transfer characteristics. The thermal mass of the Pt-Co wire was small enough to observe the temperature fluctuation due to bubbling in the boiling heat transfer. In this paper, influence of the centrifugal acceleration on the transient heat transfer and its mechanism are discussed based on the experimental results. It was observed that, for step heating with heat flux higher than maximumheat flux at steady state nucleate boiling, quasi-nucleate boiling appeared also in centrifugal acceleration field at the beginningof the heating, and that duration of the quasi-nucleate boiling was not much dependent on the acceleration field for relative high heat flux. This phenomenon was explained by bubble formation process in the boiling heat transfer. In this study, a high speed video camera was used to observe the relation of the bubble formation process and the temperature fluctuation of the Pt-Co wire in the normal gravity.

INTRODUCTION

One of the most important issues for designing the rotor field windings of a superconducting generator is estimation of the stability. A major cause of an unexpected quench of the superconducting windings is disturbance due to an abrupt wire movement.

Advances in Cryogenic Engineering, Vol. 43
Edited by P. Kittel, Plenum Press, New York, 1998

Duration time of such a disturbance is very short, less than 1 msec. The cryogenic helium coolant of the rotor windings is subject to high centrifugal acceleration field. Therefore, for the stability analysis, transient heat transfer characteristics of helium coolant in high centrifugal acceleration field should be studied. Significant amount of data on steady state heat transfer of the cryogenic helium in centrifugal acceleration field have been accumulated [1,2], but there is a little knowledge on the transient characteristics. To measure the transient heat transfer characteristics, a quick-response temperature sensor is necessary and we used thin Pt-Co wire of 20μm diameter as the temperature sensor and heater. In the experiment, the measurement sample with the Pt-Co wire was placed in a rotating cryostat and the transient heat transfer to the helium coolant in the centrifugal acceleration up to 1300G was investigated by putting a step current to the Pt-Co wire. In the range of the experiment, the helium stayed in liquid state.

It is known for the saturated liquid helium in normal gravity (1G) that just after the step heating with heat flux higher than maximum steady state heat flux in the nucleate boiling region, vapor bubbles begin to appear around the heating surface, while the temperature rise of the heating surface is kept low as in the nucleate boiling region in the steady state boiling. This quasi-nucleate boiling is followed by transition to the film boiling where the heating surface temperature rises rapidly.[3,4] It is also known that in the nucleate boiling region thin liquid helium layer appears underneath the bubble as is shown in Figure 1(a) and that, once a bubble starts to be formed, liquid is not supplied to the thin layer till the bubble departs. Helium vapor is supplied to the bubble from this thin liquid layer and the surface temperature rise is kept low because the surface is cooled by the latent heat of the evaporation of the thin layer.[5] When the heat flux is large, the liquid in the thin layer is consumed until the bubble departs from the surface (this is the quasi-nucleate boiling region). Then, the heating surface is covered with vapor and the film boiling takes place (Figure 1(b)). In the film boiling, the heat transfer to the liquid helium is deteriorated because of the vapor layer. The vapor layer grows to bubbles and the bubbles are departed from the heating surface by their buoyancy. The buoyancy of the bubble is very large in the high centrifugal acceleration field. Therefore, bubbles depart from the heating surface more frequently and higher heat transfer flux is obtained in the higher centrifugal field. As is understood from above discussions, the heat transfer is dependent on the bubbling process affected by the centrifugal acceleration.

The Pt-Co wire in our experiment could detect temperature fluctuations due to bubbling in boiling heat transfer. In our study, high speed video pictures of the bubbling process around the wire synchronized with time trace of the temperature fluctuation of the wire were taken in normal gravity (1G). Based on these results, we studied the relation of the transient heat transfer characteristics and the bubble growing and departure processes in the high centrifugal acceleration field.

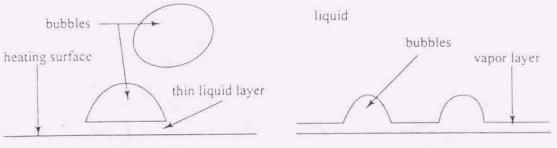

(a) nucleate boiling region (b) film boiling region

Figure 1. Vapor bubble formation in boiling heat transfer.

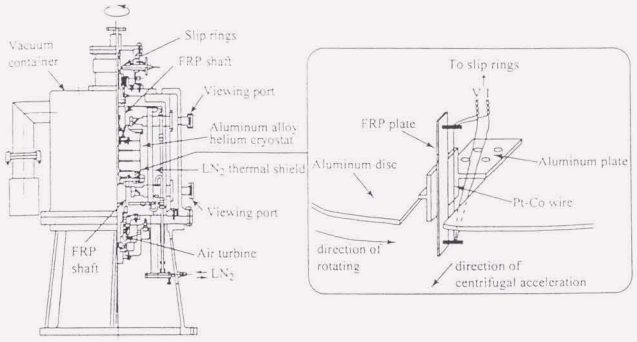

(a) rotating cryostat (b) arrangement of measurement sample

Figure 2. Cut-away view of rotational cryostat and schematic drawing of the measurement sample.

EXPERIMENTAL ARRANGEMENT

Heat Transfer Measurement in Centrifugal Acceleration Field

The experimental arrangement is shown in Figure 2. A heat transfer measurement sample with a Pt-Co wire of 20μm diameter and 48mm length (Figure 2(b)) was placed in the rotating cryostat illustrated in Figure 2(a). Details of the rotating cryostat are explained in the reference[6].

The temperature-resistance characteristic of the Pt-Co wire is shown in Figure 3. The thermal time constant of the wire was estimated as $\tau = (a^2c)/4\lambda$, where a is the radius and c the heat capacity ($\sim 9\times10^4 J/m^3K$) of the wire. The thermal conductivity of the wire was estimated as λ=~11W/mK from its electrical resistivity and the Wiedman-Franz relation. The estimated value of τ is 6×10^{-8}sec at 4.2K and 2×10^{-7}sec at 10K. The temperature was determined from the resistance of the wire measured by four terminal method and Figure 3. The response of Pt-Co wire was quick enough for the purpose of our experiment. However, the temperature resistivity of the Pt-Co wire is not so good as a carbon resistor and semiconductor resistor which are usually used in the heat transfer measurement in liquid helium.

A step current of $I(t)$ was applied to the Pt-Co wire and the transient wave form of the voltage $V(t)$ between the voltage tap on the wire was recorded by a transient recorder together with the current wave form. The surface heat flux $q(t)$ was calculated as $q(t)=I\cdot V/S$ where S is the surface area of the wire between the voltage taps. The Pt-Co wire was so thin that we could assume that the wire surface temperature was same as the wire temperature. During the step heating, the current was kept constant. $V(t)$ changed due to the temperature change of the wire, therefore, $q(t)$ changed. Our main concern is on the transient heat transfer characteristics for a few msec after the step heating and in this time range, we assumed $q(t)$ did not change. We call $q(t)$ at the beginning of the heating the initial heat flux. Data were taken by changing the rotational speed of the cryostat from 0rpm(1G) to 3600rpm(1300G). By monitoring the liquid helium level, the pressure of the helium

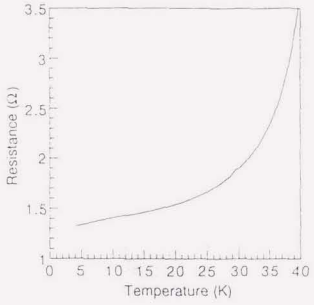

Figure 3. Temperature-resistance characteristic of the Pt-Co wire.

around the Pt-Co wire was calculated. In the experiment, the maximum pressure of the helium was 1.5×10^5Pa at 3600rpm and the helium was in the liquid state.

Observation of Bubble Formation by High Speed Video

We observed the bubble formation around the Pt-Co wire in liquid helium of normal gravity by a high speed video camera (frame speed was 9000 frames/sec) and measured the transient heat transfer characteristics at the same time. A measurement sample arrangement similar to that shown in Figure 2(b) was used in this experiment.

EXPERIMENTAL RESULTS

Bubble Formation Process and Heat Transfer Characteristics in Normal Gravity

Figure 4 shows time trace of the temperature of the Pt-Co wire and high speed video pictures of the vapor bubbles around the wire, where initial heat flux q_0=35kW/m^2 and the gravity is 1G. The pictures (1)~(8) in Figure 4(a) show the bubbles at the times denoted by (1)~(8) in the temperature time trace shown in Figure 4(b).

There is a remarkable overshoot in the temperature trace at (2) in Figure 4(b), which is followed by a temperature dip at (3) and (4). At (2), the wire is covered by vapor sheath and heat transfer to the liquid helium is deteriorated because of the vapor sheath. After that, the vapor sheath swells and starts to undulate and be divided into bubbles, while convection of the vapor around the wire begins and the wire temperature goes down. When these bubbles depart from the wire, liquid helium around the wire is replenished and the wire is cooled well having the temperature dip around at (3) and (4). After these relatively large initial bubbles depart from the wire, relatively small vapor bubbles are formed and depart. The cycle of this formation and departure of the bubble is repeated as shown in Figure 4(a)(6)~(8). Obviously from Figure 4(b), there is cyclic fluctuation of the wire temperature between (6) and (8) coinciding with the cycle of the bubble formation and departure. About 100msec after the start of the step heating, the steady state film boiling is established.

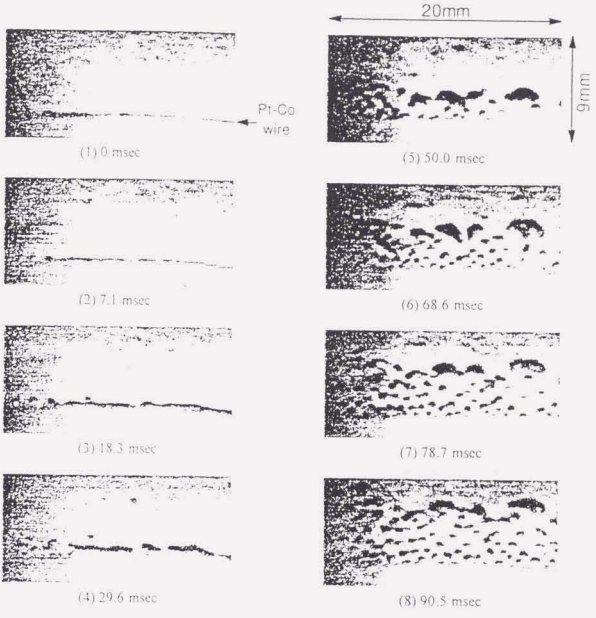

(a) high speed video pictures of bubbles around the Pt-Co wire

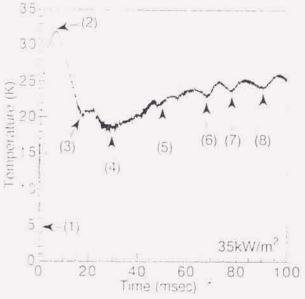

(b) temperature traces of the Pt-Co wire

Figure 4 High speed video pictures and temperature trace of the Pt-Co wire for step heating of $q_w = 35 kW/m^2$. The step heating started at $t = 0$.

Figure 5 shows temperature traces of the Pt-Co wire for step heating of 25kW/m^2~42kW/m^2 in various centrifugal acceleration field together with the case of 1G. The quasi-nucleate boiling was obviously observed also in the centrifugal field. Based on the results shown in Figure 5, specific characteristics of the transient heat transfer in the centrifugal field are summarized as follows.

1. In the range of the experiment, there are three modes in the heat transfer characteristics in the centrifugal field;

(i) steady state in the nucleate boiling region (Figure 5(a)).

(ii) gradual transition from the nucleate to the film boiling regions (Figure 5(b)and(c)).

(iii) take off from the quasi-nucleate boiling to the film boiling regions (Figure 5(c)~(e)).

whereas, there is one mode for the case of 1G, where taking off from the quasi-nucleate boiling to the film boiling. Occurrence of the mode depends on the value of G and $q(t)$. It is considered that, in the mode(ii), local nucleate boiling regions and local film boiling regions coexist and that the film boiling regions gradually overwhelm the nucleate regions.

2. Take-off time is plotted against the heat flux for various values of G in Figure 6. The take-off time is defined as the time from the start of the step heating to the time when the wire temperature takes off due to the transition to film boiling. Obviously from the figure, when the quasi-nucleate boiling appears, the take-off time is not dependent on the value of G and data can be fitted to the line $q_0=2.6\times10^4 t^{-0.25}$, where q_0 is the initial heat flux. This can be explained as follows, by assuming that the thickness of thin liquid layer underneath the vapor bubble (Figure 1(a)) is not affected by the value of G. When the thin liquid layer is consumed before the initial bubbles depart, the wire temperature takes off and the film boiling begins. The time to consume the thin liquid layer, that is the take-off time, is not dependent on the value of G because the thin liquid layer thickness does not depend on the value of G. When the vapor bubbles depart from the wire before the thin liquid layer is consumed, the nucleate boiling continues. In the high centrifugal field, the bubbles depart earlier than in normal gravity because of larger buoyancy of the bubble, and nucleate boiling is sustained in higher heat flux.

3. In the case of the mode (iii), the steady state film boiling is established in less than 1msec for the centrifugal field higher than 400G, which is much faster than the case for 1G.

4. In the steady state film boiling region, there were cyclic fluctuations in the wire temperature. These fluctuations are supposed to be caused by cyclic departure of vapor bubbles as was observed by the video camera in the normal gravity experiment. Average values of the cycle times of the fluctuations were not much dependent on $q(t)$ and are plotted against G in Figure 7. The average cycle time is dependent on $G^{-1/3}$. This dependence on $G^{-1/3}$ was also observed by a direct optical observation of the cyclic bubble departure time in other experiment conducted by using a flat heating surface.[5]

5. A temperature overshoot as was observed in the case of 1G was not observed at the beginning of the step heat in the centrifugal field except in relative low value of G (100G). The reason for this is considered as follows. In the high centrifugal field, the buoyancy of the bubble is much higher than that in 1G, therefore, convections of the liquid and vapor around the wire are established much faster and the initial bubbles depart from the wire before growing big. Without the big initial bubbles accompanying temperature overshoot, the film boiling reaches steady state right after the take-off in high centrifugal field. This supports the result described in the specific characteristic 3.

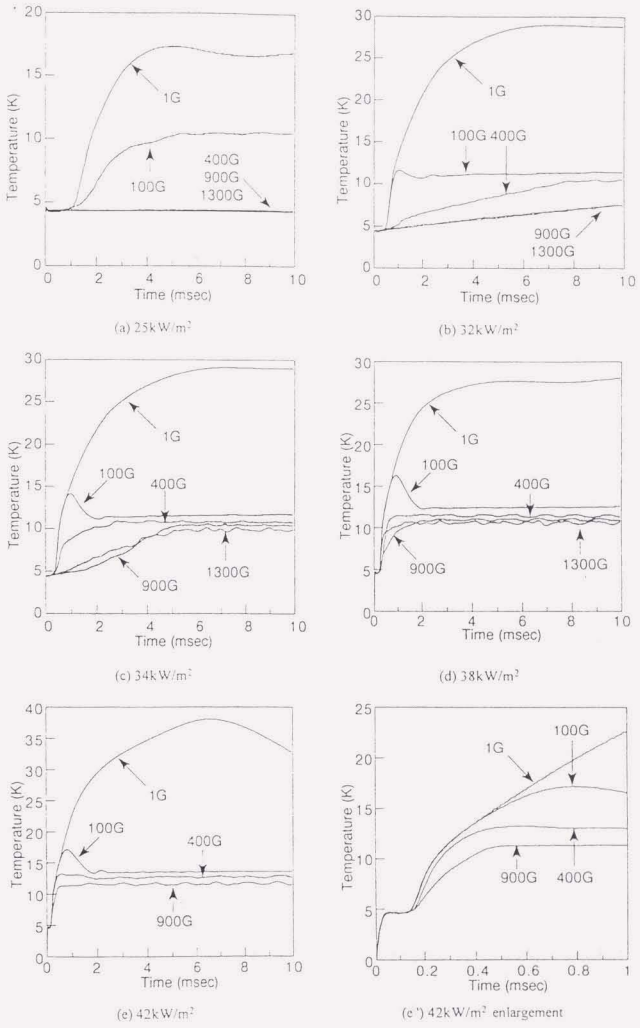

Figure 5. Transient traces of the Pt-Co wire for step heating in centrifugal field.

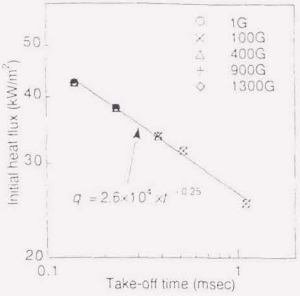

Figure 6. The relation between initial heat flux and take-off time

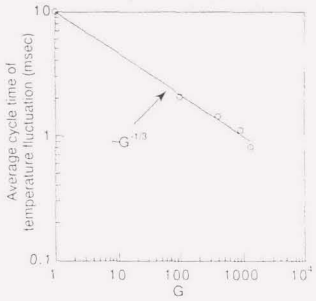

Figure 7. Plots of bubble departure time vs. centrifugal acceleration. Bubble departure time is proportional to the -1/3 power of centrifugal acceleration.

CONCLUDING REMARKS

To the knowledge of the authors, transient heat transfer characteristics of liquid helium have been measured for the first time. In the experiment, it was pointed out that the quasi-nucleate boiling was observed also in the liquid helium in centrifugal acceleration field and that the relation between the take-off time and the heat flux was same as that in the normal gravity.

Due to the limitations in the rotating speed of the rotating cryostat, the centrifugal acceleration was limited up to 1300G and the pressure of the helium was up to 1.5×10^5Pa where the helium stayed in liquid state. Whereas, in the actual superconducting generator, state of the coolant of the field windings is supercritical helium of several atms and the centrifugal acceleration field is in the range of several thousand G. Moreover, in our experiment, the heater was a thin wire. As is known, the heat transfer characteristics of a thin wire is somewhat different from those of a flat surface and thick wire. Therefore, we can not directly use our experimental results as the heat transfer data to analyze the stability of the field windings. However, our results give the following important information on the stability analysis. The film boiling heat transfer reached the steady state in very short time less than 1msec for high heat flux in 1300G because of the high centrifugal acceleration enhanced the convection of the coolant. Therefore, we may use the steady state heat transfer data measured in high centrifugal acceleration field for the stability analysis which needs the heat transfer characteristics in the time range of less than 1msec.

REFERENCES

1. R.G.Scurlock and G.K.Thornton, *Int J Heat Mass Transfer* Vol.20, pp.31-40 (1977).
2. S.Fuchino, H.Fukuda, T.Ogawa, K.Shimizu, Y.Nakabayashi, Y.Kobayashi, M.Ogihara, Y.Kamisada, N. Maki, A.Ueda, T.matsuda, *IEEE Trans. Mag* Vol.28, No.1, pp279-282 (1992)
3. O.Tsukamoto, S.Kobayashi, *J Applied Physics* Vol.46, No.3, pp1359-1364 (1975)
4. O.Tsukamoto, T.Uyemura, Y.Ishida, *Proc. of ICEC8*, pp.251-255 (1980)
5. O.Tsukamoto, *Cryogenic Engineering* Vol.11, No.3, pp.23-33 (1976) *IN JAPANESE*
6. N.Tamada, S.Fuchino, N.Natori, I.Ishii and M.Okano, *Cryogenics*, Vol.33, No.11, pp.1023-1027 (1993)

Designing Stable and High-Current Density Rotor Windings of Superconducting Generator

Osami Tsukamoto and Mitsuho Furuse
Faculty of Engineering, Yokohama National University, Yokohama, 240-8501 Japan

Tomoaki Takao
Faculty of Science and Technology, Sophia University, Tokyo, 102-8554 Japan

Masao Morita and Susumu Maeda
Mitsubishi Electric Corporation, Amagasaki, 661-8661 Japan

Toshiki Hirao
Engineering Research Association for Superconductive Generation Equipment (Super-GM), Osaka, 530-0047 Japan

Abstract — A method to statistically predict quench training characteristics of a rotor windings of a superconducting generator is presented. In the method, energy of a disturbance due to a conductor motion and a quench current are statistically estimated. We apply this method to a rotor of the 70MW class Superconducting generator being developed in the Super-GM project and study the dependence of the stability on parameters of the rotor conductors, such as amount of copper stabilizer, accuracy of conductor dimensions and operating current density. To predict the stability, compliance of the rotor winding pack is a key parameter and estimated by a finite element method. In the study, it is shown that there is an optimum value of ratio of copper to superconductor to maximize the current density of the winding pack keeping necessary stability. Based on the study, a designing method for stable and high current density rotor winding is discussed.

I. Introduction

One of key issues in designing a superconducting generator is how to design high current density rotor winding whose quench current surely exceed designed operation current. However, a method to quantitatively estimate a quench current of the winding has not been developed. This paper is related to this issue. MQE (Minimum Quench Energy) is a well-known measure of the stability of superconductors but can not be a proper measure of the stability of the superconducting windings without knowledge on the size of disturbance in the windings. Therefore, it is important to know quantitatively the size of the disturbance energy to estimate the stability.

Previously, we developed a theory to statistically predict the size of the disturbance caused by a conductor motion [1]. In the theory, parameters such as mechanical properties and amount of copper stabilizer of the conductor and configuration of winding pack are taken into consideration together with the MQE. We apply this theory to 70MW class superconducting generator under development in the Super-GM project. A key parameter of the winding pack to predict the stability is its compliance which depends on the amount of copper stabilizer of the conductor, the property of the spacer and the configuration of the winding pack. We estimated the compliance of the winding pack by the finite element method. In the paper, the validity of the theory is shown by comparing the theoretical analysis and the test results. Based on the theory, possible methods to increase the current density of the rotor winding pack keeping the necessary stability and a design method of the stability is also discussed.

Manuscript received September 14, 1998.

This work has been performed as a part of "R&D on Superconducting Technology for Electric Power Apparatuses" under the New Sunshine Program of Agency of Industrial Science and Technology, MITI, being consigned by NEDO.

II. Principle to Statistically Estimate Training Characteristics

A Disturbance Energy and Maximum Movable Length

The rotor windings are usually wound of cable conductors composed of superconducting composite strands and we consider that a quench is most probably triggered by a motion of a strand of the conductors. The strands in the windings are mainly supported by frictional forces. The strands inevitably have irregularities in their dimensions, hence, the frictional supporting forces of the strands fluctuate because contact forces between the strands fluctuate along the strands even if uniform clamping force is applied to the windings. An abrupt strand motion occurs at a poorly supported part where the electromagnetic force to the strands exceeds the frictional supporting force, and, a quench occurs when the energy released by the strand motion at the poorly supported part is larger than the MQE of the strand. Energy released by the strand motion E_d is determined by the length of the moving part of the strand, that is, that of the poorly supported part,

$$E_d = \frac{(BI)^2 (l/2)^5}{45 E I_d}, \tag{1}$$

where l is the length of the moving part of the strand, B is the magnetic field component perpendicular to the direction of the strand motion, I is the strand current, E is Young's modulus of the strand, and I_d is the geometrical moment of inertia of the strand, $I_d = \pi r^4 / 64$ for a round strand of the radius r. Knowing the relation between E_d and l, we can define the maximum movable length (MML), the maximum length of a part of the strand which can move without a quench. The MML is obtained from (1) by putting $E_d = MQE$ and given by

$$MML \propto \left\{ \frac{1440(MQE)EI_d}{(BI)^2} \right\}^{1/5} \qquad (2)$$

B. Prediction of Training Characteristics

Assuming that the random irregularity of strand dimension follows the Gaussian process, we can calculate the expected number of poorly supported parts whose lengths exceed the MML and this number is the expected number of quenches of the windings. The expected number of quenches depends on the strand current because the MQE, MML and forces to the strand depend on the strand current. We can consider that the first quench occurs at the current when the expected number of quenches becomes 1 and that the next quench follows every time at the current where the expected number of quenches increases by one. Thus training characteristics of the windings can be predicted.

III. Case Study

By applying the method mention above, we estimate the training characteristics of the rotor developed by Mitsubishi Electric Co. for the 70MW class superconducting generator as a part of the Super-GM projects.

A. Configurations of Rotor Winding and Conductor

The cross-sectional view of the rotor is shown in Fig. 1 and the specifications of the rotor are listed in Table I. The rotor windings are placed in the slots No.1~5. A cross-sectional view of the winding pack in the slot is illustrated in Fig. 2. Details of the rotor configuration are given in [2]. The cross-section of the conductor made of 9 strands is illustrated in Fig. 3 and the specifications of the conductor and strand are listed in Table II. The winding packs are surrounded by insulation spacers as shown in Fig. 2 and the compressive forces are applied to the packs and conductors by the clamping forces to the top insulation spacers. The rotor shaft with the windings in the slots was fitted in the rotor vessel by shrink-fit and the clamping forces were applied to the top insulation spacer by the vessel.

B. Forces to Conductor and Strand

When the rotor rotates and the windings are excited, the centrifugal forces and the electromagnetic forces are applied to the conductors in addition to the compressive force from the upper insulation spacer. The electromagnetic forces have two components of circumferential and radial directions of the rotor. The circumferential component of the electromagnetic force causes the strand motions. The distributions of the magnetic field and the electromagnetic forces to the conductors in the slots are estimated based on the analysis using the finite element method. The distribution of total forces to the conductors in the slots can be calculated by knowing the compliance of the winding pack in the radial direction.

C. Compliance of Rotor Winding

The strand of the rotor winding contain CuNi to reduce AC losses. Therefore, stress-strain characteristics of the rotor

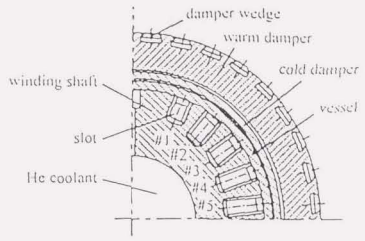

Fig. 1. Cross-section of rotor (perpendicular to center axis, quarter of the rotor).

TABLE I
SPECIFICATIONS OF 70MW CLASS SUPERCONDUCTING GENERATOR

Rotor	
Number of pole	2
Rotating velocity	3600 rpm
Diameter	890 mm
Bearing span	4900 mm
Winding	
No. of coils	10 (5 coils/pole)
Magnetic field (maximum)	4.5 T (at 3000 A)
Conductor	9 strand compacted cable

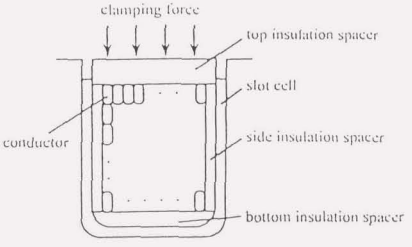

Fig. 2. Cross-sectional view of the winding pack in the slot.

winding pack in the radial direction were calculated for different values of ratio of copper stabilizer and CuNi to NbTi by the finite element method. We call this ratio nonSc/Sc after this. In the calculation, we changed nonSc/Sc by changing the amount of outer layer copper stabilizer while fixing the amount of CuNi. The compliances were calculated for the strand of same configuration shown in Fig. 3 except nonSc/Sc. In the calculation, stress-strain data of Cu, NbTi and CuNi were used and it was assumed that the core part of the strand including NbTi filamentary region stayed in the elastic region and that stabilizing copper region went in the plastic region. The stress-strain characteristics of the insulating kapton tape given in the reference [3] were also taken into consideration. The results are shown in Fig. 4. The compressive forces to the strands fluctuate around the clamping force. Therefore, the compliance of the winding pack is determined from the slope of the stress-strain curve at the stress determined by the clamping force. Obviously from Fig. 4, the compliance increases as the nonSc/Sc increase, because the amount of soft copper stabilizer increases.

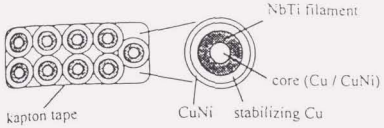

Fig. 3. Cross-sections of rotor conductor and strand.

TABLE II
SPECIFICATIONS OF CONDUCTOR AND STRAND

Conductor (compacted strand cable)	
Size in cross section	2.9 mm × 7.4 mm
No. of strands	9 strands
Critical current	5100 A (7.6 T) at 4.2 K
	4900 A (7.3 T) at 4.6 K
Strand	
Cu : CuNi : NbTi	2 : 0.7 : 1
Diameter	1.6 mm
Young's modulus	130 GPa
Geometrical moment of inertia	3.2×10^{-13} m^4

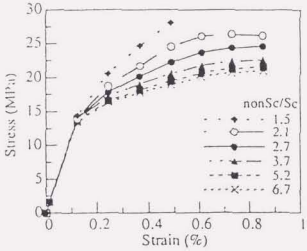

Fig. 4. Stress-strain curves of winding pack of different nonSc/Sc conductors.

D. Calculation of MQE and MML

We assume that a quench of the winding is initiated by a quench caused by a strand motion in the conductor, therefore, MQE of the single strand is calculated. Details of calculation of MQE are described in [4]. We assumed a point disturbance of 0.5 msec duration [5] and 2 mm spatial length to calculate MQE. The spatial length of the disturbance was determined by the observation of the conductor configuration. MQE's were calculated in the static and rotating conditions. In the calculation, the transient heat transfer of liquid helium was taken into account in the static condition. In the rotating condition, data of the steady heat transfer of the supercritical helium in high centrifugal field [6] were used, because, according to our experiment, the steady state heat transfer was established in very short time [7].

E. Calculation of Expected Number of Quenches and Training Characteristics

We assume the irregularity in the dimension of the conductor follows the Gaussian process of standard deviation σ, then the dimension irregularity of the winding pack also follows the Gaussian process whose standard deviation is $\sqrt{n}\sigma$, where n is the number of the layers of the winding pack. It can be considered the contact forces between the conductors also follows the Gaussian process whose standard deviation is $k\sqrt{n}\sigma$ where k is the spring constant of the winding pack which can be deduced from the compliance of the winding pack calculated by the finite element method. Then, we can numerically simulate the distribution of the fluctuation of the contact force along the conductor using the method explained in [1]. We can assume that the contact forces between conductors are equal to that between the strands of the conductor. Thus, by multiplying the contact forces by the friction coefficient μ between the strands, we can estimate the distribution of the supporting force along the strand and the number of the poorly supported parts whose lengths exceed the MML for a given conductor current. This number is the expected number of quenches till the conductor current reaches the given value.

F. Comparison of Predicted Training Characteristics with Experimental Result

The quench test of the rotor winding which is case-studied here was performed in the static condition. nonSc/Sc of the strand is 2.7. The validity of the prediction method can be checked by comparing the predicted training characteristics with the experimental result. Using the parameters listed in Table III, the accumulation of the expected number of the quenches until the conductor current reached I was calculated for the nonSc/Sc=2.7 for the static conditions. σ=33 μm was determined based on the specified dimension allowance of the conductors and μ=1.0 was determined based on experimental value of the copper vs. copper friction [8]. Fig. 5 shows the estimated training characteristics. As seen in the figure, the first quench current is 4.4 kA for the static condition. It is also seen that the first quench is followed by many successive quenches.

Result of the quench test in the static condition is shown in Fig. 6. The current at the first quench is 4.3kA and many quenches follows as is seen in the calculation result in Fig. 5. Based on this comparison, we can assume that the method to predict the training characteristics is valid.

G. Dependence of Stability on Amount of Copper Stabilizer

As nonSc/Sc increases, the spring constant k of the winding pack decreases and the standard deviation of the contact forces between the strands decreases. Therefore, the number of the poorly supported parts whose lengths exceed the MML decreases and the conductor current reaches its critical value with smaller number of the training quenches. However, high nonSc/Sc sacrifices the current density. On the other hand, low nonSc/Sc strand causes large winding pack spring constant and severe training effect.

From the standpoint of designing the rotor winding, it is important that the first quench current is high. Obviously from the discussion above, there is an optimum value of nonSc/Sc to make the first quench current maximum for given clamping force to the winding pack and σ. Fig. 7 shows the dependence of the first quench current on the nonSc/Sc. The dependence is estimated for a conductor of same dimensions shown in Fig. 3 for different values of σ by the method described above. The parameters for the calculation are same as in Table III except σ. The critical current of the conductor I_c on the load line, depending on the nonSc/Sc, is also shown in

TABLE III
PARAMETERS ON CALCULATION OF EXPECTED NUMBER OF QUENCH

σ	33 μm
μ	1.0
Spring constant of winding pack (nonSc/Sc=2.7)	5.5×10^7 [N/m/strand]/m (static condition)
	3.7×10^7 [N/m/strand]/m (rotating condition)
Clamping force to the windings	5.2×10^4 N/m/conductor (static condition)
	6.2×10^4 N/m/conductor (rotating condition)

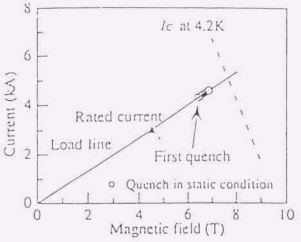

Fig. 5. Prediction of training quenches of the winding in the static condition.

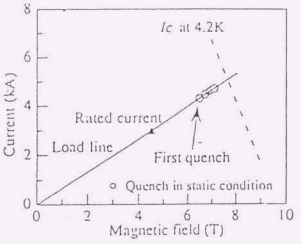

Fig. 6. Result of training quench test.

Fig. 7. For the case of σ=33μm, the first quench current becomes maximum at nonSc/Sc=3.7 and is 4.6kA which is I_c at the point. For nonSc/Sc higher than 3.7, the conductor current reaches I_c without quench but current capacity of the conductor becomes lower.

To obtain higher first quench current, it is necessary to decrease σ for a conductor of lower nonSc/Sc to reach the maximum first quench current. The maximum values are 4.9kA for σ=25μm at nonSc/Sc=2.7 and 5.1kA for σ=20μm at nonSc/Sc=2.1. The first quench can be also increased by increase of the clamping force to the winding but too high clamping force deteriorates the conductor performance damaging the conductor.

IV. CONCLUDING REMARKS - DESIGNING STABLE AND HIGH CURRENT DENSITY WINDING

Summarizing the study above, the following conclusions are obtained.

1. Quantitative estimation of the first quench and design of the stability of the winding are possible by the method described in the paper.
2. For a given value of σ and clamping force to the winding, there is an optimum value of nonSc/Sc to make the first quench current maximum. Low value of nonSc/Sc, that is, high I_c does not necessarily make the current density of the winding high. Increase of nonSc/Sc contributes to the reduction of the conductor cost by reducing the amount of NbTi.
3. Data of the compliance of the winding pack are key of our stability estimation method, we need more knowledge and data on the compliance of the winding.

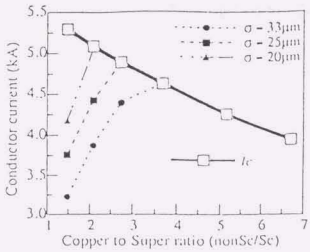

Fig. 7. Dependence of first quench current on nonSc/Sc for different values of σ.

ACKNOWLEDGMENT

The authors are very grateful to Prof. M. Shiratori and Dr. J. Gotoh of Faculty of Engineering, Yokohama National University to assist us to calculate the compliance of the winding using the finite element method.

REFERENCES

[1] T. Takao, K. Iwasaki and O. Tsukamoto, "Statistical Estimation of Disturbance Energy due to Conductor Motion in Rotor Windings of Superconducting Generator," *IEEE Trans. on Appl. Super.*, vol. 5, No. 2, pp. 361-364, 1995.

[2] T. Ohara, H. Fukuda, T. Ogawa, K. Shiobara, M. Ohi, A. Ueda, K. Itoh and H. Taniguchi, "Development of 70MW class superconducting generators," *IEEE Trans. on Magn.*, vol.27, No.2, pp2232-2239, 1991.

[3] R. P. Reed, R. E. Schramm and A. F. Clard, "Mechanical, thermal and electrical properties of selected polymers," *Cryogenics*, pp. 66-82, 1973.

[4] N. Amemiya, T. Takao and O. Tsukamoto, "Disturbance characteristics and stability of high current density superconducting wires," *Fusion Engineering Design*, vol. 20, pp. 339-344, 1993.

[5] O. Tsukamoto, "Disturbance due to conductor motion and stability of large-scale conductors," *Fusion Engineering Design*, vol. 20, pp. 327-332, 1993.

[6] R. Nakajima, K. Sato, K. Miyaike, M. Kumagai and Y. Kobayashi, "Liquid and supercritical helium heat transfer of horizontal upward facing surfaces under high centrifugal acceleration fields," HTD-Vol. 229, Heat transfer in superconducting equipment, G00721, pp. 39-44, 1992.

[7] O. Tsukamoto, M. Furuse, T. Takao, N. Tamada, S. Fuchino, I. Ishii and N.Higuchi, "Transient heat transfer characteristics of liquid helium in centrifugal acceleration field," presented at CEC/ICMC97.

[8] T. Takao, D. Yoshino, T. Kubosaka, N. Momma, I. Nitta, A. Iwabuchi, F. Odajima, "Influence of Surface Roughness and Precooling by Liquid Nitrogen on Frictional Coefficients at Liquid Helium Temperature," presented at 17th ICEC, 1998.

TRANSIENT HEAT TRANSFER OF SUPERCRITICAL HELIUM IN HIGH CENTRIFUGAL ACCELERATION FIELD

M. Furuse,[1] O. Tsukamoto,[1] T. Takao,[2]
S. Fuchino,[3] I. Ishii,[3] M. Okano,[3] and N. Tamada[3]

[1]Yokohama National University
Yokohama, Kanagawa, 240-8501, Japan

[2]Sophia University
Chiyoda, Tokyo, 102-8554, Japan

[3]Electrotechnical Laboratory
Tsukuba, Ibaraki, 305-8568, Japan

ABSTRACT

Transient heat transfer of supercritical helium in centrifugal acceleration field has been measured for studying the stability characteristics of superconducting rotor windings of a superconducting generator. A temperature resistive platinum-0.5% cobalt (Pt-Co) thin wire, having small heat mass, was used as a temperature sensor and heater to measure the heat transfer characteristics. It was observed that the steady state heat transfer of supercritical helium in 3600G (G; gravity acceleration) was established in 200μsec. In the paper, data of transient heat transfer of supercritical helium in centrifugal acceleration field are shown and their specific characteristics are studied comparing with those of liquid helium.

INTRODUCTION

Premature quenches of superconducting rotor windings of superconducting generators are mainly caused by abrupt conductor motions. Duration times of such disturbances are very short,

Advances in Cryogenic Engineering, Volume 45
Edited by Shu *et al.*, Kluwer Academic / Plenum Publishers, 2000

several 100μsec. The helium coolant for the rotor windings is in the supercritical state and subject to high centrifugal acceleration. Therefore, for stability analysis of the rotor windings, transient heat transfer data of supercritical helium in high centrifugal field are necessary.

Previously, we measured transient heat transfer characteristics of helium in centrifugal acceleration field up to 1300G where the pressure of the helium was up to 1.5×10^5Pa and the helium stayed in the liquid state. We found some specific characteristics of the transient heat transfer in the centrifugal field as follows;[1]

1. Take-off time, which is duration of quasi-nucleate boiling, was not dependent on the value of centrifugal acceleration field in the range of 1G to 1300G and relation between the take-off time τ and the heat flux of step heating q_0 was given by $q_0=2.6\times10^4\tau^{-0.25}$.
2. Steady state film boiling was established in the high centrifugal field much faster than in the case of 1G.
3. In the steady state film boiling region, the Pt-Co wire detected cyclic temperature fluctuations due to cyclic departure of bubbles from the wire surface. Average cycle time is only weakly dependent on the heat flux but proportional to the centrifugal acceleration (proportional to $a^{1/3}$; a is the centrifugal acceleration).

In the previous experiment, due to the limitation in the rotating speed of the rotating cryostat, the centrifugal acceleration was limited up to 1300G. We conducted the heat transfer experiment by increasing the rotating speed of the rotating cryostat and obtained the transient heat transfer data of the cryogenic helium in the centrifugal acceleration up to 3600G where the pressure of the helium was 2.4×10^5Pa and the helium was in the supercritical state. We observed the heat transfer of the supercritical helium had some specific characteristics different from those of the liquid helium.

EXPERIMENTAL ARRANGEMENT

We used the same experimental arrangement used in the previous experiment. Details of the arrangement are described in the reference [1]. Here, outline of the experimental arrangement is described. The experimental arrangement is schematically shown in Figure 1. A heat transfer measurement sample made of a Pt-Co wire of 20μm diameter and 40mm length shown in Figure 1(b) was placed in the rotating cryostat illustrated in Figure 1(a). The Pt-Co wire was used as the heater and temperature sensor. Thermal time constant of Pt-Co wire is less than 10μsec, the thermal response of the Pt-Co wire is sufficiently fast to measure transient heat transfer characteristics in the range of several tens μsec. The temperature was determined from the resistance of the wire measured by the four terminal method. A step current of $I(t)$ was applied to the Pt-Co wire and the transient wave form of the voltage $V(t)$ between the voltage tap on the wire (length 40mm) was recorded by a transient recorder together with the current wave form. The surface heat flux $q(t)$ was calculated as $q(t)=IV/S$ where S was the surface area of the wire between the voltage taps. The Pt-Co wire has low thermal mass and we can assume that the wire surface temperature agreed to the wire temperature. During the step heating, the current was kept constant but $V(t)$ changed due to the temperature change of the wire, therefore, $q(t)$ changed. Our main concern is on the transient heat transfer characteristics for a few msec

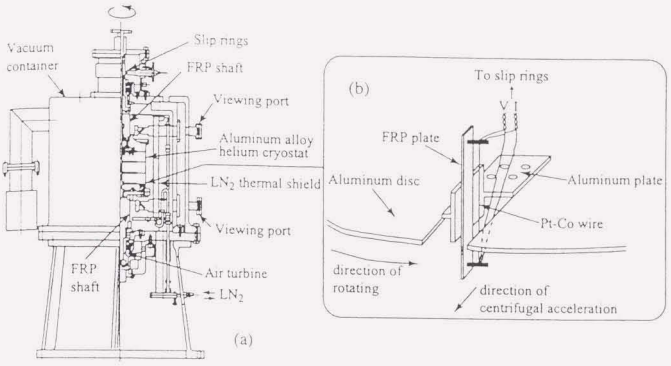

Figure 1. Cut-away vies of (a) rotational cryostat and (b) schematic drawing of the measurement sample.

after the step heating and in this time range, we assumed $q(t)$ did not change. We call the value of $q(t)$ at the beginning of the heating the initial heat flux. Data were taken by changing the rotational speed of the cryostat from 0rpm (1G) to 6000rpm (3600G). By monitoring the liquid helium level, the pressure of the helium around the Pt-Co wire was calculated. The helium stayed in liquid state below 4000rpm (1600G) and became supercritical state at 6000rpm (3600G). The bath temperature and pressure of the helium in the rotating cryostat varied 4.2K~4.7K and 1.0~2.4×10^5 Pa depending to the rotating speed of the cryostat.

EXPERIMENTAL RESULTS

Figure 2 shows temperature traces of the Pt-Co wire for step heating of 23kW/m^2~47kW/m^2 in various centrifugal acceleration field together with the case of 1G. It was found in our previous work that the steady state film boiling was established in early stage of the step heating for liquid helium in high centrifugal acceleration field and that cyclic temperature fluctuations caused by bubbling of the liquid helium were observed. In the supercritical helium of 3600G, the cyclic temperature fluctuations were also observed and the heat transfer reached steady state earlier for the step heating than in the liquid state helium. The average cycle of the temperature fluctuations T_b in the supercritical state are plotted against acceleration field a together with those in the liquid state in Figure 3. T_b's of the supercritical helium for a=3600G are shorter than those of the liquid helium of lower a and on the line of $T_b \propto a^{1/3}$ same as of T_b's of the liquid helium. Pressure of the supercritical helium at 3600G was about 2.4×10^5 Pa where the density of the supercritical helium is strongly dependent on the temperature. Therefore, it is considered that quasi-bubbling occurred in the supercritical helium and that large centrifugal acceleration aids departure of the bubble to shorten T_b.

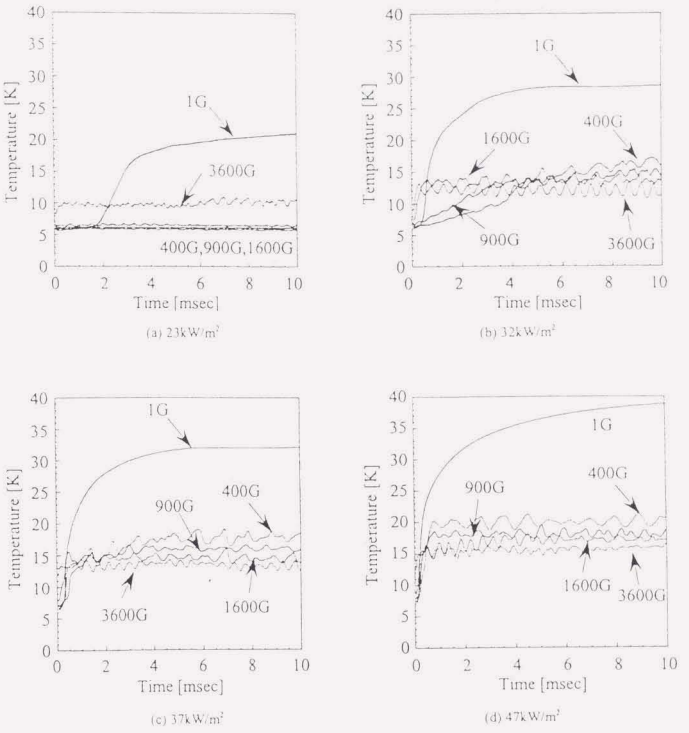

Figure 2. Transient time traces of temperature of Pt-Co wire for step heating in centrifugal field.

Obviously from Figure 2(a), the nucleate boiling region with good heat transfer appearing in the liquid state does not appear in the supercritical state because the supercritical helium is mono phase. Figure 4 shows the heat transfer characteristics at the early stage of the step heating for the heat flux 47kW/m^2. As seen in Figure 4, the heat transfer of supercritical helium reaches the steady state in 200μsec and the quasi-nucleate boiling which is observed in the liquid helium is not observed for the supercritical helium of 3600G and those characteristics were commonly observed in the range of the heat flux 23kW/m^2~47kW/m^2 where we conducted the experiment.

The temperature rise of the wire ΔT in the steady state is plotted against the heat flux for various centrifugal fields in Figure 5. The heat transfer in the supercritical state of 3600G is

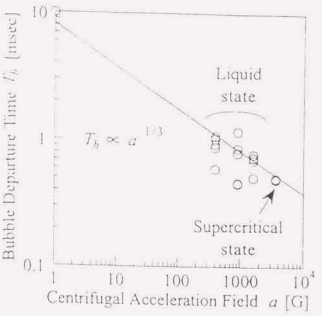

Figure 3. Plots of bubble departure time vs. centrifugal acceleration.

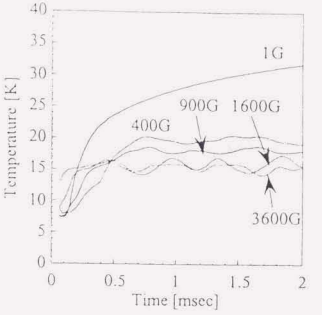

Figure 4. Enlargement of Figure 2. (d) 47kW/m^2.

worse in the low heat flux region below 25kW/m^2 and better in the high heat flux region above 26kW/m^2 compared with that in the liquid state of 400G~1600G. The nucleate boiling occurs in the liquid helium even when the helium is subject to the centrifugal acceleration and good heat transfer is obtained. On the other hand, the nucleate boiling does not occur in the supercritical state and the heat is removed from the wire surface by free convection of the helium. The heat transfer in the nucleate boiling region is better than that by the free convection even in the high centrifugal field. Therefore in the low heat flux range, the heat transfer of the supercritical state is lower than that of the liquid state. When the heat flux in the liquid state exceeds a certain threshold, the maximum nucleate boiling heat flux, the boiling moves to the film boiling where the heat transfer by the boiling much decreases and the free convection cooling becomes dominant. The heat transfer by the free convection increases as the centrifugal acceleration increases. Therefore, the heat transfer in the supercritical state created by higher centrifugal field is higher than that in the liquid state subject to lower centrifugal field.

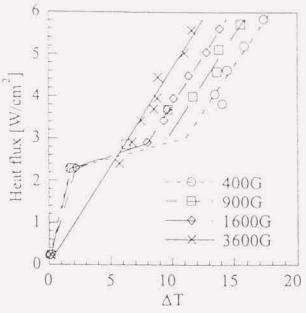

Figure 5. Steady state heat transfer characteristics.

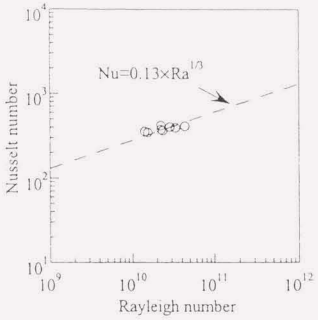

Figure 6. Steady state heat transfer data of supercritical helium of 3600G plotted in Rayleigh vs. Nusselt numbers.

Our steady state heat transfer data for the supercritical helium of 3600G are plotted in a graph of Nusselt vs. Rayleigh numbers in Figure 6. Our data are on the line $Nu=0.13\times Ra^{1/3}$ which is derived from the steady state heat transfer data for a flat heating surface in the supercritical helium in the centrifugal field.[2] The line in Figure 6 follows the well-known equation which is for the convection cooling.[2]

Based on the above study, we conclude that the heat transfer of the supercritical helium in high centrifugal field is dominated by the steady state free convection cooling and that the steady state heat transfer is established in about 200μsec after the start of the heating. For the stability analysis of the superconducting rotor windings subject to disturbances caused by conductor motions, we consider that the steady state heat transfer data can be used.

1156

CONCLUSIONS

Transient heat transfer of supercritical helium in high centrifugal acceleration field was measured. The results of the study based on the experiment are summarized as follows.

1. The heat transfer reached the steady state in about 200μsec.
2. The nucleate boiling and quasi-nucleate boiling were not observed in the supercritical state while they were observed in the liquid state.
3. The steady state heat transfer of the supercritical helium was lower in the lower heat flux region and higher in the higher heat flux region than that of the liquid state.
4. The heat transfer is considered to be dominated by the free convection cooling because the data expressed in terms of Nusselt and Rayleigh numbers follow the line for the free convection cooling.
5. Based on the experimental results, we consider that the steady state heat transfer data in the supercritical helium can be used to the stability analysis of the superconducting rotor winding where duration of the disturbances causing premature quenches are several 100μsec.

REFERENCES

1. O. Tsukamoto, M. Furuse, T. Takao, N. Tamada, S. Fuchino, I. Ishii and N. Higuchi, Transient Heat Transfer Characteristics of Liquid Helium in Centrifugal Acceleration Field, *Advances in Cryogenic Engineering*, Vol.43B, Plenum Press, New York(1998), pp.1489-1496.
2. R. Nakajima, K. Sato, K. Miyake, M. Kumagai and Y. Kobayashi, Liquid and Supercritical Helium Heat Transfer of Horizontal Upward Facing Surfaces under High Centrifugal Acceleration Fields, ASME HTD-Vol.229, Heat Transfer in Superconducting Equipment, Book No. G00721 (1992), pp.39-44.

Analytical Estimation of Quench Current of Large Bore Superconducting Magnet

Mitsuho Furuse and Osami Tsukamoto
Faculty of Engineering, Yokohama National University, Yokohama, 240-8501 Japan

Tomoaki Takao
Faculty of Science and Technology, Sophia University, Tokyo, 102-8554 Japan

Kiyoshi Yoshida
Japan Atomic Energy Research Institute, Ibaraki, 311-0193 Japan

Abstract — Previously we developed a theory to estimate the stability of a magnet by statistical estimation of size of disturbance caused by conductor motion. In the theory, various conductor and magnet parameters such as mechanical properties and fluctuation in dimensions of the conductor, electromagnetic and mechanical forces to the conductors and configurations of the magnet winding are taken into consideration together with minimum quench energy (MQE). We applied this theory to a large bore magnet developed by Japan Atomic Energy Research Institute (JAERI) for a test facility for large superconductors. The magnet showed training phenomena at excitation tests. In this paper, quench characteristics of the magnet are quantitatively estimated using our statistical method. The reasons for the unexpected quenches are studied and possible modification of the magnet design is discussed to increase the stability.

I. Introduction

Stability of a superconductor is commonly measured by MQE. However, MQE can not measure the stability of a magnet properly without knowledge on disturbance energy. It is widely accepted that a main cause of a quench of a high current density magnet is an abrupt conductor motion due to electromagnetic force applied to the conductor. Previously we developed a theory to quantitatively estimate quench currents of a magnet by estimating size of a disturbance caused by a conductor motion and confirmed validity of the theory by applying it to various superconducting magnets [1]-[3].

In this theory, it is assumed that frictional supporting force of a conductor fluctuates because of irregularities in dimensions of conductors and spacers even if uniform clamping force is applied to the winding and that the conductor motions occur at poorly supported parts where electromagnetic force exceeds the frictional supporting force to the conductor. By counting number of places along the conductor where conductor motions occur and release energy exceeding MQE, training behavior of a magnet can be statistically estimated. In this paper, we apply this theory to a large bore magnet and compare with excitation test results. We also discuss a possible method to increase the stability.

II. Large Bore Magnet and Its Training Behaviors

A large bore superconducting magnet was developed for a test facility for large superconductors by JAERI. The magnet was pool-cooled and consisted of 34 double pancake coils of 1.5m inner and 1.8m outer diameters. Specifications of the magnet are shown in Table I. The pancake coils were tied together by clamping bolts with GFRP spacers between the pancakes. A schematic illustration of the magnet windings is shown in Fig. 1. The magnet showed training behaviors as shown in Fig. 2 where two series of training, Case 1 and Case 2, are shown. The Case 1 is for the first series of training and the Case 2 for the second series after the clamping forces to the pancake coils were increased by narrowing the diameter of the bolts and more stretching the bolts. Compared with the Case 1, the quench currents were increased in the Case 2. Acoustic sensors were attached on the magnet and acoustic burst signals were observed just before quenches, which suggested the quenches were caused by conductor motions.

Critical current of the conductor vs. magnetic field is also shown in Fig. 2. As seen from this figure, the magnet has large current margin and potential to increase magnetic field. A key method to increase the stability against the conductor motion is to ensure the supporting forces to the conductors. In this magnet, the supporting forces to the conductors are applied by the clamping bolts and, in this paper, required mechanical properties of the bolts are quantitatively estimated for the quench current to exceed a certain required level.

TABLE I
SPECIFICATIONS OF THE LARGE BORE MAGNET

Conductor	Rectangular shape monolithic
Size	4.0mm width, 7.9mm thick
NbTi : Cu	1:3.2
Magnet	34 pool-cooled double pancakes
Outer/Inner diameter of coil	1.8m/1.5m
Total number of turns	2236
Stored Energy	21MJ (at 6T)

1051-8223/00$10.00

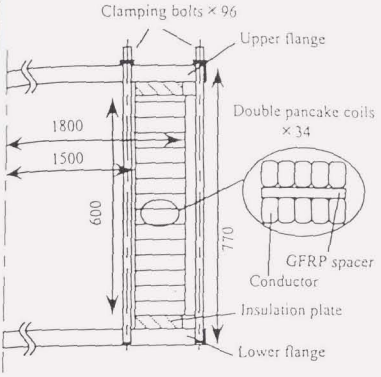

Fig. 1. Schematic illustration of magnet windings.

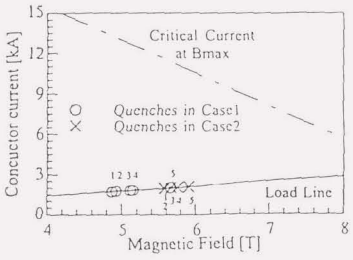

Fig. 2. Critical current on the load line of the magnet and training characteristics. Serial numbers at quench points denote orders of quench events for the Case 1 and Case 2.

III. Principle to Estimate Training

In the magnet studied here, the conductors are supported against radial electromagnetic forces mainly by frictional forces between the conductors and the GFRP spacers placed between the pancake coils. The conductors and spacers inevitably have irregularities in their dimensions. The frictional supporting forces fluctuate because contact forces between the conductors and spacers fluctuate along the conductors and poorly supported parts appear. An abrupt conductor motion occurs at the poorly supported part and a quench occurs when the energy released by the conductor motion is larger than the MQE of the conductor. Energy released by the conductor motion E_d can be calculated by the following equation [4].

$$E_d = \frac{(BI)^2(l/2)^5}{45EI_d} \qquad (1)$$

Where l is the length of the moving part of the conductor, B is the magnetic field component perpendicular to the direction of the conductor motion, I is the conductor current, E is Young's modulus of the conductor, and I_d is the geometrical moment of inertia of the conductor. $I_d = bh^3/12$ for a rectangular shape conductor whose width and thickness are b and h respectively. By putting E_d = MQE, we can determine the maximum length of a part of the conductor which can move without a quench. We define this length the Maximum Movable Length (MML). The MML is given by [4]

$$MML = \left\{ \frac{1440(MQE)EI_d}{(BI)^2} \right\}^{1/5}. \qquad (2)$$

The clamping force is applied to the winding by the flanges and clamping bolts to axial direction (Fig. 1). When the magnet is excited, the coil windings shrink in axial direction due to the electromagnetic forces and the clamping forces decrease. Then the number of poorly supported parts and chances of quenches increase. The distributions of the electromagnetic forces to the conductors can be calculated by the finite element method, and the contact forces between conductors and spacers can be estimated by knowing the compliance of the windings and clamping bolts. We made an analytical model as shown in Fig. 3 to calculate the contact forces between the conductors and spacers. In the model, compliance of the coil windings is expressed as a spring and that of the clamping bolt also. k is the spring constant of one layer of a double pancake for axial displacement. We assume that the axial displacement of a pancake coil is uniform in the radial direction. We assume also that the top and bottom flanges are solid plates to which the 96 bolts apply clamping forces and that the axial displacement of the flanges are uniform in the radial direction. k_0 is the spring constant expressing the total axial-direction compliance of the 96 bolts. f_{di} (i = 1 ~ 68) is electromagnetic force to i th layer of the pancake coils and f_0 is the clamping force the coils applied by the clamping bolts.

We assume the irregularities in the dimensions of the conductor and spacers follow the Gaussian process. Then, the contact forces between the conductors and spacers fluctuate according to the Gaussian process of a standard deviation σ_F ; $\sigma_F = k \cdot n^{1/2}\sigma_0$, where n is the total number of layers of the pancake coils (n = 68) and σ_0 is the standard deviation of the thickness irregularities of the double pancakes and spacers. σ_0 is given by $\sigma_0 = (\sigma_c^2+\sigma_t^2)^{1/2}$, where σ_c and σ_t are the standard deviations of irregularities of thicknesses of one double pancake coil and a spacer respectively. Based on above assumptions and the model shown in Fig. 3, the fluctuation of the contact forces can be statistically evaluated along the conductor using the method explained in the reference [5]. Multiplying the evaluated contact forces by the friction coefficient μ between conductors and spacers, statistical distribution of the supporting forces to the conductors against the hoop stresses can be evaluated and we can count the number of poorly supported parts of the conductors whose lengths exceed the MML. This number is the expected number of quenches of the magnet. The expected number of quenches depends on the conductor current because the MML and forces to the conductor depend on the conductor current. We can consider that the first quench occurs at the current where the expected number of

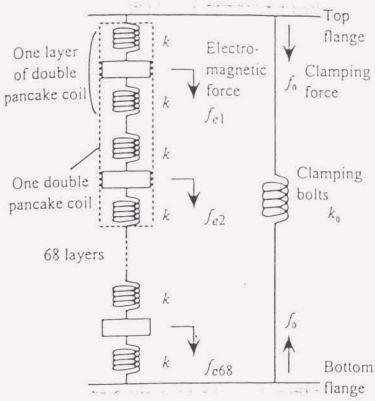

Fig. 3. Winding model of the magnet to calculate contact forces between the conductors.

quenches becomes 1 and that the next quench follows every time at the current where the expected number of quenches increases by one. Thus training characteristics of the magnet can be predicted.

IV. Estimation of Quench Characteristics of Large Bore Coil

Parameters of the conductor and magnet used in the analysis are shown in Table II. σ_c is determined based on the specified dimension allowance of the conductors and we put $2\sigma_c$ = the dimension allowance. σ_s is assumed equal to σ_c. $\mu = 0.7$ is determined based on experimental value of the epoxy vs. epoxy friction [6]. The Young's modulus of the coil is determined by measuring the displacement of the top flange against the bottom flange during the excitation of the magnet using strain gauges attached on the clamping bolts. The Young's modulus of the bolts is that of the stainless steel at 4.2K. The large bore magnet was tested twice, Case 1 and Case 2, by changing the clamping forces as explained in the section II. In the analysis, changes in the clamping

TABLE II
Parameters on Calculation of Expected Number of Quench

σ_c , σ_s	25μm
μ	0.7
Young's modulus of the conductor	130GPa
I_d	$4.2\times10^{-11}m^3$
Young's modulus of the coil	5GPa
Young's modulus of the clamping bolts	200GPa
Diameter of clamping bolts	Case1 : 16mm Case2 : 13mm
Clamping force to the coils f_0	Case1 : 10.5MPa Case2 : 12.0MPa

conditions in the two cases are taken into consideration by changing clamping force f_0 and spring constant of clamping bolts k_0. MQE of the conductor is calculated assuming a point disturbance of 0.5msec duration and 20mm spatial length that is width of the spacer. Details of calculation of MQE are described in [7]. In the analysis, supporting forces and electromagnetic forces to the conductors are calculated by increasing the conductor current from zero and the accumulation of the expected number of the quenches until the conductor current reaches I is calculated by a way explained in the section III. The results are plotted against I in Fig. 4. In the analysis, it is assumed that displacement of the conductor in a poorly supported area is limited when the moving part of the conductor touches a conductor in the neighboring turn. We assume the limit of the radial displacement of the conductor fluctuates also according to the Gaussian process of standard deviation σ_c.

V. Comparison of Experimental and Analytical Results and Discussion on Coil Design Modification

Statistically estimated training behaviors obtained from Fig. 4 and experimental results are compared in Fig. 5. As obvious from Fig. 5, analytical results well coincide with experimental results.

In the calculation, it is shown in both of the Case 1 and Case 2, the first quench occurred around a current where the clamping forces applied by the flanges and bolts were lost by increase of the electromagnetic forces in the axial direction. Considering this fact, we can increase quench current by increasing initial clamping force or more effectively by decreasing spring constant of the clamping bolts for the clamping forces not to be lost even when the magnet current reaches high level. The first quench currents are calculated by changing k_0 while f_0 is fixed to the value in Case 2 and the results are shown in Fig. 6. As seen in Fig. 6, quench current can reach the critical current without training by reducing the value of k_0 to 30% of that for the Case 2. k_0 can be reduced by use of spring washers and longer clamping bolts. The first quench current can be also increased by increasing the initial clamping force but too high clamping force damages the conductors and deteriorates the conductor performance.

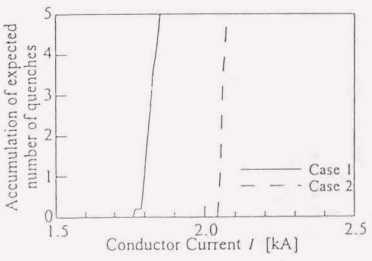

Fig. 4. Accumulation of expected number of quenches (Case 1 and Case 2).

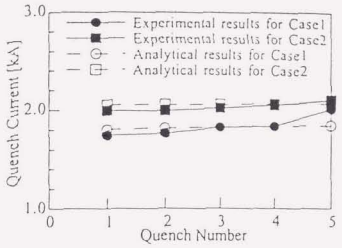

Fig. 5. Analytically calculated quench current and experimental results of training.

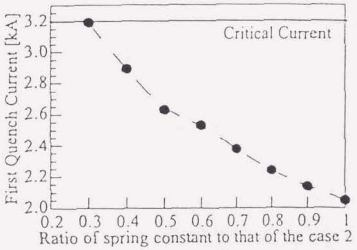

Fig. 6. Dependence of first quench current on total spring constant of clamping bolts. f_0 is fixed to the value of the Case 2.

By decreasing σ_0 and k, σ_F is decreased and the first quench current can be increased. However, in this large bore magnet, lack of the clamping force is main cause of conductor motion. Therefore an effective way to substantially increase the first quench current is decrease of k_0.

VI. Conclusions

The training characteristics of the large bore magnet were quantitatively analyzed by our statistical method and the analytical results well coincided with experimental results. It was also shown by the analysis that the first quench current could be increased by decreasing spring constant of the clamping bolts for the clamping force not to be lost when the magnet current reached to a rated current.

From these results, we consider that our method to statistically estimate stability of superconducting magnet can be a powerful tool for designing stable magnets.

References

[1] T.Takao, O.Tsukamoto, M.Furuse and K.Tsuchiya, "Statistical Estimation of Quench Characteristics of Quadrupole Magnets," *IEEE Trans. on Appl. Super.*, Vol.7, No.2, pp.183-186, 1997

[2] O.Tsukamoto, M.Furuse, T.Takao, M.Morita and T.Hirao, "A Method to Estimate the Stability of Rotor Winding of Superconducting Generator in Rotating Condition," proceedings of 15th International Confereng on Magnet Technology, Part one, pp.522-525

[3] O.Tsukamoto, M.Furuse, T.Takao, M.Morita, S.Maeda and T.Hirao, "Designing Stable and High-Current Density Rotor Windings of Superconducting Generator," *IEEE Trans. on Appl. Super.*, Vol.9, No.2, pp.244-247, 1999

[4] T.Takao, O.Tsukamoto and S.Honjo, "Probability of Premature Quenches Due to Conductor Motion in Superconducting Windings," *Cryogenics*, Vol.31, pp.504-509, 1991

[5] T.Takao, K.Iwasaki and O.Tsukamoto, "Statistical Estimation of Disturbance Energy due to Conductor Motion in Rotor Windings of Superconducting Generator," *IEEE Trans. on Appl. Super.*, Vol.5, No. 2, pp.361-364, 1995

[6] A.Iwabuchi, H.Arai, Y.Yoshino, T.Shimizu, M.Sugimoto, K.Yoshida, T.Kashima and H.Inui, " Frictional Properties of Ceramics, MoS_2 Coated Films and Polyethylene Fibre Reinforced Plastics at 4.2K in Liquid Helium," Cryogenics, Vol. 35, No. 1, pp.35-40, 1995

[7] N.Amemiya, T.Takao and O.Tsukamoto, "Disturbance Characteristics and Stability of High Current Density Superconducting Wires," *Fusion Engineering Design*, Vol. 20, pp.339-344, 1993

Transient Heat Transfer of Liquid Helium in Rotating Machines

Shuichiro Fuchino, Itaru Ishii and Noriharu Tamada
Electrotechnical Laboratory, Tsukuba, Ibaraki ,Japan

Osami Tsukamoto and Mitsuho Furuse
Yokohama National University, Yokohama, Kanagawa, Japan

Tomoaki Takao
Sophia University, Tokyo, Japan

Abstract— Transient heat transfer characteristics of liquid helium under centrifugal acceleration fields have been investigated using a Platinum-0.5 at% Cobalt (Pt-Co) thin wire. Step heat inputs ranging from 1 to 5 W/cm^3 are applied to the 20 μm diameter wire in a rotating cryostat containing liquid helium. The maximum centrifugal acceleration is around 1300 times larger than gravitational acceleration at 3600 rpm. The temperature rise is measured by the resistivity of the Pt-Co wire. As the result, the take-off time (onset of film boiling) can be described by a power fit of the heat flux. The cyclic temperature fluctuations have been observed, the times of which can be also described by a power fit of the centrifugal acceleration. These results are discussed on the basis of the bubble departure time.

I. Introduction

Superconducting generators have advantages of generation efficiency improvement, their reduced sizes and weights, and higher power system stability. In the case of superconducting generators, superconducting field windings are affected by the centrifugal acceleration and bubbles or lower density parts caused by heating are moved away very fast by large buoyancy. Thereafter, it is very important to investigate the behavior of liquid helium under centrifugal acceleration to estimate the stability of the superconducting field windings.

Consequently it is well studied about steady state heat transfer under centrifugal field [1], [2].

It is also well known that the mechanical disturbance just like a wire movement or micro cracks in the structural material may trigger the normal transition of superconducting magnets, and these mechanical disturbances are happened quickly, usually within 1 millisecond [3].

Considering these facts, it is very important to investigate the transient heat transfer characteristics under the centrifugal acceleration fields. In this paper, transient heat transfer characteristics of liquid helium under centrifugal acceleration fields have been measured using the Pt-Co thin wire and results are discussed on the basis of the bubble departure time.

Manuscript received October 20, 1997.
S. Fuchino, 81-298-54-5819, fax 81-298-54-5822, fuchino@etl.go.jp; I. Ishii, 81-298-54-5814, fax 81-298-54-5822, iishi@etl.go.jp; N. Tamada, 81-298-54-5812, fax 81-298-54-5822, tamada@etl.go.jp; O. Tsukamoto, 81-45-339-4121, fax 81-45-338-1157, osami@tsukalab.dnj.ynu.ac.jp; M. Furuse, 81-45-335-4124, fax 81-45-338-1157, mf@tsukalab.dnj.ynu.ac.jp; T. Takao, 81-3-3238-3327, fax 81-3-3238-3321, takao@toshi.ee.sophia.ac.jp

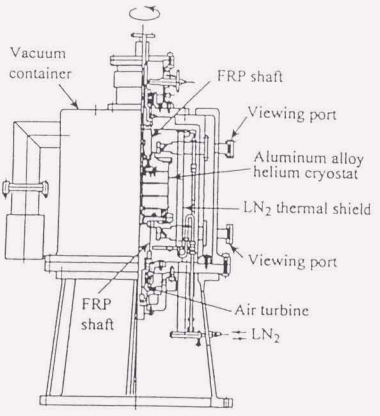

Fig. 1 Cut away view of high speed rotating cryostat.

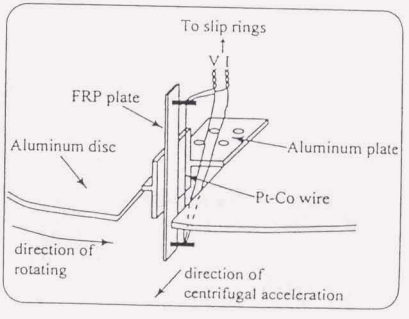

Fig. 2 Configuration of sample holder.

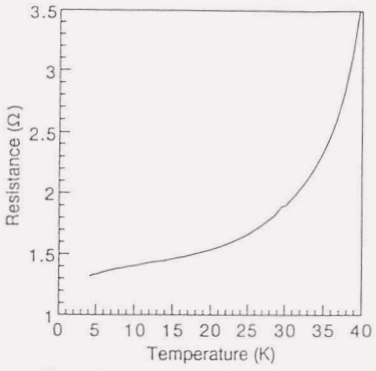

Fig. 3 Resistance-temperature characteristics.

II. Experiments

Fig. 1 shows a cut-away view of the high speed rotating cryostat used in our experiment. The rotating helium cryostat is made from aluminum alloy, and is 20cm in diameter and 20cm in height. The helium cryostat can be driven by fiber reinforced plastic (FRP) shafts connected to a base-mounted air turbine. The maximum centrifugal acceleration of the cryostat is 10,000 times larger than that of normal gravity (1G=9.8 m/s^2) at 10,000rpm. Fig. 2 shows the configuration of a sample holder with the Pt-Co thin wire placed on the disc in the rotating helium cryostat. Step heat inputs ranging from 1 to 5 W/cm^2 are applied to the thin wire with 20 μm in diameter and 48mm in length. The maximum centrifugal acceleration is around 1300 times larger than gravitational acceleration at 3600 rpm. The temperature rise can be known by the resistivity of the Pt-Co wire. Fig. 3 shows the resistance-temperature characteristics of the Pt-Co thin wire.

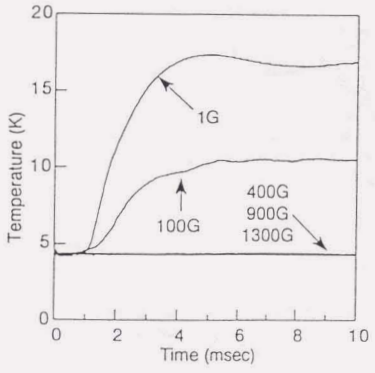

(a)25kW/m^2

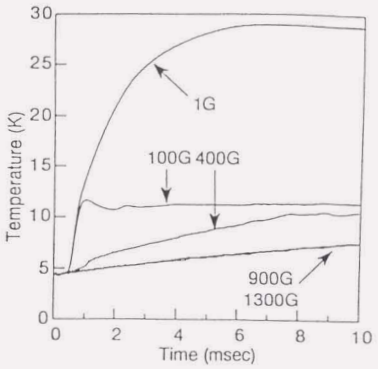

(b)32kW/m^2

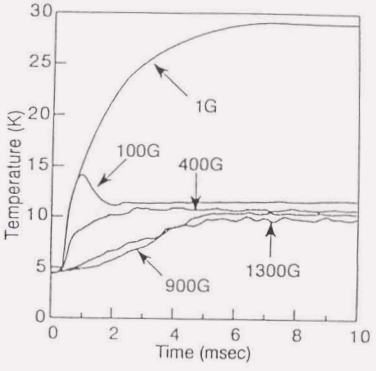

(c)34kW/m^2

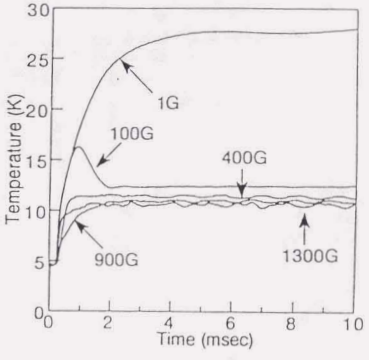

(d)38kW/m^2

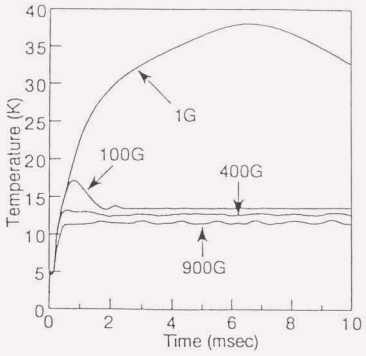

(e)42kW/m^2

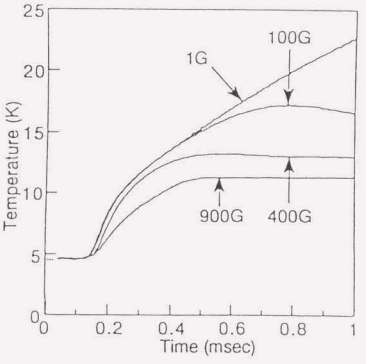

(e')42kW/m^2 enlargement

Fig. 4 Temperature traces of Pt-Co wire for various power input

III. Results and Discussion

Fig. 4 shows temperature traces of Pt-Co wire for varying power inputs under the various centrifugal acceleration fields. Based on these results, specific characteristics of the transient heat transfer were summarized in [4]. From these data, take-off times can be plotted for various heat fluxes. Here the take-off time is defined as the onset time of film boiling from the start of the step heating.

Fig. 5 shows the take-off times versus heat flux. From Fig. 5, the take-off time, t_{to} can be described by a power fit of the initial heat flux, q_i as $t_{to} \sim q_i^{-4}$. Though Schmidt [5] has proposed that this exponent of q_i is -2 theoretically and -2.8 experimentally, this value is dependent on the bath temperature. The higher the bath temperature is, the smaller the exponent is in his data, for example, the exponent is -2.8 at 3.0K and -3.5 at 4.2K. In our experiment, the bath temperature is around 4.3K by the adiabatic compression, therefore our fitting line doesn't deviate from his data. Other parameter to affect this exponent is helium pressure. The pressure of the outer part of the rotor is higher than 1.013 bar by centrifugal acceleration force, for example, the pressure is 1.2 bar at 2,000rpm. The exponent becomes smaller with increased pressure [6], for example, the exponent is -2.5 at 1.02bar and -4 at 1.63bar.

The cyclic temperature fluctuations in the wire are shown in Fig. 6. These fluctuations are supposed to be caused by cyclic departure of vapor bubbles as was observed by the video camera in the normal gravity [4]. The average cyclic times were not much dependent on q_i and are plotted against G at 42kW/m^2 in Fig. 7. This cyclic time is dependent on $G^{-1/3}$. This dependence on $G^{-1/3}$ was also observed by a direct optical observation for a flat heating surface in the same cryostat [7]. This dependence on $G^{-1/3}$ can be explained qualitatively as follows. Jacob [8] has proposed that fD is constant, where f is the frequency of bubble departure and D is the departure diameter of the bubble. Zuber [9] has also proposed that D is dependent on $G^{-1/3}$. Consequently the cyclic time of bubble departure (the inverse of the frequency) is proportional to $G^{-1/3}$.

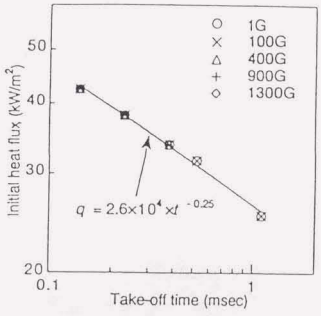

Fig. 5 take-off times versus heat flux.

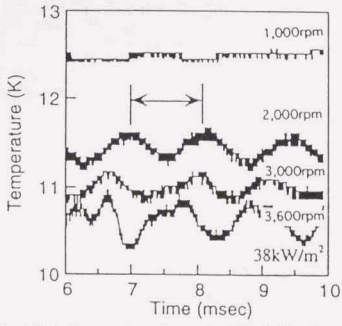

Fig. 6. Periodic temperature fluctuation in the Pt-Co wire.

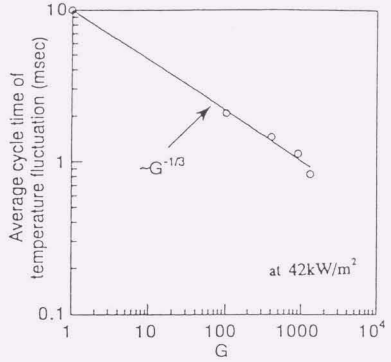

Fig. 7. Average cyclic time dependence on centrifugal acceleration.

IV. Conclusions

Transient heat transfer characteristics of liquid helium under centrifugal acceleration fields have been investigated using a Pt-Co thin wire. As the result, the take-off time can be described by a power fit of the heat flux and the discrepancy from Schmidt's data can be explained by the influence of the temperature and pressure.

The cyclic temperature fluctuations have been observed, the times of which can be also described by a power fit of the centrifugal acceleration. This dependence can be explained quantitatively by the frequency and the diameter of the bubble departure.

References

[1] R. G. Scurlock and G. K. Thornton, "Pool heat transfer to liquid and supercritical helium in high centrifugal acceleration fields," *Int. J. Heat Mass Transfer*, Vol.20, No.1, pp. 31-40, 1977.

[2] S. Fuchino, H. Fukuda, T. Ogawa, K. Shimizu, Y. Nakabayashi, Y. Kobayashi, M. Ogihara, Y. Kamisada, N. Maki, A. Ueda, T. Matsuda, "Development of 70MW class superconducting generators," *IEEE Trans. Magn.*, Vol.28, No.1, pp279-282, 1992

[3] S. Fuchino, Y. Iwasa, "A cryomechanics technique to measure dissipated energies of 10nJ," *Experimental Mechanics* Vol.30, No.4, pp356-359, 1990

[4] O. Tsukamoto, M. Furuse, T. Takao, N. Tamada, S. Fuchino, I. Ishii, N. Higuchi, "Transient heat transfer characteristics of liquid helium in centrifugal acceleration field," *Proc. CEC/ICMC '97*, to be published

[5] C. Schmidt, "Transient heat transfer and recovery behaviour of supers," *IEEE Trans. Magn.*, Vol.17, No.1, pp738-741, 1981.

[6] D. L. Kingsbury and S. W. Van Sciver, "Transient heat transfer in channel of liquid or supercritical helium," *Cryogenics*, Vol.35, No.9, pp573-579, 1995.

[7] N. Tamada, S. Fuchino, N. Natori, I. Ishii and M. Okano, "Optical measurement of transient phenomenon of liquid helium boiling under very high centrifugal operation," *Cryogenics*, Vol. 33, No.11, pp1023-1027, 1993

[8] M. Jacob, *Heat transfer*, Vol.1, John Wiley, New York, 1949.

[9] N. Zuber, *AEC Report, AECU-4439*, pp85-136, 1959

A Method to Estimate the Stability of Rotor Winding of Superconducting Generator in Rotating Condition

Osami Tsukamoto, Mitsuho Furuse
Faculty of Engineering, Yokohama National University, Yokohama, 240 Japan

Tomoaki Takao
Faculty of Science and Technology, Sophia University, Tokyo, 102 Japan

Masao Morita
Mitsubishi Electric Corporation, Amagasaki, Hyogo, 661 Japan

Toshiki Hirao
Engineering Research Association for Superconductive Generation Equipment (Super-GM), Osaka, 530 Japan

Abstract — Stability and training characteristics of rotor windings of a superconducting generator in rotating condition are estimated and compared with those in static condition. A major cause of unexpected quenches of the rotor windings is a disturbance caused by an abrupt conductor motion. We developed a method to statistically estimate the quench characteristics of a superconducting coil caused by conductor motions. We apply this method to a superconducting rotor of the 70 MW class generator developed as a part of Super-GM projects. In the paper, the method is explained and results of the stability estimation are presented.

I. Introduction

One of the most important issues of a generator with superconducting field windings is how to estimate the stability of the windings in rotating condition. A major cause of unexpected quenches of the rotor windings is a disturbance caused by an abrupt conductor motion. The released energy by the conductor motion depends on many factors, such as stiffness, compliance and irregularities in dimensions of the conductors, electrical and mechanical forces to the conductors, fixing structure of the conductors. We developed a method to statistically estimate the disturbance energy due to conductor motion taking into account of these factors [1]-[4]. Once the disturbance energy is known, the stability of the windings can be estimated by knowing MQE (Minimum Quench Energy) of the conductor. To calculate the MQE of the conductor of the rotor winding in the rotating condition, we should know the transient heat transfer characteristics of the helium coolant in the rotating condition. We showed that the steady state heat transfer characteristics were established in short time less than 1 msec when the centrifugal gravity was high as was in the rotor in the rotating condition [5]. By applying our method to statistically estimate the disturbance energy and using the steady state heat transfer characteristics of helium coolant in the rotating condition, we estimate the stability and training characteristics of the rotor windings developed as a part of the Super-GM project in the rotating condition.

Manuscript received October 22, 1997.

O.Tsukamoto, +81-45-339-4121, fax +81-45-338-1157, osami@tsukalab.dnj.ynu.ac.jp; M.Furuse, +81-45-339-4124, mf@tsukalab.dnj.ynu.ac.jp; T.Takao, +81-3-3238-3327, fax +81-3-3238-3321, takao@toshi.ee.sophia.ac.jp; M.Morita, +81-6-497-7127, fax +81-6-497-7288, morita@ele.crl.melco.co.jp; T.Hirao, +81-6-361-1051, fax +81-6-361-1437, LDM04314@niftyserve.or.jp

This work has been performed as a part of "R&D on Superconducting Technology for Electric Power Apparatuses" under the New Sunshine Program of Agency of Industrial Science and Technology, MITI, being consigned by NEDO.

II. Method to Statistically Estimate Stability

Conductors in windings are mainly supported by frictional forces. The conductors inevitably have irregularities in their dimensions, hence the frictional supporting forces to conductors fluctuate because contact forces between the conductors fluctuate along the conductors even if uniform compressive force is applied to the windings. An abrupt conductor motion occurs at a poorly supported part where the electromagnetic force to the conductor exceeds the frictional supporting force, and when the energy released by the conductor motion at the poorly supported part is larger than the MQE of the conductor, the conductor is quenched. Energy released by the conductor motion is determined by the length of the poorly supported part and we can define the MML (Maximum Movable Length), the maximum length of the conductor segment which can move without a quench [6],[7]. We developed a theory to statistically estimate the number of the poorly supported parts whose lengths exceed the MML, assuming that the random irregularities of the conductor dimensions follow the Gaussian process.

A. Maximum Movable Length

The rotor windings whose stability we estimate are wound of cable conductors composed of superconducting composite strands and we consider that a quench is most probably triggered

by a motion of a strand of the conductors.

The disturbance energy E_d released by a strand motion can be given by the following equation [6],[7].

$$E_d = \frac{(Bl)^2 (l/2)^5}{45 E I_d}, \qquad (1)$$

where l is the length of the moving segment of the strand, B the magnetic field component perpendicular to the direction of the strand motion, I the strand current, E Young's modulus of the strand, and I_d the geometrical moment of inertia of the strand, $I_d = \pi r^4 / 64$ for a round strand of the radius r. When the released energy E_d is greater than MQE, a quench occurs. The MML is obtained by putting $E_d = MQE$ and given by

$$MML = \left\{ \frac{1440\,(MQE)\,E I_d}{(Bl)^2} \right\}^{1/5} \qquad (2)$$

B. Steps for Estimation

To estimate the training characteristics of the rotor windings by applying our theory, the following steps are taken.

1. Calculation of the MQE of the strand of the rotor conductor for given operating condition.
2. Calculation of the MML based on the calculated values of MQE of the strand.
3. Estimating the statistical distribution of the length of the poorly supported part for given stress conditions of the supporting force, electromagnetic force, and centrifugal force, by assuming that the dimension irregularity follows the Gaussian process.
4. Counting the number of the poorly supported parts whose lengths exceed the MML.

III. Forces to Superconductors in the Rotor Winding

Forces to the conductors in the rotor winding should be known to estimate the stability characteristics and are dependent on the winding configuration, the rotating speed and the distribution of the magnetic field in the slots.

A. Configurations of Rotor Windings

We estimate the stability of the rotor developed by Mitsubishi Electric Co. for the 70 MW class superconducting generator as a part of the Super-GM projects. The cross-sectional view of the rotor is shown in Fig. 1 and the specifications of the rotor are listed in Table I. The rotor windings are placed in the slots No.1~5. A cross sectional view of the winding pack in the slot is illustrated in Fig. 2. Details of the rotor configuration is given in [8]. The cross section of the conductor made of 9 strands is illustrated in Fig. 3 and the specifications of the conductor and strand are listed in Table II.

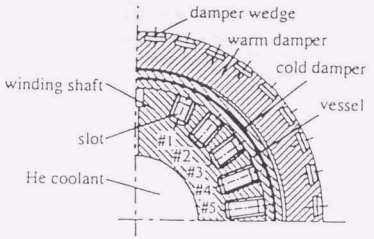

Fig. 1. Cross section of rotor (perpendicular to center axis, quarter of the rotor).

TABLE I
SPECIFICATION OF 70 MW CLASS SUPERCONDUCTING GENERATOR

Rotor	
Number of poles	2
Rotating velocity	3600 rpm
Diameter	890 mm
Bearing span	4900 mm
Winding	
No. of coils	10 (5 coils/pole)
Magnetic field (maximum)	4.5 T (at 3000 A)
Conductor	9-strand compacted cable

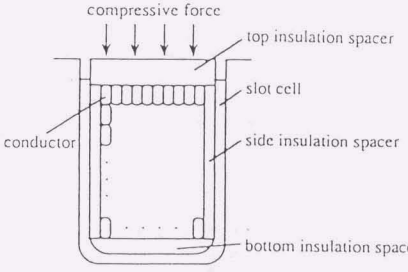

Fig. 2. Cross sectional view of the winding pack in the slot.

B. Forces to Conductors in Winding

The winding packs are surrounded by insulation spacers as is shown in Fig. 2 and the compressive forces are applied to the packs by the forces to the top insulation spacers. The rotor shaft with the windings in the slots was fitted in the rotor vessel by shrink-fit and the forces were applied to the top insulation spacer by the vessel.

When the rotor rotates and the windings are excited, the centrifugal forces and the electromagnetic forces are applied to the conductors in addition to the compressive force from the top insulation spacer. The centrifugal forces are in the opposite direction to the compressive forces. The distribution of forces to the conductors due to the compressive and centrifugal forces in the slots can be calculated knowing the Young's modulus of the winding pack in the radial direction. The Young's modulus was measured and estimated 68.8 MPa. The

TABLE II
SPECIFICATIONS OF CONDUCTOR AND STRAND

Conductor (compacted strand cable)	
Size in cross section	2.9 mm × 7.4 mm
No. of strands	9 strands
Critical current	5100 A (7.6 T) at 4.2 K 4900 A (7.3 T) at 4.6 K
Strand	
Cu : CuNi : NbTi	2 : 1 : 1
Diameter	1.6 mm
Young's modulus	130 GPa
Geometrical moment of inertia	3.2×10^{-13} m^4

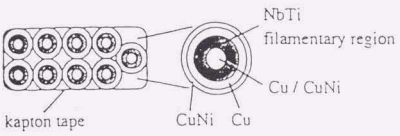

Fig. 3. Cross sections of rotor conductor and strand.

compressive force to the winding pack in the slot is estimated 5.2×10^4 N/m in static condition and 6.2×10^4 N/m in rotating condition in this study. This difference in the compressive forces is due to the difference in the ways to apply the forces to the top insulation spacers. The electromagnetic forces have two components of circumferential and radial directions of the rotor. The circumferential component of the electromagnetic forces cause the strand motions. The distributions of the magnetic field and the electromagnetic forces to the conductors in the slots are estimated based on the analysis using the finite element method.

IV. STATISTICAL ESTIMATION OF EXPECTED NUMBER OF QUENCH OF ROTOR WINDING

A. Calculation of MQE and MML

We assume that a quench of the winding is initiated by a quench caused by a strand motion in the conductor, therefore, MQE of the single strand is calculated. Details of calculation of MQE are described in [9]. We assumed a disturbance of 0.5 msec duration and 2 mm spatial length for the MQE calculation. MQE s were calculated for the static and rotating conditions. In the calculation, the transient heat transfer of liquid helium was taken into account in the static condition. In the rotating condition, data of the steady heat transfer of the supercritical helium in high centrifugal field [10] were used because according to our experiment, the steady state heat transfer was established in very short time.

The temperature of the helium coolant is 4.6 K in the rotating condition at the rated rotating speed and 4.2 K in the static condition. The MQE depends on the magnetic field, current and coolant temperature. MQE's of the strand were calculated for the static and rotating conditions as a function of the current and the field to which the strand was subject. The MQE's of the strand in the places of highest and lowest fields in the windings are plotted against the conductor current in Fig. 4. The MML of the strand was calculated from (2) based the calculated MQE and is a function of the current and the place in the slots as the MQE is.

B. Calculation of Expected Number of Quenches and Training Characteristics

We assume the irregularity in the dimension of the conductor follows the Gaussian process of standard deviation σ_n, then the dimension irregularity of the winding pack also follows the Gaussian process whose standard deviation is $\sqrt{n}\sigma_n$, where n is the number of the layers of the winding pack. It can be considered the contact forces between the conductors also follows the Gaussian process whose standard deviation is $k\sqrt{n}\sigma_n$ where k is the spring constant of the winding pack which can be deduced from the Young's modulus of the pack. Then, we can numerically simulate the distribution of the fluctuation of the contact force along the conductor using the method explained in [2]. We can assume that the contact force between conductors are equal to that between the strands of the conductor. Thus, by multiplying the contact force by the friction coefficient μ between the strands, we can estimate the distribution of the supporting force along the strand and the number of the poorly supported parts whose lengths exceed the MML for a given conductor current. This number is the expected number of quenches. Using the parameters listed in Table III, the accumulation of the expected number of the quenches until the conductor current reached I was calculated and is plotted against I in Fig. 5 for the static and rotating conditions. Fig. 6 shows the training characteristics which is obtained by assuming that a quench occurs at each time when the accumulation of the expected number of quenches increases by one. As is seen from the figure, the initial quench currents are 4.5 kA for the static condition and 4.2 kA for the rotating condition. The stability is deteriorated in the rotating condition but the initial quench is expected to exceed the rated current. It is also seen that after the initial quench, many quenches occurs successively in both conditions.

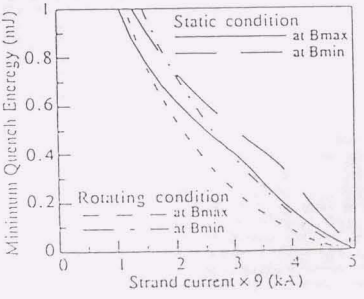

Fig. 4. Calculated MQE of strand in static and rotating conditions.

V. Comparison of Estimation with Experimental Results

The quench test of the rotor windings was performed in the static conditions and the result is shown in Fig. 7. As is shown Fig. 7, in the static condition, the current at the initial quench is 4.3 kA and many quenches follow. In the rotating condition, excitation test of the windings was also performed and it was demonstrated no quench occurred up to the rated current. These results well coincide with the estimation described above.

TABLE III
Parameters on Calculation of Expected Number of Quench

σ_n	50.0 μm
μ	1.0
Young's modulus of winding pack	68.8 MPa
compressive force to the windings	5.2×10^4 N/m (static condition)
	6.2×10^4 N/m (rotating condition)

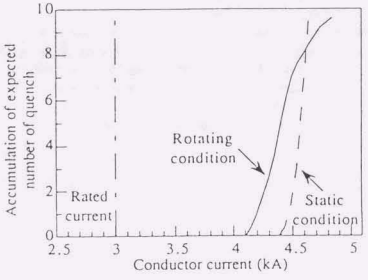

Fig. 5. Accumulation of expected number of quenches in static and rotating conditions.

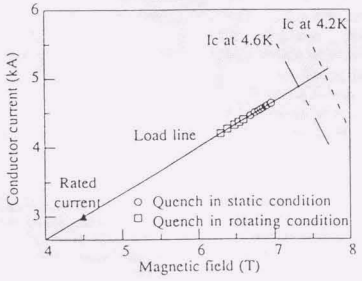

Fig. 6. Analytical result on training quenches of winding in static and rotating conditions.

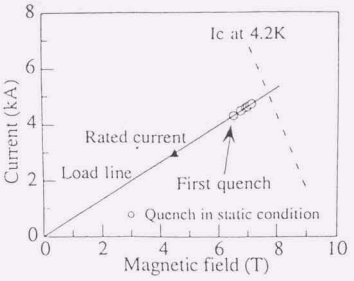

Fig. 7. Training quenches of winding in static condition.

VI. Concluding Remarks

The method to statistically estimate the quench characteristics of the superconducting rotor windings is explained and it is shown that the method can be a powerful tool for designing the rotor windings. With this method, we can figure out actual design parameters of the conductor and windings such as MQE of the conductors, the allowance in the dimensions of the conductor, and the compressive forces to the winding packs. However more works should be done to make the estimation more precise.

References

[1] T.Takao, P.C.Michael and O.Tsukamoto, "Influence of copper-to-superconductor ratio on the stability of high current density superconductor," *IEEE Trans. on Magn.*, vol. 30, No. 4, Part II, pp.2439-2442, 1994.

[2] T.Takao, K.Iwasaki and O.Tsukamoto, "Statistical Estimation of Disturbance Energy due to Conductor Motion in Rotor Windings of Superconducting Generator," *IEEE Trans. on Appl. Super.*, vol. 5, No. 2, pp.361-364, 1995.

[3] T.Takao, O.Tsukamoto, T.Hirao, M.Morita and B.Ikeda, "Quench Characteristics of Rotor Winding of Superconducting Generator in Static and Rotating Conditions," *IEEE Trans. on Magn.*, vol. 32, No. 4, pp.2365-2368, 1996.

[4] T.Takao, O.Tsukamoto, M.Furuse and K.Tsuchiya, "Statistical Estimation of Quench Characteristics of Quadrupole Magnets," *IEEE Trans. on Appl. Super.*, vol. 7, No. 2, pp.183-186, 1997.

[5] O.Tsukamoto, M.Furuse, ,T.Takao, N.Tamada, S.Fuchino, I.Ishii and N.Higuchi, "Transient heat transfer characteristics of liquid helium in centrifugal acceleration field," *presented at CEC/ICMC 97*

[6] T.Takao, O.Tsukamoto and S.Honjo, "Probability of premature quenches due to conductor motion in superconducting windings," *Cryogenics*, vol. 31, pp.504-509, 1991.

[7] O.Tsukamoto, "Disturbance due to conductor motion and stability of large-scale superconductors," *Fusion Engineering Design*, vol. 20, pp.327-332, 1993.

[8] T.Ohara, H.Fukuda, T.Ogawa, K.Shobara, M.Ohi, A.Ueda, K.Itoh and H.Taniguchi, "Development of 70MW class superconducting generators," *IEEE Trans. on Magn.*, vol.27, No.2, pp2232- , 1991

[9] N.Amemiya, T.Takao and O.Tsukamoto, "Disturbance characteristics and stability of high current density superconducting wires," *Fusion Engineering Design*, vol. 20, pp.339-344, 1993.

[10] R.Nakajima, K.Sato, K.Miyaike, M.Kumagai and Y.Kobayashi, "Liquid and supercritical helium heat transfer of horizontal upward facing surfaces under high centrifugal acceleration fields," HTD-Vol. 229, Heat transfer in superconducting equipment, G00721, pp.39-44, 1992

Study on Designing High Current Density Rotor Windings of Superconducting Generator and Relation of the Stabilities in Static and Rotating Conditions

Mitsuho Furuse, Osami Tsukamoto, Shinji Torii, Shirabe Akita and Masatoyo Shibuya

Abstract— **It is critically important to realize high current density superconducting rotor windings to make a superconducting generator economically competitive to a conventional one. High current density rotor windings inevitably suffer from instability problems. Therefore, the rotor windings should be designed for the quench currents to surely exceed the maximum operational currents in the rotating condition. In the next step of the Super-GM project, the current density required is 30% higher than that of the rotor winding developed in the former Super-GM project. To test the stability of the rotor windings, usually quench tests are conducted in a static and pool-cooled condition for the simplicity of the test but presently the relation between the stabilities in the static and rotating conditions is not clear. In the paper, we study what information can be obtained and how the stability in the rotating condition can be estimated from the static test. Based on this study, we investigate a method to design quench currents of high current density rotor windings to exceed a required value and discuss what level for the quench current to exceed in the static condition to satisfy the requirement in the rotating condition.**

Index Terms—**Conductor motion, minimum quench energy, stability of superconducting rotor winding, superconducting generator.**

I. Introduction

One of the most important issues in designing rotor windings of a superconducting generator is how to design high current density windings whose quench current exceed a required value. In a high current density superconducting coil, it is well known that the main causes of unexpected quenches are conductor motions. We developed a method to quantitatively estimate training quench characteristics of superconducting windings by use of statistical method [1]-[3]. In the method, energy of a disturbance due to a conductor motion is estimated statistically and transient heat transfer characteristics of helium coolant and compliance of the winding packs are taken into account. Using this method, we estimated the quench current of one of the rotors of the 70MW class superconducting generator which was developed in the Super-GM project and the estimation well explained the results of the excitation tests [2].

In the next step of the Super-GM project, the operational current density of the rotor winding pack required is 30% higher than that of the winding pack developed in the former project for the superconducting generator to be economically competitive to a conventional one. In this paper, based on our method, we study how to modify the design parameters of the superconductors and windings to satisfy the requirement in the next step of the project.

To test the stability of the rotor winding, quench test is usually performed in a static and pool cooled condition for the simplicity of the test. However, in a rotating condition, the forces to the conductor and heat transfer characteristics are different, and therefore the stability characteristics are different from the case of the static condition. In this paper, we discuss also the relation between the stability characteristics in static and rotating conditions by studying the differences of the supporting force of the conductors and heat transfer characteristics. Based on this discussion, required quench characteristics of the winding in the static condition is estimated to verify the stability in the rotating condition.

II. Principle of Method to Estimate Quench Characteristics

The rotor of the Super-GM superconducting generator is wound of cable conductors composed of copper stabilized superconducting composite strands. We consider that a quench is triggered by a motion of a strand of the conductor.

The strands are mainly supported by frictional forces. The stands and conductors inevitably have irregularities in dimensions. Therefore, the frictional supporting forces of the strands fluctuate because contact forces between the strands fluctuate along the strands even if uniform compressive force is applied to the winding pack. An abrupt strand motion occurs at a poorly supported part where the electromagnetic force to the strand exceeds the frictional supporting force, and a quench occurs when the energy released by the strand motion at the poorly supported part is larger than the Minimum Quench Energy (MQE) of the strand. Energy released by the strand motion is given by the following equation by knowing the length of the moving part,

$$E_d = \frac{(BI_s)^2 (l/2)^5}{45EI_d}, \qquad (1)$$

where l is the length of the moving part of the strand, B is the magnetic field component perpendicular to the direction of the strand motion, I_s is the strand current, E is Young's modulus of the strand, and I_d is the geometrical moment of inertia of the

Manuscript received September 18, 2000.

Mitsuho Furuse and Osami Tsukamoto are with Yokohama National University, Yokohama, Japan (telephone: 81-45-339-4124 or 4121, e-mail: mf@tsukalab.dnj.ynu.ac.jp, osami@tsukalab.dnj.ynu.ac.jp).

Shinji Torii and Shirabe Akita are with Central Research Institute of Electric Power Industry (CRIEPI), Tokyo, Japan (telephone: 81-3-3480-2111, e-mail: tori@criepi.denken.or.jp, akita@criepi.denken.or.jp).

Masatoyo Shibuya was with Engineering Research Association for Superconductive Generation Equipment (Super-GM), Osaka, Japan. He is now with CRIEPI, Tokyo, Japan (telephone: 81-468-56-2121, e-mail: shibuya@criepi.denken.or.jp).

strand, $I_d = \pi r^4/64$ for a round strand of radius r. To determine the length of the poorly supported part, we assume that the irregularities in conductor dimensions follow Gaussian process and that its spectrum density is proportional to the spatial frequency to the –4th power. The standard deviation of the dimension irregularity of the winding pack is given by $\sqrt{n}\sigma$, where σ is standard deviation of the dimension irregularity of the conductor including the insulation layer and n is the number of layers of the winding. It can be assumed from the above assumption that the contact forces between the conductors produced by the compressive force applied to the winding pack follow the Gaussian process whose standard deviation is $k\sqrt{n}\sigma$ where k is the spring constant of the winding pack. Based on the above assumptions, we can numerically simulate statistical distribution of the frictional supporting forces of the conductors and strands. Thus we can statistically determine the length of the poorly supported part and count the expected number of the parts whose lengths exceed the maximum movable length (MML). This number is the expected number of quenches. MML is the maximum length of the strand segment which can move abruptly without a quench and calculated by putting E_d = MQE.

MQE's of the strand of the rotor windings in static and rotating conditions are calculated by numerically solving a one dimensional thermal equilibrium equation for a strand subject to a point disturbance. In the calculation, transient heat transfer characteristics of liquid helium are taken into account for the calculation of MQE in static condition. Data of steady state heat transfer of supercritical helium in high centrifugal acceleration field are used for the rotating condition because, according to our experiment, the steady state heat transfer is established in very short time, less than 200μsec in rotating condition [4].

Based on the theory explained above, we can estimate quench characteristics of the rotor windings.

III. Distribution of Forces in Rotor Windings and Parameters Used in Analysis

To estimate the quench characteristics, we should know the distributions of forces applied to the conductors and strands in the winding. The conductors and strands are subject to electromagnetic forces and centrifugal forces. The former forces can be calculated by numerical calculation of the magnetic field distributions in the winding by use of the finite element method. The later can be calculated from the formula of the centrifugal force. From these force distributions, the supporting forces of the conductors and strands are calculated using an analytical model of the winding explained in the following.

In the calculation, we assume that the cross-sectional configurations of the rotor windings and conductors are the same as those developed in the former Super-GM project.

A. Configurations of Rotor Winding and Conductor

The rotor windings are placed in the slots of the rotor shaft. Cross-sectional views of the winding pack and the conductor in a slot are illustrated in Fig. 1. The conductors are made of 9 strands. Details of the rotor configuration are given in [5]. The winding packs are surrounded by insulation spacers and the compressive pressures are applied to the winding packs by the clamping forces to the insulation spacers placed on the top of the winding packs. The winding shaft with the windings in the slots is fitted in the rotor vessel by shrink-fit and the clamping forces are applied by the shrunken vessel.

B. Model to Calculate Distributions of Forces

Distributions of contact forces between conductors can be calculated by an analytical model shown in Fig. 2. In the model, a conductor is described as a mass point m connected to the neighboring conductors with two springs of spring constant $k/2n$ which represent elastic deformation of the conductor by the contact forces, and electromagnetic force and centrifugal force to the conductor are applied to the mass point. We neglect force interaction in the circumferential direction because deformation of conductors in circumferential direction by circumferential compressive force is considered to be smaller than that in the radial direction. When the rotor rotates and the windings are excited, the windings shrink in the radial direction by radial electromagnetic forces and centrifugal forces and depart from bottom insulation plate at a certain conductor current. In this case, the component of the radial force to the conductor due to the pre-compressive forces which are initially applied to the winding pack disappeared. We assume the contact forces between conductors are uniformly conducted to the strands composing the conductor. We assume also that a strand moves abruptly in circumferential direction when the circumferential force to the strand exceeds the frictional supporting force produced by the contact forces between the strands.

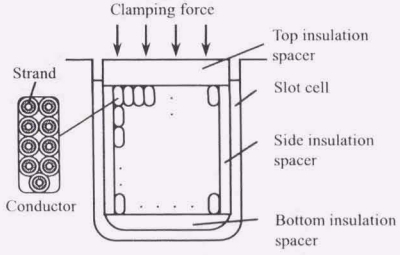

Fig. 1. Cross-sectional view of the winding pack in the slot of winding shaft.

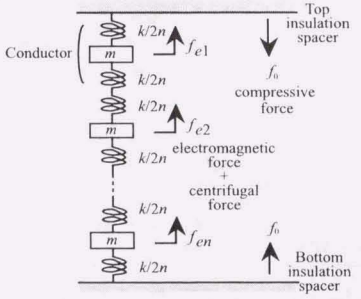

Fig. 2. Analytical model to calculate distribution of contact forces between conductors.

C. Compliance of Rotor Windings

As mentioned above, the contact forces between strands fluctuate along the strand around the value calculated by the spring model because of the irregularity in dimensions of the conductors and insulators. The standard deviation of fluctuation of the contact force is $k\sqrt{n}\sigma$. Stress-strain characteristics of the rotor winding pack in the radial direction were calculated for different values of ratio of copper stabilizer and CuNi to NbTi (nonSc/Sc) by finite element method. Details of calculation are described in [2]. The calculation results are shown in Fig. 3. We determine the value of k from the slope of the stress-strain curve at the stress determined by the compressive force to the winding pack.

We measured, in liquid helium, compliance of a test winding pack which simulated that of the rotor windings. Measured results are also shown in Fig. 3. As seen in Fig. 3, there is hysterisis, but the slope of the stress-strain curve is almost in the same level as the calculation results. Therefore, we consider that the calculation results are valid. The value of k used in the analysis is determined by $k=K\times 2.9\text{mm}/7.4\text{mm}/n$ where K is the slope of the stress-strain curve of winding pack shown in Fig. 3.

D. Parameters Used for Numerical Calculation

Parameters of the conductor, strand and winding pack used for the numerical analysis are listed in Table I. Dimensions of the conductor and strand are the same as those used in the rotor winding developed in the Super-GM project. Three cases of external field dependence of the conductor I_c , the standard case and high cases I and II, are assumed as shown in Fig. 4 (at 4.6K). The load line of the windings is also shown in Fig. 4. I_{max0}=3.6kA and I_{max1}=4.7kA in Fig. 4 are maximum operation currents of the former and next step Super-GM projects, respectively. The performance in the standard case is in the same level as that of the conductor used in the former Super-GM. I_c at 7.3T and 4.6K is assumed 30% higher in the high case I and 50% higher in the high case II than that in the standard case. In Fig. 4, non Sc/Sc is assumed 2.7. In all of those cases, the conductor and strand dimensions are the same.

Distribution of frictional supporting force can be given by multiplying the numerically calculated contact force distribution by the frictional coefficient μ between the strands. Analytical results show that the quench currents are not sensitive to μ in the range of μ=0.5~1.0. Therefore, we put μ=0.7. σ=33 μm is determined based on the specification of dimension allowance of the conductors.

IV. Estimation of First Quench

We consider that the first quench current of the rotor winding is an important measure of the stability. By counting expected number of strand segments where circumferential electromagnetic forces to the segments exceed the frictional supporting forces and their lengths exceed MML, we can estimate the expected number of quenches. The first quench current is determined as the current where the expected number of quenches exceed 1 during the excitation of the winding.

A. Dependence of First Quench Current on Non-super to Super Ratio and Methods to Increase Winding Current Density

Fig. 5 shows first quench currents estimated for various values of nonSc/Sc for the standard case and high cases I and II

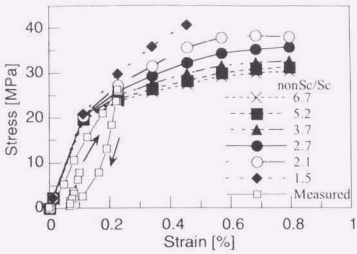

Fig. 3. Stress-strain curves of winding pack of different nonSc/Sc conductors

TABLE I
PARAMETERS OF CONDUCTOR, STRAND AND WINDING PACK ASSUMED IN CALCULATION

Conductor (compacted strand cable)	
Size in cross section	2.9 mm × 7.4 mm
No. of strands	9 strands
Standard deviation of dimension irregularity σ (including insulation layer)	33 μm
Strand	
Cu : CuNi : NbTi	1.0~5.3 : 0.5~1.4 : 1
Diameter	1.6 mm
Young's modulus	130 GPa
Geometrical moment of inertia	3.2×10^{-13} m^4
Frictional coefficient μ	0.7
Winding pack	
Spring constant k (depend on nonSc/Sc)	37GPa/m ~ 81GPa/m
Compressive force	18Mpa ~ 21MPa

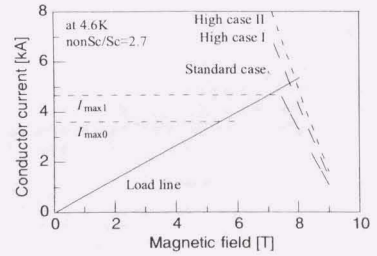

Fig.4. I_c vs. B characteristics used in the numerical analysis.

assuming that the pre-compressive pressure to the winding pack is 18MPa. In the estimation, we assume configurations of the windings and conductors including the dimensions in the cases I and II are the same as those in the standard case.

As nonSc/Sc increases, the spring constant of the conductor decreases and the standard deviation of the contact forces between the strands $k\sqrt{n}\sigma$ decreases. Therefore, the number of the poorly supported parts whose lengths exceed the MML decreases and the first quench current increase. However, high nonSc/Sc sacrifices the current density of the conductor. On

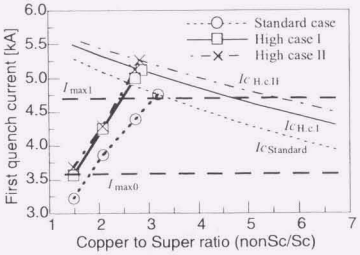

Fig. 5. Dependence of first quench current on nonSc/Sc

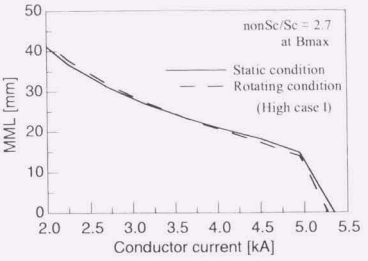

Fig. 6. MML vs. conductor current in static and rotating conditions.

the other hand, low nonSc/Sc strand causes the spring constant of the conductor to be large and the first quench current to decrease. As is shown in Fig. 5, there is an optimum value of the nonSc/Sc to make the first quench current maximum. In the standard case, the first quench current reaches critical current I_c=4.8kA at the nonSc/Sc=3.2.

To satisfy the requirement of 30% increase of the current density of the rotor winding, the first quench current should surely exceed 4.7kA. Obviously from Fig. 5, the conductor of the standard case is hard to exceed the required level but the conductors of the high cases I and II can well exceed the required level if proper values of the nonSc/Sc are selected.

B. Relation between Stabilities in Static and Rotating Conditions

In the rotating condition, centrifugal forces are applied to the conductors. The direction of the centrifugal force is opposite to the compressive force and the contact forces between strands become smaller in rotating condition than that in static condition. Bath temperature and heat transfer characteristics which affect MQE are also different in the static and rotating conditions. Fig. 6 shows MML vs. conductor current in the static and rotating conditions for the conductor of the high case I and nonSc/Sc=2.7. Values of MML are not much changed except in the range near to I_c's as shown in Fig. 6. In Fig. 6, I_c dependence on the bath temperature T_b are considered (T_b=4.2K and 4.6K for the static and rotating conditions respectively). Therefore, the contact force between the strands, that is related to the supporting force of the conductor, dominates the difference between the stabilities in the static and rotating conditions. The supporting force of the conductor directly depends on the compressive force to the winding pack. Fig. 7 shows the first quench currents vs. the pre-compressive pressure to the winding pack in the static and rotating conditions for the conductor of the high case I with nonSc/Sc=2.7. Knowing the first quench current in the static condition, we can estimate the effective value of the compressive force and the first quench current in the rotating condition from Fig. 7. For example, for the first quench to exceed 4.7kA in the rotating condition, the first quench current should exceed 5.2kA in the static condition.

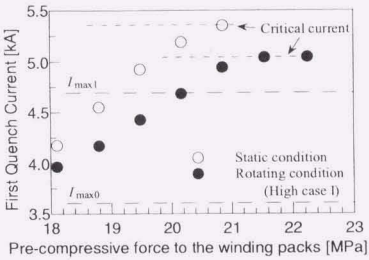

Fig. 7. Dependence of first quench current on compressive force.

V. Concluding Remarks

The first quench currents of the superconducting rotor windings are quantitatively estimated for various cases. In this study, the following are shown.

1. The current density of the winding can be improved by properly selecting the amount of the copper of the conductor because the conductor motions are suppressed.
2. The quench test in the static and pool cooled condition gives information on the pre-compressive forces to the winding pack and the quench currents in the rotating condition.
3. The requirement of the 30% increase of the operating current density can be satisfied by 30% increase of the critical current density of the conductor and by proper selection of the nonSc/Sc and the pre-compressive forces to the winding packs.

References

[1] T. Takao, O. Tsukamoto, M. Furuse and K. Tsuxhiya, "Statistical Estimation of Quench Characteristics of Quadrupole Magnets," *IEEE Trans. on Appl. Super.*, Vol. 7, No. 2, pp. 183-186.

[2] O. Tsukamoto, M. Furuse, T. Takao M. Morita, S. Maeda and T. Hirao, "Designing Stable and High-Current Density Rotor Windings of Superconducting Generator," *IEEE Trans. on Appl. Super.*, Vol. 9, No. 2, pp. 244-247.

[3] M. Furuse, O. Tsukamoto, T. Takao and K. Yoshida, "Analytical Estimation of Quench Current of Large Bore Superconducting Magnet," *IEEE Trans. on Appl. Super.*, Vol. 10, No. 1, pp. 653-656.

[4] M. Furuse, O. Tsukamoto, T. Takao, S. Fuchino, I. Ishii, M. Okano and N. Tamada, "Transient Heat Transfer Characteristics of Supercritical Helium in High Centrifugal Acceleration Field," *Advances in Cryogenic Engineering*, Vol. 45, pp. 1151-1158.

[5] T. Ohara, H. Fukuda, T. Ogawa, K. Shiobara, M. Ohi, A. Ueda, K. Itoh and H. Taniguchi, "Development of 70MW class superconducting generators," *IEEE Trans. on Magn.*, vol.27, No.2, pp. 2232-2239.

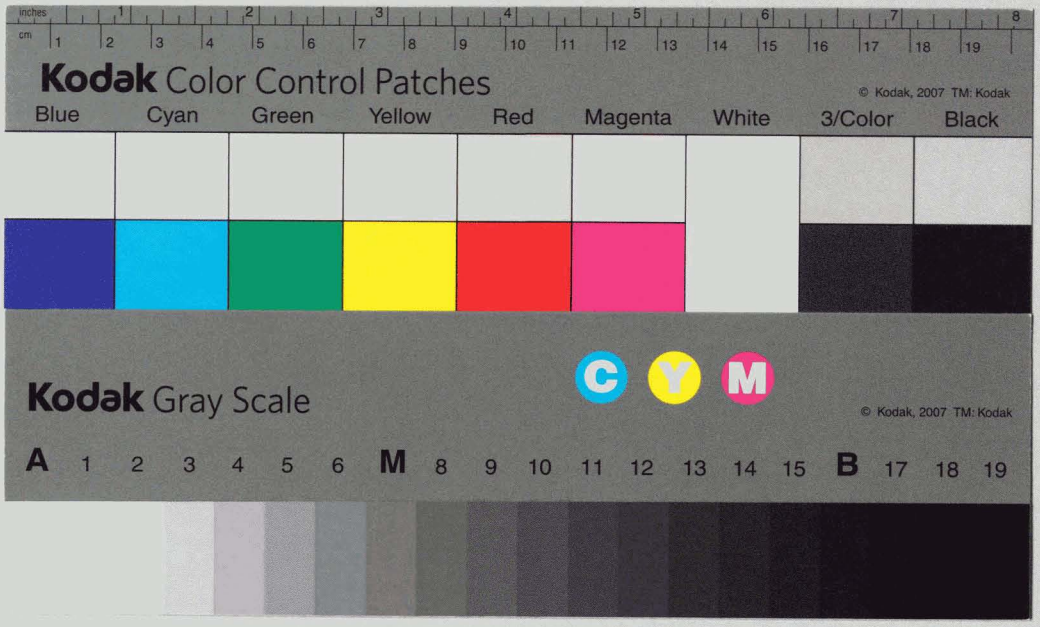
inches
cm
Kodak Color Control Patches
© Kodak, 2007 TM: Kodak
Blue
Cyan
Green
Yellow
Red
Magenta
White
3/Color
Black
Kodak Gray Scale
C
Y
M
© Kodak, 2007 TM: Kodak
A 1 2 3 4 5 6 M 8 9 10 11 12 13 14 15 B 17 18 19